CHARACTERIZATION OF THE MITOCHONDRIAL SCAFFOLD PROTEIN SLP2

Inaugural – Dissertation zur

Erlangung des Doktorgrades

der Mathematisch-Naturwissenschaftlichen Fakultät

der Universität zu Köln

vorgelegt von

Britta Ingrid Gudrun Thewes

aus Bergisch Gladbach

Köln, 2022

Berichterstatter:

Prof. Dr. Thomas Langer
Prof. Dr. Jan Riemer

Tag der mündlichen Prüfung:

02.12.2022

Abstract

Mitochondria are essential organelles that perform diverse functions in eukaryotic cells. They possess a complex ultrastructure with two membranes and multiple compartments in which mitochondrial- and nuclear-encoded proteins ensure mitochondrial function in an organized manner. This organization within mitochondria is maintained by various proteins, protein complexes, and lipids, e.g., the ATP synthase, respiratory chain (super)complexes, the MICOS complex, the GTPase OPA1, the lipid cardiolipin, and the structural proteins PHB, PHB2 and SLP2.

In contrast to the essential prohibitin complex, little is known about the functions of SLP2. Together with the proteases PARL and YME1L, SLP2 forms the so-called SPY complex at the inner membrane of mitochondria and influences respiratory chain supercomplex formation, mitochondrial calcium homeostasis and stress-induced hyperfusion of mitochondria.

To understand the function of SLP2 in mitochondria, immunoprecipitation experiments of SLP2 as well as various omics approaches and biochemical experiments were performed in human SLP2 deficient cells. We found that SLP2 interacts with a variety of mitochondrial proteins and is thus tightly linked to the mitochondrial network. Loss of SLP2 resulted in global impairment of mitochondrial gene expression and increased turnover of the mitochondrial small ribosomal subunit and the interactors TMBIM5, DNAJC15 and APOO. This gene expression defect led to respiratory chain deficits and secondarily to impairment of the TCA cycle and a stress response of the cell, the integrated stress response.

In conclusion, we show in this work that SLP2 is required for optimal mitochondrial function via gene expression. Furthermore, we uncover previously unknown connections of SLP2 to the protein import machinery, the MICOS complex and the respiratory chain, and discover protein-specific effects of SLP2 on protein turnover. Thus, with the results presented in this thesis, we demonstrate that SLP2 is an important structural protein with diverse roles in maintaining mitochondrial function.

Table of content

1 Introduction

1.1 Mitochondrial organization

Mitochondria are essential organelles that harbor their own genome and participate in a wide range of cellular functions, including the well-known task of ATP production together with the tricarboxylic acid (TCA) cycle, but also metal metabolism via heme and Fe-S clusters, Ca^{2+} buffering as well as lipid biosynthesis (Lill et al., 2020; Nunnari and Suomalainen, 2012; Rizzuto et al., 2000). This variety of functions requires a high level of organization within mitochondrial compartments. Consistent with their proposed origin from α-proteobacteria, these compartments are created by two membranes, the outer (OM) and the inner (IM) membrane which in mitochondria form specific dynamic membrane invaginations called cristae. The IM can be subdivided into the inner boundary (IBM), closest to the OM, and the cristae membrane (CM) forming the actual cristae (Freya and Mannellab, 2000; Kühlbrandt, 2015; Palade, 1953; Werner and Neupert, 1972). The cristae and cristae junctions harbor the respiratory chain (super)complexes, the ATP synthase, the mitochondrial contact site and cristae organizing system (MICOS) complex and optic atrophy protein 1 (OPA1) which aid in maintaining mitochondrial shape (Harner et al., 2011; Hoppins et al., 2011; Vogel et al., 2006) The dimeric complexes of the ATP synthase have been shown to assemble into rows and induce local membrane curvature thus probably enabling the formation of the cristae (Blum et al., 2019) (Fig. 1).

The cristae junctions are highly enriched for the MICOS complex which also forms contact sites with the OM (Harner et al., 2011; Hoppins et al., 2011). In mammals the MICOS complex consists of two subcomplexes with different MICOS subunit proteins (1) MIC60, MIC25, MIC19 and (2) MIC10, MIC26 (APOO), MIC27 (APOOL) and MIC13 (Khosravi and Harner, 2020). Downregulation or complete loss of the MICOS subunits MIC10, MIC60, MIC13 and MIC19 leads to strong cristae defects with a drastic decrease in cristae junctions while loss of MIC25, APOO or APOOL barely display any cristae phenotype (Mukherjee et al., 2021; Stephan et al., 2020a) (Fig. 1 b).

The MICOS complex has been reported to interact with another mitochondrial shaping factor, OPA1 (Darshi et al., 2011). OPA1 is a dynamin-like GTPase of the inner membrane with large portions exposed to the intermembrane space (IMS) where it regulates fusion and fission of the IM (Akepati et al., 2008; Olichon et al., 2003). Long and short OPA1 forms are generated via proteolytic cleavage by the IM proteases

metalloendopeptidase OMA1 and ATP-dependent zinc metalloprotease YME1L1 in balance to maintain a tubular mitochondrial network. Excessive accumulation of S-OPA1 by hyperactivation of OMA1 due to mitochondrial stress and cellular insults leads to fragmentation of mitochondria and increased fission (Anand et al., 2014; Wai and Langer, 2016). Fusion and fission of the outer mitochondrial are mediated by mitofusins (MFN1, MFN2) and dynamin-related protein 1 (DRP1/ DNM1L) respectively (Santel and Fuller, 2001; Smirnova et al., 2001). Mitochondrial dynamics are controlled by metabolic demands and stress conditions (Youle and Van Der Bliek, 2012). Fusion is promoted under starvation conditions and can take forms such as stress-induced mitochondrial hyperfusion in cultured cells, a process that is dependent on the scaffold protein stomatin-like protein 2 (STOML2, here SLP2) and L-OPA1 and provides optimal respiratory function of mitochondria (Tondera et al., 2009) (Fig. 1 a).

Mitochondrial shape is not maintained by proteins alone but also by its lipids. The mitochondrial IM contains phospholipids like phosphatidylethanolamine (PE), phosphatidylinositol (PI), phosphatidylcholine (PC), phosphatidylserine (PS), and phosphatidic acid (PA), as well as phosphatidylglycerol (PG) and cardiolipin (CL) (Horvath and Daum, 2013). CL makes up for up to 20 % of total lipids in the IM and is synthesized from PA by the enzymes phosphatidate cytidylyltransferase (TAMM41), phosphatidylglycerol phosphate synthase (PGS1), protein-tyrosine phosphatase mitochondrial 1 (PTPMT1) and cardiolipin synthase (CRLS1/CLS1). It is then further remodeled by phospholipases and acylated by tafazzin (TAZ) to form mature CL (Dudek, 2017). CL has been shown to exert chaperone-like activity by interaction with various proteins and protein complexes of the IM. Among them are the respiratory chain complexes and supercomplexes, mitochondrial carrier proteins like pyruvate carrier (MPC1/2) and ADP/ATP translocase 1 (ANT1/SLC25A4) and the mitochondrial calcium uniporter (MCU) associated calcium uptake proteins 1 and 2 (MICU1, MICU2). Other essential mitochondrial proteins and machineries such as OPA1 and the import complexes translocase of outer membrane (TOM), sorting and assembly machinery (SAM), translocase of the inner membrane TIM22 and TIM23, presequence translocase-associated motor (PAM), the MICOS complex, specifically MIC60 and the apolipoproteins APOO and APOOL, as well as the mitochondrial ribosome have been associated with CL (Dudek, 2017; Lee et al., 2020a; Schlame and Ren, 2009).

Many genes coding for mitochondrial shaping factors have been shown to be involved in human diseases. OPA1 has been associated with optic atrophy, YME1L with

mitochondriopathy with optic atrophy, DRP1 with encephalopathy and optic atrophy, MIC60 with Parkinson's disease and MIC13 with lethal infantile hepato-encephalopathy (Delettre et al., 2000; Hartmann et al., 2016a; Tsai et al., 2018; Waterham et al., 2007; Zeharia et al., 2016). The gene for TAZ which is required for CL remodeling is mutated in Barth syndrome (BTHS). In all of these diseases mitochondrial morphology is altered to varying extents and e.g., with disconnected cristae or fragmentation (Navaratnarajah et al., 2021; Schlame and Ren, 2006). Loss of mitochondrial shape further correlates with age and decreased mitochondrial function (Brandt et al., 2017; Sohal, 1970; Walker and Benzer, 2004).
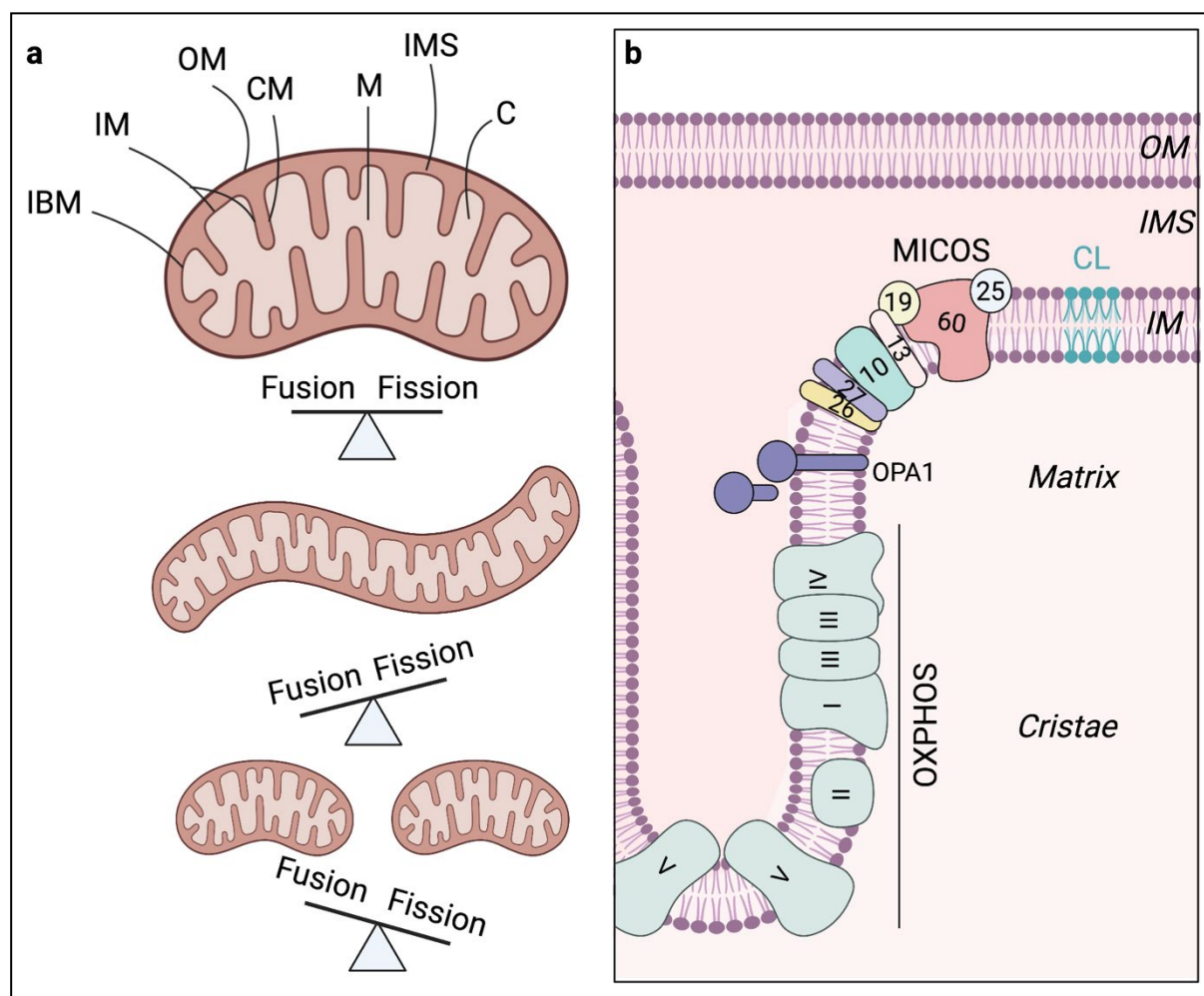
Figure 1: Mitochondrial structure and organization

(a) Schematic illustration of mitochondrial structure with the outer membrane (OM) and inner membrane (IM) which is subdivided into inner boundary membrane (IBM) and cristae membrane (CM), the compartments of the intermembrane space (IMS), matrix (M) and cristae (C). Mitochondrial fusion and fission is in balance to allow for a tubulated mitochondrial network. A shift towards more fusion leads to hyperfused and elongated mitochondria while more fission results in fragmentation. **(b)** Shaping factors of the mitochondrial inner membrane include the MICOS complex with MIC60, MIC25, MIC19, MIC10, MIC13, MIC26 (APOO) and MIC27 (APOOL), the

proteolytic cleavage of OPA1 into long and short forms, the respiratory chain with emphasis on the ATP synthase (V) dimers at the tip of the cristae and the phospholipid cardiolipin (CL).

1.2   SPFH protein family

Other mitochondrial shaping factors are found in the stomatin/prohibitin/flotillin/HflK/C (SPFH)/ prohibitin/Band 7 family of proteins which are prone to oligomerize into high molecular weight complexes. Members of this protein family include non-mitochondrial ERLIN1/2, flotillin FLOT1/2, podocin, stomatin, as well as mitochondrial prohibitin PHB1/2 and SLP2. Besides the C-terminal SPFH domain most of them also contain a C-terminal coiled coil region for oligomerization as well as a N-terminal intra- or transmembrane region. SPFH proteins are found at various subcellular membranes such as the plasma membrane, endosomes, lipid droplets, Golgi, endoplasmic reticulum (ER), nucleus and mitochondria where they exert a range of different functions (Browman et al., 2007). The prohibitins and SLP2 are the only members which localize to mitochondria. In the ER membrane the complex of erlin 1 and 2 was shown to promote degradation of inositol 1,4,5-trisphosphate (IP3) receptors (IP3Rs) which control ER calcium stores (Pearce et al., 2009). Mutation of erlin 2 further caused hereditary spastic paraplegia (HSP) (Rydning et al., 2018). Flotillins localize to the plasma membrane and have been associated with endocytosis, insulin receptor signaling and possibly T cell receptor signaling (Otto and Nichols, 2011). Another scaffold protein found at the plasma membrane but also in lipid droplets and endosomes is stomatin. The *C. elegans* homolog mechanosensory protein 2 (MEC2) of stomatin is involved in mechanosensation while human stomatin was shown to regulate the gating of acid-sensing ion channels (ASICs) (Price et al., 2004a).

In the mitochondrial IM PHB and PHB2 form large ring complexes of approx. 1 MDa consisting of co-translationally dependent hetero-oligomers (Berger and Yaffe, 1998; Tatsuta et al., 2005) (Fig. 2). Complete absence of the mitochondrial PHB complex is embryonic lethal in flies, *C. elegans* and mice (Sanz et al., 2003; Theiss and Sitaraman, 2011). Prohibitins were further shown to be important in prancreatic β-cells to protect from diabetes and low prohibitin levels were detrimental in neurons of Parkinson's disease (Dutta et al., 2018; Supale et al., 2013). PHB and PHB2 have also been proven to be involved in mitochondrial nucleoid organization and diseases such as neurodegeneration and obesity in mice (Ande et al., 2016; Kasashima et al., 2008; Merkwirth et al., 2012). The loss of prohibitins in cells leads to destabilization of long

isoforms of OPA1, thus resulting in abnormal cristae morphology, fragmentation and increased susceptibility to apoptosis (Merkwirth et al., 2008; Morrow and Parton, 2005). As chaperones they stabilize newly synthesized mitochondrial translation products and support mitochondrial gene expression (He et al., 2012; Nijtmans et al., 2000). They are also required for respiratory chain supercomplex formation (Jian et al., 2017). Prohibitins additionally form the PMA complex with the *m*-AAA protease to negatively regulate *m*-AAA-mediated membrane protein degradation and interact with the mitochondrial chaperone DnaJ homolog subfamily C member 19 (DNAJC19) to enable CL remodeling (Richter-Dennerlein et al., 2014; Steglich et al., 1999). Surprisingly, PHB2 was recently shown to function as an IM mitophagy receptor that is essential for parkin-mediated mitophagy (Wei et al., 2017).

Recently the structure of the assembled *E. coli* SPFH proteins HflK/C in a complex with the ATP-dependent zinc metalloprotease FtsH was resolved by cryo-EM. The structure revealed that the SPFH complex encloses the protease and thus presents a cage for it by which it putatively limits the activity and substrate access of the protease (Daumke and Lewin, 2022; Ma et al., 2022).

1.3 SLP2

The only other mitochondrial member of the SPFH family besides PHB and PHB2 is SLP2 which is found in the matrix but attaches to the IM by an unknown mechanism as it lacks a transmembrane region (Lapatsina et al., 2012) (Fig. 2). At the IM SLP2 forms a 2 MDa complex termed SPY with the *i*-AAA protease YME1L and the presenilin-associated rhomboid-like protease PARL. In association with the SPY complex SLP2 was found to facilitate PARL-mediated PTEN-induced putative kinase protein 1 (PINK1) cleavage and to negatively regulate phosphoglycerate mutase family member 5 (PGAM5) processing by PARL upon stress conditions. The same publication also described an increased OMA1 mediated cleavage of OPA1 in the absence of SLP2 (Wai et al., 2016). Similar conditions induce stress-induced mitochondrial hyperfusion (SiMH) which occurs to enable optimal respiration by altering mitochondrial shape and requires MFN1, L-OPA1 and SLP2 (Tondera et al., 2009). SLP2 further regulates the stability of specific mitochondrial proteins such as complex I and IV subunits of the respiratory chain (Da Cruz et al., 2008a). Increased uncoupled mitochondrial respiration as well as decreased supercomplex formation and mitochondrial membrane potential was observed upon SLP2 loss in T cells

(Mitsopoulos et al., 2015a). SLP2-deficient activated T cells further displayed a mild mitochondrial translation defect (Mitsopoulos et al., 2017). In various cancer cell lines silencing of SLP2 led to a proliferation defect and was sometimes accompanied by an induction of cell death (Huang et al., 2017; Wang et al., 2009; Yang et al., 2018). On the contrary, SLP2 expression correlated with tumor progression in tissue samples of cervical cancer, breast cancer and invasion in esophageal squamous cell carcinoma (Cao et al., 2007, 2013; Xiao et al., 2015). Reminiscent of stomatin which modulates acid-sensing ion channels, SLP2 was shown to negatively regulate mitochondrial calcium homeostasis, resulting in a lower calcium storage capacity of mitochondria, lower mitochondrial and higher cytosolic Ca^{2+} elevations (Da Cruz et al., 2010; Price et al., 2004a). SLP2 has also been associated with CL as it selectively precipitated CL-containing vesicles and its overexpression led to increased CL synthesis (Christie et al., 2011a).
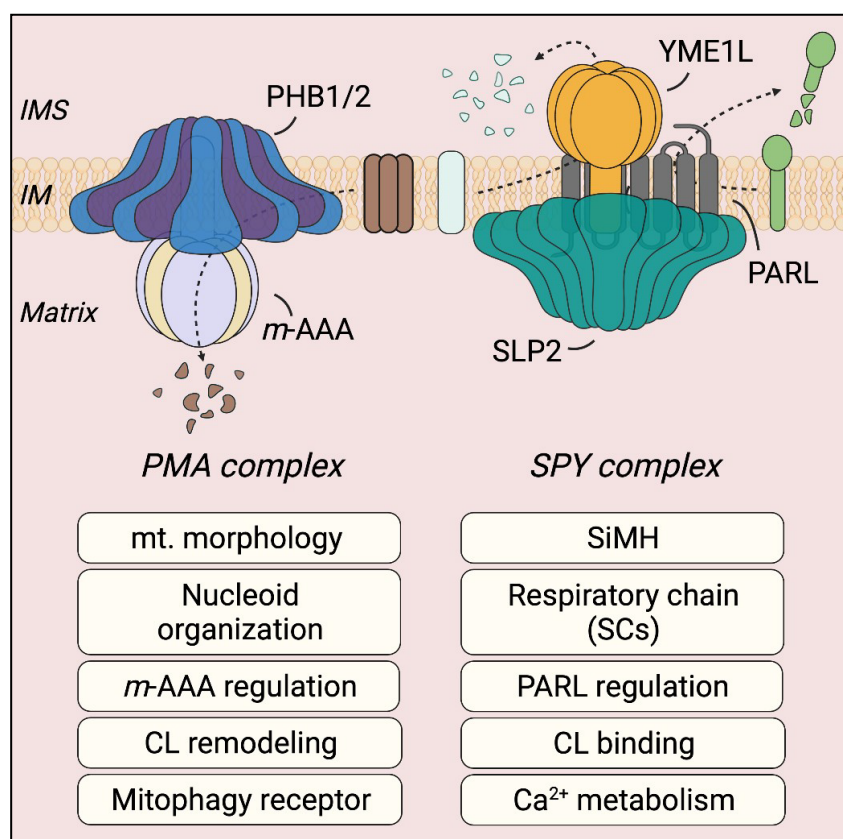
Figure 2: The mitochondrial SPFH scaffold proteins prohibitin and SLP2
Schematic illustration of PHB1/2 and SLP2 within the PMA (prohibitin/ *m*-AAA) complex and SPY (SLP2/ PARL/ YME1L) complex at the inner mitochondrial membrane. Prohibitins (left) have been linked to mitochondrial morphology, nucleoid organization, *m*-AAA regulation, cardiolipin (CL) remodeling and mitophagy. SLP2 (right) has been shown to have functions in stress-induced mitochondrial hyperfusion (SiMH), respiratory chain (super)complexes, PARL substrate cleavage within SPY, CL binding and calcium homeostasis.

1.4   Mitochondrial proteases

The prohibitin complex and SLP2 both associate with mitochondrial proteases which exert protein quality control and other regulatory functions. The proteolytic system of mitochondria consists of 18 catalytically active proteases which can be divided into four functional categories (Deshwal et al., 2020). Mitochondrial processing peptidases like the mitochondrial processing peptidase (MPP) or inner membrane protease (IMMP) are best known to cleave targeting sequences and promote maturation of newly imported proteins (Poveda-Huertes et al., 2017). Another processing peptidase PARL in the IM rather regulates dual protein localization by cleaving within transmembrane domains of its substrates. PARL substrates include steroidogenic acute regulatory protein (StAR)-related lipid transfer protein 7 (STARD7), PGAM5, PINK1, Diablo IAP-binding mitochondrial protein (DIABLO, SMAC) and Tetratricopeptide repeat protein 19 (TTC19) (Jin, 2010; Saita et al., 2017, 2018; Sekine et al., 2012). This demonstrates the involvement of PARL in mitochondrial and cellular processes like lipid transfer, mitophagy, apoptosis and oxidative phosphorylation (OXPHOS). Loss of PARL has been associated with Parkinson's and LHON disease (Phasukkijwatana et al., 2010; Wüst et al., 2015). The main substrate of the stress- activated processing peptidase OMA1 has been described in 1.1 and is OPA1 (Anand et al., 2014). Other substrates however like DAP3 Binding Cell Death Enhancer 1 (DELE1) which directly links OMA1 to the integrated stress response have been suggested (Fessler et al., 2020; Guo et al., 2020).

The second largest group of mitochondrial proteases contains those dependent on ATP. One of them is the *m*-AAA protease, an either homo- or heterooligomeric hexamer of AFG3-like protein 2 (AFG3L2) with paraplegin (SPG7), and one of two ATPases associated with diverse cellular activities (AAA) proteases in mitochondria (Koppen et al., 2007). The *m*-AAA protease sits within the IM and is active on the matrix side where it regulates mitochondrial gene expression by cleaving the mitochondrial large ribosomal subunit protein bL32m (MRPL32) and thus translation (Bonn et al., 2011; Nolden et al., 2005). In addition, mitochondrial calcium signaling was shown to depend on the *m*-AAA protease as it cleaves the essential MCU regulator (EMRE) and thereby limits MCU assembly and Ca^{2+} overload (König et al., 2016; Tsai et al., 2017). Recently more substrates of the *m*-AAA protease were identified which include links to protein import via DnaJ homolog subfamily C member 15 (DNAJC15), calcium signaling via transmembrane BAX inhibitor motif-containing protein 5 (GHITM, here

TMBIM5), OXPHOS, gene expression and other mitochondrial pathways (Patron et al., 2022). Mutations in AFG3L2 or SPG7 have been shown to cause dominant spinocerebellar ataxia (SCA28) and hereditary spastic paraplegia (HSP7) respectively (Casari et al., 1998; Pierson et al., 2011).

The second AAA protease is the *i*-AAA protease which acts on the IMS side of mitochondria. Besides OPA1 as discussed in 1.1, substrates of YME1L include proteins involved in lipid transfer, import, respiration and metabolism in steady-state conditions and upon oxygen or nutrient deprivation (MacVicar et al., 2019). In detail, YME1L affects mitochondrial import by cleaving the TIM23 complex constituents translocase of inner mitochondrial membrane 17A (TIMM17A) and reactive oxygen species modulator 1 (ROMO1) and was shown to degrade the non-assembled respiratory chain subunits NADH-ubiquinone oxidoreductase chain 6 (MT-ND6), NADH dehydrogenase [ubiquinone] 1 beta subcomplex subunit 6 (NDUFB6) and cytochrome c oxidase subunit 4 (COX4) among other substrates (MacVicar et al., 2019; Ohba et al., 2020; Rainbolt et al., 2013; Richter et al., 2019; Stiburek et al., 2012). Recently YME1L was further described to be involved in nucleotide synthesis by regulating the pyrimidine nucleotide carrier solute carrier family 25 member 33 (SLC25A33) which was linked mtDNA release and an inflammatory response (Sprenger et al., 2021). Loss of YME1L has been associated with mitochondriopathy and neurological dysfunction (Hartmann et al., 2016b; Sprenger et al., 2019).

The two remaining ATP-dependent proteases in the mitochondrial matrix are Lon protease homolog (LONP1) and CLPXP which consists of seven caseinolytic peptidase subunit P (CLPP) and six caseinolytic peptidase subunit X (CLPX) subunits (Baker and Sauer, 2012; Pinti et al., 2016). CLPP was shown to be involved in mitochondrial translation by degrading the GTPase Era (ERAL1) which needs to be removed from the 28S subunit to allow for interaction with the 39S subunit (Szczepanowska et al., 2016). Deficiency of CLPP further causes Perrault syndrome (Jenkinson et al., 2013). Similarly, also LONP1 was described to be involved in mitochondrial gene expression. Its substrates include transcription factor A (TFAM), single-stranded DNA-binding protein (SSBP1), transcription termination factor 3 (MTERF3) and FAST kinase domain-containing protein 2 (FASTKD2) thus closely linking LONP1 to mitochondrial DNA maintenance and transcription among other processes (Matsushima et al., 2010; Zurita Rendón and Shoubridge, 2018). LONP1 has been associated with various human diseases and its mutation causes cerebral,

ocular, dental, auricular, skeletal anomalies (CODAS) syndrome (Bota and Davies, 2016) (Fig. 3).

Microsomal endopeptidase (MEP) and pitrilysin metallopeptidase 1 (PITRM1) are mitochondrial oligopeptidases (Mzhavia et al., 1999). High temperature requirement mitochondrial serine protease A2)/Omi (HTRA2) and β-lactamase-like protein (LACTB) are proteases of the IMS and carry out functions in apoptosis and filament formation respectively (Deshwal et al., 2020; Keckesova et al., 2017; Suzuki et al., 2001).
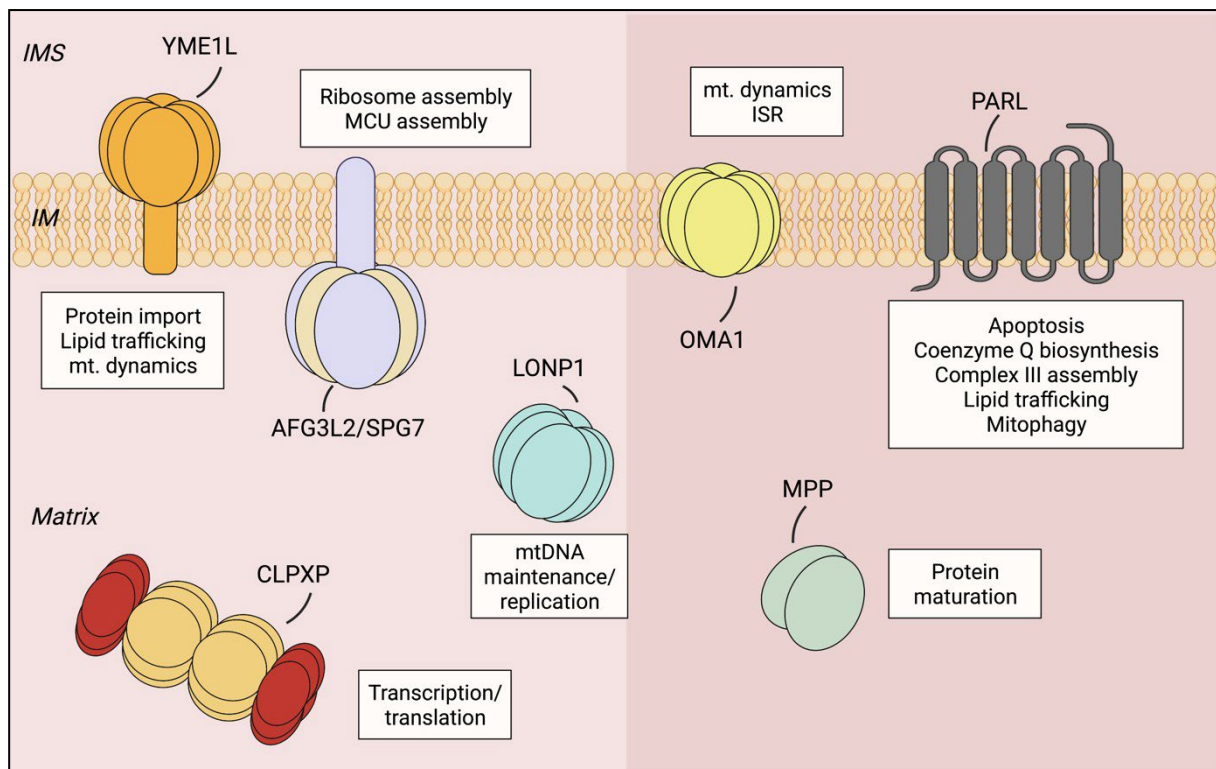
Figure 3: The mitochondrial proteolytic system
The ATP-dependent mitoproteases (left) YME1L (*i*-AAA), AFG3L2/SPG7 (*m*-AAA), LONP1 and CLPXP regulate mitochondrial processes such as protein import, lipid trafficking, dynamics and different aspects of gene expression. The processing peptidases (right) OMA1, PARL and MPP support dynamics, the integrated stress response, apoptosis, synthesis of coenzyme Q (CoQ), complex III assembly, lipid trafficking, mitophagy and maturation of proteins.

1.5   Mitochondrial gene expression

Mitochondria contain their own genome, the ~16 kb circular double-stranded mitochondrial DNA (mtDNA) which encodes for 11 mRNAs (13 proteins) for the respiratory chain, 22 tRNAs and 2 rRNAs (Anderson et al., 1981; Fernández-Silva et al., 2003). mtDNA is mainly maternally inherited and multiple copies of it are packed into nucleoids by TFAM (Ekstrand et al., 2004; Shoubridge, 2000). The promoter regions for the two strands of mtDNA, heavy (H) and light (L) with the heavy-strand

(HSP) and light-strand promoter (LSP), are found in the non-coding regulatory region (NCR) and transcription initiation results in long polycistronic transcripts (Aloni and Attardi, 1971; Anderson et al., 1981). Transcription initiation of mtDNA requires the sequential recruitment of TFAM, mitochondrial DNA-directed RNA polymerase (POLRMT) and mitochondrial transcription factor B2 (TFB2M) (Hillen et al., 2018). Elongation is supported by transcription elongation factor (TEFM) while termination is poorly understood and has partially been associated with transcription termination factor 1 (MTERF1) (Fernández-Silva et al., 2003; Yakubovskaya et al., 2010).

The transcripts are then processed by elaC ribonuclease Z 2 (ELAC2, RNase Z) and RNase P which consists of tRNA methyltransferase 10C (TRMT10C, MRPP1), hydroxysteroid 17-beta dehydrogenase 10 (HSD17B10, MRPP2) and protein-only RNase P catalytic subunit (PRORP) and results in the excision of tRNAs which punctuate most transcripts (Holzmann et al., 2008; Ojala et al., 1981). Mt-mRNAs (except *MT-ND6*) are further modified by 3'-adenylation via mitochondrial poly(A) polymerase (MTPAP) and methylation as well as pseudouridylation have been suggested (Carlile et al., 2014; Safra et al., 2017; Tomecki et al., 2004). Mitochondrial tRNA modifications include 3' addition of CCA by tRNA nucleotidyl transferase 1 (TRNT1) among others followed by aminoacylation via aminoacyl-tRNA synthetases (aaRS) (D'Souza and Minczuk, 2018; Nagaike et al., 2001). FASTKD family members are involved in various steps of mitochondrial gene expression including processing, translation and assembly of the ribosome (Kotrys and Szczesny, 2020; Suzuki et al., 2011).

The stability of mitochondrial transcripts is mediated by the complex of leucine-rich penticopeptiderich domain containing protein (LRPPRC) and stem–loop interacting RNA-binding protein (SLIRP) in which LRPPRC supports RNA polyadenylation and translation (Lagouge et al., 2015; Ruzzenente et al., 2012; Sasarman et al., 2010; Sterky et al., 2010). Degradation of non-coding mtRNA species from the L-strand, rRNAs and overall mt-mRNA turnover is facilitated by another complex consisting of ATP-dependent RNA helicase SUPV3L1 (SUV3) and polynucleotide phosphorylase (PNPase, PNPT1) (Borowski et al., 2013; Chen et al., 2006; Toompuu et al., 2018).

The translation of mitochondrially encoded mRNAs requires the independent assembly of the mitochondrial ribosome which is made up of the large 39S (mtLSU, LSU) and small 28S (mtSSU, SSU) subunit (Brown et al., 2014; Greber et al., 2014, 2015; Kaushal et al., 2014; Sharma et al., 2003). Mitoribosome assembly starts close to

mtDNA and was suggested to continue in RNA granules (Antonicka and Shoubridge, 2015). The 28S subunit consists of 30 ribosomal proteins and 12S rRNA. Its assembly is made up of sequential clusters and requires various assembly factors including the RNA modifying enzymes dimethyladenosine transferase 1 (TFB1M), 5-methylcytosine rRNA methyltransferase NSUN4, tRNA (uracil-5-)-methyltransferase homolog B (TRMT2B) and the GTPase Era (ERAL1) which stabilizes the 12S RNA (Dennerlein et al., 2010; Metodiev et al., 2009a, 2014; Powell and Minczuk, 2020). The 39S subunit contains the 16S RNA, tRNA^{Val} or tRNA^{Phe} and 52 ribosomal proteins which follow a similar assembly pattern that that of the small subunit. Assembly of the LSU requires many assembly factors including the RNA modifying enzymes rRNA methyltransferase 1-3 (MRM1-3), tRNA (adenine(58)-N(1))-methyltransferase (TRMT61B), pseudouridylate synthase RPUSD4, the ATP dependent RNA helicases DHX30 and DDX28 as well as the mitochondrial ribosomal GTPases GTPBP5/6/7/10 and others (Antonicka and Shoubridge, 2015; Antonicka et al., 2017; Bar-Yaacov et al., 2016; Cipullo et al., 2021; Hilander et al., 2021; Lee and Bogenhagen, 2014). Translation is initiated by the binding of mRNA to the SSU and recognition of fMet-tRNA^{Met} in the ribosomal P site with the help of the initiation factors IF2 and IF3 (Spencer and Spremulli, 2004). This is followed by translation elongation during which the aminoacylated tRNA is delivered, a peptide bond is formed and the mRNA-tRNA module is translocated (Hammarsund et al., 2001; Ling et al., 1997). Nascent chains are co-translationally inserted into the IM via the mitochondrial inner membrane protein OXA1L (OXA1L), supported by MRPL45 as the membrane anchor of the LSU subunit (Jia et al., 2003; Kummer et al., 2018; Szyrach et al., 2003). Finally, translation is terminated upon recognition of a stop codon via the four putative termination factors peptide chain release factor 1 and 1a (mtRF1, mtRF1a), peptidyl-tRNA hydrolase ICT1 (ICT1) and mitochondrial translation release factor in rescue (C12ORF65) and the ribosome is recycled (Kummer and Ban, 2021). The co-translational membrane insertion and assembly of nascent chains is best described for cytochrome c oxidase subunit 1 (MT-CO1 or COX1) of complex IV. This process not only requires OXA1L as mentioned above but also the mitochondrial translation regulation assembly intermediate of cytochrome c oxidase (MITRAC) complex and the translocase of the inner mitochondrial membrane (TIMM21). The MITRAC complex exists as an early and late form together with newly synthesized COX1. MITRAC$_{early}$ contains cytochrome c oxidase assembly protein (COX14, C12ORF62) and cytochrome c

oxidase assembly factor 3 homolog (COA3, MITRAC12) while MITRAC$_{late}$ additionally recruits surfeit locus protein 1 (SURF1), cytochrome c oxidase assembly factor 1 homolog (COA1, MITRAC15) and COX assembly mitochondrial protein (CMC1). The TIM21 complex facilitates transport of newly imported nuclear complex IV subunits from TIM23 to MITRAC to allow for assembly (Mick et al., 2012; Richter-Dennerlein et al., 2016a; Wang et al., 2020; Weraarpachai et al., 2012). Translation of mitochondrially encoded CIV subunits is tightly coordinated with the import of its nuclear subunits as COX1 translation is stalled in the absence of nuclear COX4 (Richter-Dennerlein et al., 2015, 2016b) (Fig. 4, fig. 5).

Replication of mtDNA requires the DNA polymerase γ (POLG), the mtDNA twinkle (TWNK) and SSBP (Gray and Wongs, 1992; Gustafsson et al., 2016; Mignotte et al., 1985; Spelbrink et al., 2001). Mitochondrial DNA mutations cause a variety of clinical disorders such as Mitochondrial Encephalopathy, Lactic Acidosis, and Stroke-like episodes (MELAS) which is caused by mutations in MT-ND1, MT-ND5 or TRNL1 or Leber's hereditary optic neuropathy (LHON) that is due to MT-ND1, MT-ND4 and MT-ND6 mutations (Taylor and Turnbull, 2005). However, mutations in nuclear genes involved in mitochondrial gene expression have been shown to cause disorders as well. These include mutations in amino-tRNA synthetases, ribosomal proteins and other translation factors (Boczonadi and Horvath, 2014) as well as replication factors like POLG and TWNK (Holt et al., 2022).
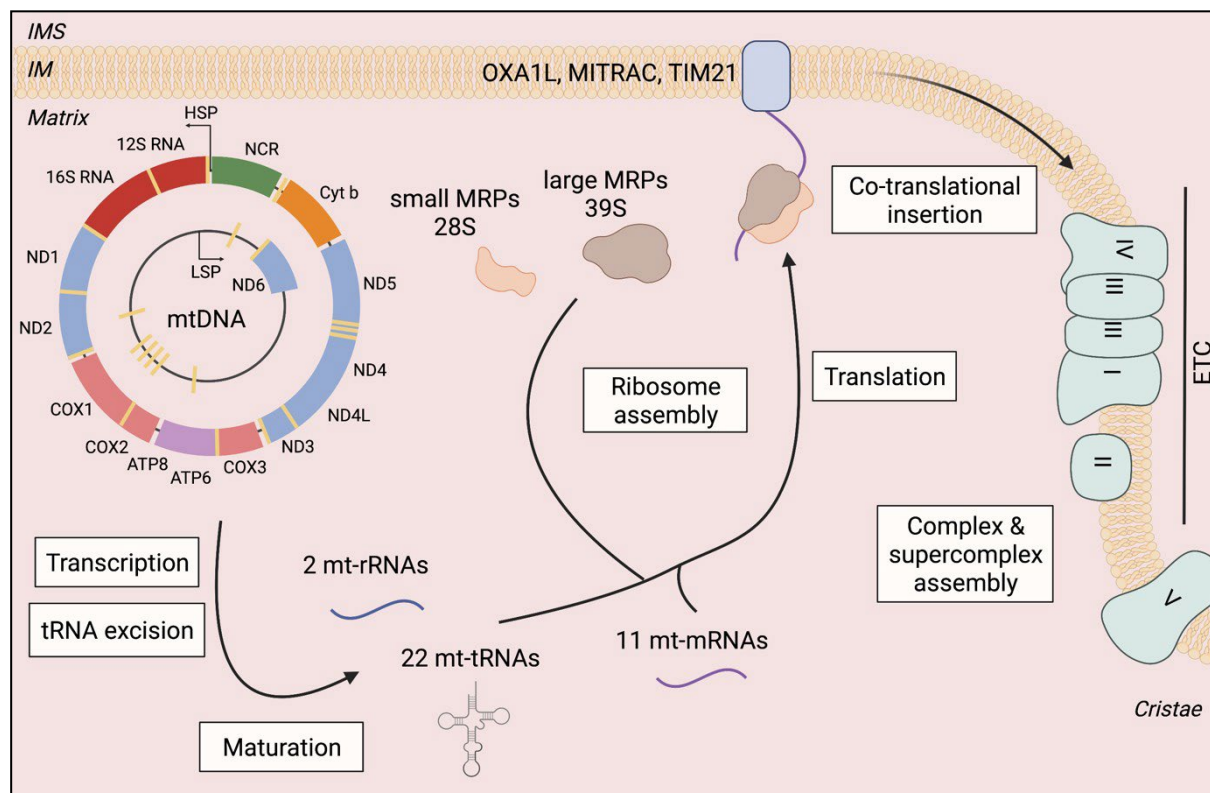
Figure 4: Mitochondrial gene expression

Schematic overview of mitochondrial gene expression. The heavy and light strand of the mitochondrial genome (mtDNA) are transcribed to give rise to 2 mt-rRNAs (12S, 16S), 22 mt-tRNAs and 11 mt-mRNAs by tRNA excision and different processing and maturation steps. The mitoribosome (55S) is then assembled from nuclear encoded ribosomal subunit proteins, 12S, 16S and tRNA^{Val} or tRNA^{Phe} which first form the small (28S) and large (39S) ribosome. Mitochondrial mRNAs are then translated and co-translationally inserted into the inner membrane where they assemble into respiratory chain (super)complexes together with imported nuclear OXPHOS subunits.

1.6 Mitochondrial protein import

Besides the 13 OXPHOS proteins encoded by the mitochondrial DNA more than 1000 nuclear encoded proteins have to be imported across two membranes to allow for proper function of the organelle (Rath et al., 2021). Roughly, mitochondrial protein import is facilitated by the multi-protein complexes TOM, SAM, mitochondrial import (MIM), mitochondrial IMS import and assembly (MIA), TIM22 and TIM23 and PAM which coordinate to allow for five different import pathways (Chacinska et al., 2009; Kang et al., 2018; Wiedemann and Pfanner, 2017). The two pathways for IM and matrix protein import are briefly discussed in the following.

Most mitochondrial proteins carry cleavable presequences and are thus imported via the presequence pathway. This requires the receptors translocase of outer mitochondrial membrane TOM20 and TOM22 followed by translocation via TOM40 (Ahting et al., 2001; Backes et al., 2018; Saitoh et al., 2007; Van Wilpe et al., 1999). The protein is then handed over to the TIM23 complex and TIM21 for lateral sorting into the IM or the TIM23 and PAM complex for import into the matrix (Bhattacharyya et al., 1995; Borges et al., 2003; Dekker et al., 1993; Guo et al., 2004; Sinha et al., 2010; Yamamoto et al., 2002). The TIM23 complex was suggested to exist as an indispensable form with TIMM17B and DNAJC19 or together with TIMM17A and DNAJC15 as an non-essential complex (Sinha et al., 2014). MPP removes the targeting sequences in both cases. As metabolic hubs mitochondria contain many metabolic carriers which do not contain presequences but are imported into the IM via the carrier pathway instead. They are transported across the OM by TOM20, TOM70 and TOM40 and subsequently handed to the TIM22 complex and released into the IM (Kang et al., 2017; Okamoto et al., 2014; Sirrenberg et al., 1996) (Fig. 5).
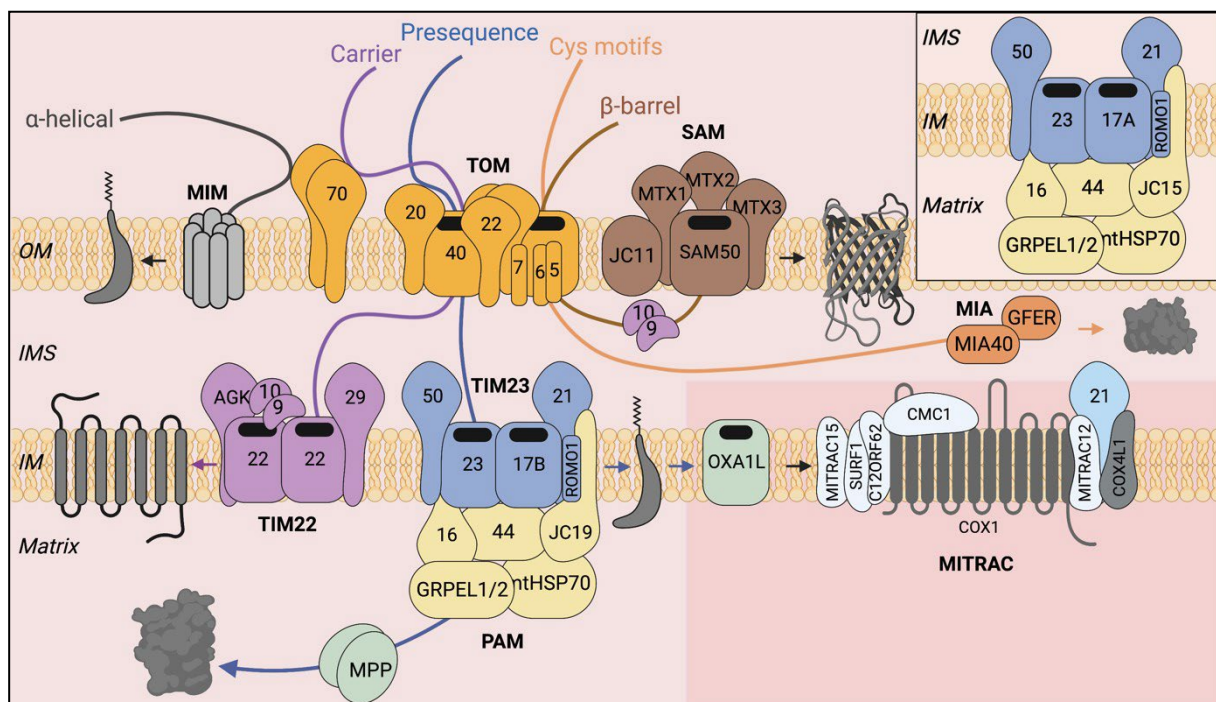
Figure 5: Mitochondrial import and insertion pathways

Schematic overview of mitochondrial import pathways in humans. Most nuclear encoded mitochondrial proteins are imported first via the TOM complex (TOMM40, TOMM20, TOMM22, TOMM5, TOMM6, TOMM7, TOMM70) or the MIM complex in the case of α-helical OM proteins. The SAM complex (SAMM50, MTX1, MTX2, MTX3, DNAJC11) accepts precursors from TOM for the import of β-barrel proteins. Proteins that carry a presequence are imported via TOM and specifically TOM20 before associating with the TIM23 complex (predominantly: TIMM23,

TIMM17B, TIMM50, TIMM21, ROMO1). In association with the TIM23 complex, TIMM21 supports lateral sorting into the inner membrane while the PAM complex (predominantly: TIMM16, TIMM44, DNAJC19, GRPEL1/2, mtHSP70) facilitates import of matrix proteins. For both MPP removes the presequence. OXA1L mediates the co-translational insertion of mitochondrially encoded proteins together with the MITRAC complex and TIMM21 in case of COX1. Inner membrane carrier proteins are imported via TOM40 and specifically TOMM70 and the TIM22 complex (TIMM22, AGK, TIMM29, TIMM9, TIMM10). The MIA complex (MIA40, GFER) facilitates import of IMS proteins with conserved cysteine motifs such as COX17 and small TIMs (Banci et al., 2009).

1.7   Respiratory chain

Mitochondrial gene expression products together with the import of nuclear encoded proteins make up the respiratory chain. The respiratory chain is best-known feature of mitochondria and uses NADH and succinate to generate an electrochemical proton gradient across the mitochondrial inner membrane. In the matrix NADH and succinate are generated in the TCA cycle from acetyl-CoA that is produced by glycolysis and fatty acid β oxidation (Krebs and Johnson, 1980). The inner membrane harbors the respiratory chain complexes complex I (NADH:ubiquinone oxidoreductase), complex II (succinate dehydrogenase SDH), complex III (cytochrome bc1 oxidoreductase) and complex IV (cytochrome c oxidase) in addition to the two electron carriers ubiquinone and cytochrome c (Letts and Sazanov, 2017).

The largest complex with 45 subunit is the L-shaped complex I which enables the oxidoreduction of NADH and ubiquinone to pump four protons across the IM into the IMS (Jones et al., 2017; Zhu et al., 2016). Complex II on the other hand does not pump protons and is the smallest complex with only four subunits. Complex II is responsible for the oxidation of succinate to fumarate in the TCA and at the same time the reduction of ubiquinone to ubiquinol (Rasheed et al.). The ubiquinol pool generated by complex I and II is then used by complex III which couples the oxidation of ubiquinol to the reduction of cytochrome c and at the same time pumps four protons into the IMS (Mitchell, 1976; Xia et al., 2013). Cytochrome c delivers these electrons to complex IV which in turn uses them to reduce oxygen to water and transfers four protons across the IM (Timón-Gómez et al., 2018; Yoshikawa and Shimada, 2015). Complex III and IV consist of 11 and 14 subunits respectively. The flux of protons into the IMS causes an electrochemical proton gradient across the IM. The mitochondrial ATP synthase or complex V uses this gradient for oxidative phosphorylation of ADP to ATP (Mitchell, 1961; Pinke et al., 2020; Zhu et al., 2016).

The assembly of each respiratory chain complex requires a set of assembly factors. Surprisingly, by far the most are identified for the assembly of complex IV which assembles into three subcomplexes. Each subcomplex contains one mitochondrially encoded core protein and numerous nuclear encoded subunits (Timón-Gómez et al., 2018). This tightly connects mitochondrial protein import with respiratory chain assembly and function. OXPHOS complexes are contain different cofactors such as iron-sulfur clusters in CI, II and III, haem in CIII and IV or cupper, magnesium and zinc in CIV (Cardenas-Rodriguez et al., 2018; Swenson et al., 2020; Vercellino and Sazanov, 2021). The organization of the respiratory chain complexes goes beyond the assembly of individual complexes which together assemble into supercomplexes (SCs). The respirasome consists of the complexes I+III$_2$+IV and other compositions like I+III$_2$ or III$_2$+IV have been described (Acín-Pérez et al., 2008; Chance et al., 1963; Schägger and Pfeiffer, 2000). Why and if supercomplexes are needed however remains controversial. It has been hypothesized that supercomplexes could support the stability of individual complexes, limit reactive oxygen species (ROS) production or increase the efficiency of electron transport (Blanchi et al., 2004; Lapuente-Brun et al., 2013; Maranzana et al., 2013; Sousa et al., 2016).

1.8   Aims of this thesis

Mitochondria are cellular signaling hubs with functions ranging from ATP production to lipid biosynthesis. These functions are carried out in six mitochondrial compartments by over 1100 nuclear and mitochondrially encoded proteins. These diverse functions require further organization by specific proteins and their complexes such as the MICOS complex or scaffold proteins such as the prohibitins and SLP2. SLP2 forms a large complex at the inner mitochondrial membrane where it interacts with the proteases PARL and YME1L in the SPY complex and allows for stress-induced mitochondrial hyperfusion, respiratory chain supercomplex assembly and calcium homeostasis.

Despite the proposed functions of SLP2 in mitochondria, little is known about its scaffolded proteins and in-depth consequences of *SLP2*$^{-/-}$. The severe effects of a loss of the closely related prohibitin complex however suggest functions of SLP2 that have yet been discovered. Here we aim to identify the expanse of the SLP2 interactome and the consequences of *SLP2*$^{-/-}$ in a human cancer cell line on the mitochondrial proteome as well as its turnover, mitochondrial respiration, metabolism and ultrastructure by mass spectrometry methods, biochemical approaches and electron microscopy. Based on our results, we further investigate mitochondrial gene expression in detail at the levels of mtDNA maintenance, transcription, ribosome assembly and translation by isotope labeling and biochemical approaches in human cells or isolated mitochondria to shed light on this poorly understood role of SLP2 on mitochondrial protein synthesis.

2 Materials and methods

2.1 Materials

2.1.1 Chemicals

Chemicals were obtained from Thermo Fisher Scientific (Schwerte), Sigma Aldrich (Steinheim), Merck (Darmstadt), Roth (Karlsruhe), Serva (Heidelberg), or VWR International GmbH (Darmstadt) or New England Biolabs (Ipswich) if not indicated otherwise.

2.1.2 Cell lines

Table 1 contains all cell lines used in this thesis and their origin. All cell lines were Henrietta Lacks cervical tumour cells (HeLa).

Table 1: Cell lines used in this study

Cell line	Reference
HeLa *wildtype (WT)*	S. Saita
HeLa *SLP2$^{-/-}$*	S. Saita
HeLa *SLP2$^{-/-}$ + SLP2^{FLAG}*	S. Saita

2.1.3 siRNAs and esiRNAs

Table 2 contains all siRNAs (Thermo Fisher, Invitrogen) and esiRNAs (Sigma) used for transient knockdown of gene expression. The procedure is described in 2.2.1.3.

Table 2: esiRNAs and siRNAs

esiRNA	Product number
EGFP	EHUEGFP
SLP2	EHU145711
siRNA	Product number
Negative control medium GC	12935300
SLP2	HSS116547
YME1L	HSS116546

2.1.4 Antibodies

Table 3 contains the antibodies used in this thesis.

Table 3: Antibodies

Antibody	Product number	Dilution
AFG3L2	(unavailable) (Biogenes)	1:1000
ASS1	HPA020934 (Sigma)	1:1000
ATP5A	ab14748 (abcam)	1:1000
COX2	ab110258 (abcam)	1:1000
COX4	459600 (Thermo)	1:10000
DNAJC15	16063-1-AP (Proteintech)	1:500
LC3	3868S (Cell signaling)	1:1000
APOO	MA5-15493 (Invitrogen)	1:1000
APOOL	PA5-51427 (Invitrogen)	1:1000
MPV17L2	HPA043111 (Sigma)	1:500
NDUFV1	11238-1-AP (Proteintech)	1:1000
NME4	TA501114 (Origene)	1:500
PARL	G038 (Genscript)	1:500
PRELID1	PA5-31087 (Invitrogen)	1:1000
P62	P6248 (Sigma)	1:1000
SDHA	ab14715 (abcam)	1:2000
SLP2	10348-1-AP (Proteintech)	1:2000
STARD7	HPA064958 (Sigma)	1:1000
TMBIM5	16296-1-AP (Proteintech)	1:1000
Tubulin	Sc-17787 (Santa Cruz)	1:2000
UQCRC2	ab14745 (abcam)	1:1000
Vinculin	13901 (Cell Signaling)	1:1000
YME1L	11510-1-AP (Proteintech)	1:1000

2.1.5   Quantitative real-time PCR primers

Table 4 lists all primers used for qPCR.

Table 4: qPCR primers

Target	ID/ sequence
TaqMan	
ACTB	Hs99999903_m1
12S RNA	Hs02596859_g1
16S RNA	Hs02596860_s1

SYBR Green	
ACTB	FWD CTGTGGCATCCACGAAACTA
	REV AGTACTTGCGCTCAGGAGGA
Dloop2	FWD CGGGAGCTCTCCATGCATTT
	REV CAGCGTCTCGCAATGCTATC
Dloop3	FWD CCCCTCCCACTCCCATACTA
	REV GGGCGGGGGTTGTATTGAT

2.2 Methods

2.2.1 Cell biology

2.2.1.1 Cell culture

HeLa cells were cultured in a 95 % humidified incubator with 5 % CO_2 at 37 °C in DMEM-GlutaMAX (4.5 g/l glucose, Gibco) supplemented with 10 % fetal bovine serum (FCS, Biochrom). Cells were tested routinely for mycoplasma infections.

2.2.1.2 Cell culture for pulse-chase SILAC

For the measurement of protein turnover in a pulse-chase SILAC experiment HeLa cells were cultured in DMEM without arginine, lysine and glutamine (Silantes) supplemented with glutamine (Gibco), 10 % dialyzed FCS (Gibco), stable heavy isotopes $^{13}C_6^{15}N_4$ arginine (Arg10) and $^{13}C_6^{15}N_2$ lysine (Lys8) for 5 doublings. The medium was then exchanged to one with light isotopes $^{12}C_6^{15}N_4$ arginine (Arg0) and $^{12}C_6^{15}N_2$ lysine (Lys0) for the indicated time points (2, 4, 8, 12 h) before collection by scraping.

2.2.1.3 Transient knockdown by siRNA and esiRNA transfection

Target genes were transiently knocked by RNA interference by small interfering RNA (siRNA) or endoribonuclease-prepared siRNA (esiRNA) oligonucleotides (Table 2). Non-targeting scrambled siRNA with medium GC content was transfected as negative control for siRNA-mediated knockdown. As control for esiRNA-mediated knockdown cells were transfected with esiRNA targeting *EGFP*. Cells were harvested by scraping 72 h after transfection.

2.2.1.4 Oxygen consumption rate (OCR) measurement by Seahorse

Measurement of cellular respiration was performed using the Mito Stress Kit and the Seahorse Extracellular Flux Analyzer XFe96 (Agilent). 30000 cells/ well of a 96-well plate HeLa cells were seeded for the assay. Cells were incubated at 37°C in a CO_2-free incubator for 1 h prior to measurement. OCR and extracellular acidification rate (ECAR) were assessed by sequential addition of oligomycin (2 µM); FCCP (0.5 µM) and rotenone and antimycin A (0.5 µM).

2.2.1.5   Electron microscopy (EM)

The mitochondrial ultrastructure of cells was analysed by EM at the CECAD imaging facility. Cells plated on Aclar film were fixed in fixation buffer (2 % glutaraldehyde, 2.5 % sucrose, 3 mM $CaCl_2$, 100 mM HEPES-KOH pH 7.2) at room temperature for 30 min and 4°C for 30 min. Samples were washed three times in 1 % osmium tetroxide, 1.25 % sucrose, and 1 % potassium ferrocyanide in 0.1 M sodium cacodylate buffer. After dehydration in alcohol gradient series and propylene oxide, the tissue samples were embedded. Ultrathin sections were cut on a Leica ultramicrotome and placed on copper grids (Science Services, 100mesh). Sections were stained with uranyl acetate (Plano, 1.5 %) and lead citrate (Sigma) and examined with an electron microscope (JEM 2100 Plus, JEOL) with a OneView 4 K camera (Gatan) with DigitalMicrograph software at 80 kV.

2.2.1.6   *In cellulo* mitochondrial translation assay

For labelling of newly synthesized mitochondrial proteins HeLa cells were starved in minimal DMEM (-Cys, -Met, Gibco) and cytosolic translation was inhibited by 100 µg/ml emetine for 1 h. 50 µCi/ 6 well of ^{35}S methionine/ cysteine was added to the cells for different 15, 30, 45, 60 min before harvesting and lysis by RIPA. For *in organello* translation see 2.2.2.6.

2.2.2   Biochemistry

2.2.2.1   Preparation of cell lysates

Cells were harvested by scraping in cold phosphate buffered saline (PBS) and centrifuged at 700 x g for 3 min, 4 °C. The pellet was resuspended in RIPA buffer (1 % (v/v) Triton X-100, 0.1 % (w/v) SDS, 0.5 % (w/v) sodium deoxycholate, 1 mM EDTA, 50 mM HEPES-KOH pH 7.6, 150 mM NaCl, 1x protease inhibitor complete (Roche))

and vigorously shaken for 20 min on a Vibrax shaker at 4°C before centrifugation at 16,100 x g for 20 min.

2.2.2.2   SDS-PAGE and immunoblotting

For sodium dodecyl sulfate polyacrylamide gel electrophoresis (SDS-PAGE) gels containing 10, 12 or 15 % acrylamide were used with the TRIS-tricine buffer system. Electrophoresis was performed in SE600X Chroma Units (Hoefer Inc.) or PerfectBlue gel system (PEQLAB) using anode buffer (0.2 M TRIS, pH 8.9) and cathode buffer (0.1 M TRIS pH 8.25, 0.1 M Tricine, 0.1 % (w/v) SDS). Cell lysates were mixed with 4x Lämmli buffer (2 % SDS, 10 % glycerol, 75 mM Tris–HCl pH 6.8, 0.02 % bromphenol blue, 5% beta-mercaptoethanol) and heated at 40 °C for 15 min before loading. After the run gels were transferred onto nitrocellulose membranes by semi-dry electroblotting for 2-3 h at 400 mA. Membranes were then blocked with 5 % milk powder (w/v) in TBS-Tween for 30 min at room temperature and incubated with the antibodies listed in Table 3 in dilutions 1:500-1:2000 in 5 % milk or 2 % BSA (w/v) in TBS-Tween overnight at 4 °C. Membranes were incubated with a specific antibody solution (1:500 – 1:10,000 in 0.5 % milk powder (w/v) in TBS-Tween) over night at 4°C. The signal was detected with the Intas Chemostar ECL and Fluorescence imager (Intas).

2.2.2.3   Blue native polyacrylamide gel electrophoresis (BN-PAGE)

BN-PAGE was performed as described previously (Wittig et al., 2006). Enriched mitochondrial fractions were lysed for 30 min at 4 °C in solubilization buffer (25 mM NaCl, 2.5 mM 6-aminohexanionic acid, 25 mM Imidazole/HCL pH 7.0, 5 % Glycerol, 25 mM KPi-buffer pH 7.4) containing digitonin at a concentration of 2 g/g protein before centrifugation at 16,100 x g for 20 min at 4 °C. Samples were loaded with 0.1 % Coomassie G250 to homemade 3-13% acrylamide gels. Proteins were separated overnight using 25 mM Imidazole anode buffer and cathode buffer (50 mM Tricine, 7.5 mM Imidazole, 0.002 % Coomassie G250). Proteins were transferred to PVDF membranes and blotted as in 2.2.2.2.

2.2.2.4   Isolation of enriched mitochondrial fractions

Cells harvested from at least one 150 mm cell culture plate were resuspended in Mito buffer (220 mM mannitol, 70 mM sucrose, 5 mM HEPES pH 7.4, 1 mM EGTA, 0.2 %

BSA, 1x complete protease inhibitor (Roche)) and left to swell on ice for 15 min. The mixture was homogenized 10 times using a 1 ml syringe and 27G needle (0,40 x 25 mm, Sterican) and centrifuged at 1,000 x g at 4 °C for 5 min. The supernatant was transferred and the pellet was homogenized 10 times again before centrifugation. The supernatants were then pooled and centrifuged at 12,000 x g for 15 min to pellet mitochondria. The protein content was measured by resuspension in Mito buffer without BSA and Bradford assay before usage or storage at -80 °C.

2.2.2.5 Co-immunoprecipitation

Enriched mitochondrial fractions were lysed with buffer containing 30 mM TRIS-HCl pH 7.4, 150 mM KAc, 1x complete protease inhibitor (Roche) and 2 g/g digitonin for 30 min at 4 °C, slowly shaking before centrifugation for 30 min at 16,100 x g at 4 °C. 20 µl of EZview™ Red ANTI-FLAG® M2 affinity gel (Sigma) per 1 mg enriched mitochondrial fraction was washed (30 mM TRIS-HCl pH 7.4, 150 mM Kac, 1x complete protease inhibitor (Roche), 0.1 % digitonin) 3 times before incubation with the lysate for 2 h at 4 °C on a rotator. After three washes the IP was eluted competitively by FLAG peptide (Sigma) for 15 min.

2.2.2.6 *In organello* mitochondrial translation assay

For labelling of newly synthesized mitochondrial proteins an enriched mitochondrial fraction was isolated as described in 2.2.2.4 in the presence of 200 µg/ml emetine and washed twice with translation buffer (Table 5). 300 µCi ^{35}S-methionine were added to 1 mg enriched mitochondrial fraction and incubated at 37 °C for 0.5 or 1 h before washing them twice in translation buffer. Pulse samples were then placed on ice while 60 µg/ml methionine in translation buffer was added to chase samples for 3 h. Afterwards all samples were lysed with 2 g/g digitonin as described in 2.2.2.3 for SDS-PAGE and BN-PAGE.

Table 5: Translation buffer for *in organello* translation

Chemical	Final concentration
2x translation buffer	
Mannitol	200 mM
Sodium succinate dibasic hexahydrate	20 mM
KCl	160 mM

MgCl$_2$ hexahydrate	10 mM
KH$_2$PO$_4$, pH 7.4	2 mM
HEPES, pH 7.4	50 mM
1x translation buffer	
2x Translation buffer, pH 7.4	1x
17-amino-acid stock	60 µg/ml
Cysteine	60 µg/ml
Tyrosine	60 µg/ml
ATP	5 mM
GTP	200 µM
Creatine phosphate	6 mM
Creatine kinase	60 µg/ml

2.2.2.7   Isolation of RNA

Total RNA was isolated from cells using NucleoSpin RNA kit (Macherey-Nagel) according to the manufacturer's protocol. RNA concentration and quality were measured by NanoDrop (VWR).

2.2.2.8   Isolation of genomic DNA

Genomic DNA was isolated from cells using DNeasy Blood and Tissue Kit (Qiagen) according to the manufacturer's protocol. DNA concentration and quality were measured by NanoDrop (VWR).

2.2.2.9   Real-time quantitative PCR (RT-qPCR)

RNA was isolated from cells as described in 2.2.2.7 and cDNA was synthesized from 2 µg by PCR using GoScript Reverse Transcription Mix (Promega) before dilution of 1:4. RT- qPCR was performed using Power SYBR Green Master Mix (ThermoFisher) or LightCycler TaqMan (Roche) according to the manufacturer's protocol in a QuantStudio 6 Flex Real-Time PCR System (Thermo Fisher). Data was quantified using the $2^{-\Delta\Delta Ct}$ method using a housekeeping gene as control. Primer sequences are listed in Table 4.

2.2.2.10 Sucrose gradient ultracentrifugation for ribosome analysis

Enriched mitochondrial fractions were isolated from cells according to 2.2.2.4 but without EGTA or BSA and lysed as stated in Table 6 for 20 min on ice with occasional vortexing before centrifugation at 10,000 x g for 45 min at 4 °C. Gradients were prepared as stated in Table 6 by the Gradient Master (Biocomp) using the settings SW41, short, 10-30 % sucrose, 1 step gradient and chilled before usage. 400 µl was removed from the top of the gradient before loading the sample. The gradients were run in a pre-chilled ultracentrifuge (Beckamn Coulter) in a SW41 rotor 15 hours at 71,000x g and 4° C (Accel: 1, Decel: 4). After the run fractionation in 750 µl steps was carried out using the Piston Gradient Fractionator (Biocomp), Triax Flow cell (Biocomp) and fraction collector. TCA precipitation followed as described in 2.2.2.11.

Table 6: Lysis buffer and gradient preparation for ribosome analysis via sucrose gradient ultracentrifugation

Chemical	Final Concentration
Lysis buffer	
Sucrose	260 mM
KCl	100 mM
$MgCl_2$	20 mM
1 M TRIS-HCl, pH 7.5	10 mM
Digitonin	2 %
Protease inhibitor	1x
rRNAsin	0.08 U/ml
Gradient	
Sucrose	10 %, 30 %
KCl	100 mM
$MgCl_2$	20 mM
TRIS-HCl, pH 7.5	10 mM
Protease inhibitor (w/o EDTA)	1x

2.2.2.11 TCA precipitation

A 750 µl sample from sucrose gradient fractionation (4.2.2.10) was mixed with 1 % sodium deoxycholate to 0.5 % final and 100 % trichloroacetic acid (TCA) to 20 % final. The mixture was vortexed and incubated for 10 min on ice before centrifugation for 30

min at 16,100 x g and 4 °C. The resulting pellet was washed twice with ice-cold acetone (15 min, 16,1000 x g, 4 °C) before drying it at room temperature for 20 min and resuspension in 1x Lämmli buffer for gel loading.

2.2.2.12   Complex I and IV in gel activity assay

Complex I and IV activities were assessed directly after BN-PAGE on the gels. For complex I activity the gel was incubated in 2 mM TRIS-HCl pH 7.4 with 0.1 mg/ml NADH and 2.5 mg/ml NBT. Complex IV activity was assessed by incubation of the gel in 0.05 M KH_2PO_4 pH 7.4 with 0.5 mg/ml DAB, 0.02 mg/ml catalase, 1 mg/ml cytochrome C and 0.075 g/ml sucrose. The gels were lightly shaken at room temperature until sufficient staining and scanned.

2.2.3   Proteomics

2.2.3.1   Interactome

Protein Digestion: Proteins were eluted from FLAG M2 (Sigma Aldrich) beads using 4% SDS in 100 mM HEPES, pH 8.5. Proteins were precipitated using ice-cold acetone and reconstituted in 6M Urea/ 2M Thio-Urea in 50 mM HEPES, pH 8.5. Proteins were reduced (TCEP) and alkylated (CAA) for 45 min at room temperature in the dark and digested overnight at room temperature using Trypsin (Sigma Aldrich) and LysC (Wako). Generated peptides were desalted using the StageTip technique.

Liquid Chromatography and Mass Spectrometry: LC-MS/MS instrumentation consisted of an Easy-LC 1200 (Thermo Fisher Scientific) coupled via a nano-electrospray ionization source to a QExactive HF-x mass spectrometer (Thermo Fisher Scientific). For peptide separation, an in-house packed column (inner diameter: 75 μm, length: 40 cm) was used. A binary buffer system (A: 0.1 % formic acid and B: 0.1 % formic acid in 80% acetonitrile) was applied as follows: Linear increase of buffer B from 4% to 32% within 33 min, followed by a linear increase to 55 % within 5 min. The buffer B content was further ramped to 95 % within 2 min. 95 % buffer B was kept for a further 5 min to wash the column. Before each sample, the column was washed using 6 μL buffer A and the sample was loaded using 7 μL buffer A.

The mass spectrometer operated in a data-dependent mode and acquired MS1 spectra at a resolution of 60000 (at 200 m/z) using a maximum injection time of 20 ms and an AGC target of 3e6. The scan range was defined from 350-1650 m/z and the data type was set to profile. MS2 spectra were acquired at a 15000 resolution (at 200

m/z) using an isolation window of 1.4 m/z and normalized collision energy of 24,26,28 (multi-inject). The Top22 peaks were targeted for MS2 spectra acquisition. The first mass was set to 110 m/z. Dynamic exclusion was enabled and set to 20s.

Data analysis: Raw files were analyzed using MaxQuant (1.6.4) (Cox and Mann, 2008) and the implemented Andromeda search engine (Cox et al., 2011). MS2 Spectra were correlated against the in-silico digested human reference proteome. Label-free quantification was enabled using default settings. The Match-between runs algorithm was enabled using default settings. LFQ quantification with default settings was used. Proteins were considered putative interactors with a log2 ratio of > 1 and FDR < 5 %.

2.2.3.2   Whole cell proteome

Protein Digestion: 40 µL of 4% SDS in 100 mM HEPES ph = 8.5 was pre-heated to 70°C and added to the cell pellet for further 10 min incubation at 70°C on a ThermoMixer (shaking: 550 rpm). The protein concentration was determined using the 660 nm Protein Assay (ThermoFisher Scientific, #22660). 50 µg of protein was subjected to tryptic digestion. Proteins were reduced (10 mM TCEP) and alkylated (20 mM CAA) in the dark for 45 min at 45 °C. Samples were subjected to SP3-based digestion (Hughes et al., 2014). Washed SP3 beads (Hughes et al., 2014) (SP3 beads (Sera-Mag(TM) Magnetic Carboxylate Modified Particles (Hydrophobic, GE44152105050250), Sera-Mag(TM) Magnetic Carboxylate Modified Particles (Hydrophilic, GE24152105050250) from Sigma Aldrich) were mixed equally, and 3 µL of bead slurry were added to each sample. Acetonitrile was added to a final concentration of 50% and washed twice using 70 % ethanol (V=200 µL) on an in-house made magnet. After an additional acetonitrile wash (V=200µL), 5 µL digestion solution (10 mM HEPES pH = 8.5 containing 0.5µg Trypsin (Sigma) and 0.5µg LysC (Wako)) was added to each sample and incubated overnight at 37°C. Peptides were desalted on a magnet using 2 x 200 µL acetonitrile. Peptides were eluted in 10 µL 5% DMSO in LC-MS water (Sigma Aldrich) in an ultrasonic bath for 10 min. Formic acid and acetonitrile were added to a final concentration of 2.5% and 2%, respectively. Samples were desalted further using SDP-RP stage tips and stored at -20°C until subjected to LC-MS/MS analysis.

Liquid Chromatography and Mass Spectrometry: LC-MS/MS instrumentation consisted out of an Easy-LC 1200 (Thermo Fisher Scientific) coupled via a nano-electrospray ionization source to a QExactive HF-x mass spectrometer (Thermo Fisher Scientific). For peptide separation, an in-house packed column (inner diameter: 75 µm,

length: 40 cm) was used. A binary buffer system (A: 0.1 % formic acid and B: 0.1 % formic acid in 80% acetonitrile) was applied as follows: Linear increase of buffer B from 4% to 27% within 69 min, followed by a linear increase to 45% within 5 min. The buffer B content was further ramped to 65 % within 5 min and then to 95 % within 6 min. 95 % buffer B was kept for a further 10 min to wash the column. Prior to each sample, the column was washed using 5 µL buffer A and the sample was loaded using 8 µL buffer A.

The RF Lens amplitude was set to 55%, the capillary temperature was 275°C and the polarity was set to positive. MS1 profile spectra were acquired using a resolution of 60,000 (at 200 m/z) at a mass range of 320-1150 m/z and an AGC target of 1×106. For MS/MS independent spectra acquisition, 48 windows were acquired at an isolation m/z range of 15 Th, and the isolation windows overlapped by 1 Th. The fixed first mass was 200 Th. The isolation center range covered a mass range of 350–1065 m/z. Fragmentation spectra were acquired at a resolution of 15,000 at 200 m/z using a maximal injection time of 22 ms and stepped normalized collision energies (NCE) of 24, 27, 30. The default charge state was set to 3. The AGC target was set to 1e6. MS2 spectra were acquired as centroid spectra.

Data analysis: Spectronaut (13.11.200127.43655) (Bruderer et al., 2015) using a HeLa peptide library obtained from offline high-pH fractionation (24 fractions, pooled from 60s fraction collections, which were measured and analyzed as described (Eiyama et al., 2021)) and the Uniprot human reference proteome (approx. reviewed 20,000 entries). Default settings were used including a precursor and protein FDR of 0.01. The MaxLFQ algorithm was enabled for label-free quantification.

2.2.3.3   Pulse-chase SILAC

Protein Digestion: The protein digestion was performed as described above for the whole proteome.

Liquid Chromatography and Mass Spectrometry: The protein digestion was performed as described above for the whole proteome.

Data analysis: Spectronaut (15.0.210615.50606) (Bruderer et al., 2015) was used in directDIA mode using the human Uniprot reference proteome for in-silico digestion. Channel two was defined as 'Arg10 and Lys8'. Two missed cleavages were allowed and the MS1 and MS2 mass tolerance strategy was set to 'automatic'. The number of maximum variable modifications was set to 5 and Acetylation at the protein N-term and methionine oxidation were defined as variable modifications. Peptide intensities for the

'light' and 'heavy' channels were used to calculate the peptide SILAC ratio. The median SILAC ratio (remaining fraction, RF) for each peptide was used to obtain a protein ratio. Only those peptides were used for the RF decreased with every time point and which contained at least 3 valid values. A linear fit of lnRF was applied to generate slope values. The slope difference of *WT* and *SLP2*^{−/−} was used to quantify the difference. Only proteins with 4 valid RF values were considered for later analysis.

2.2.4   Transcriptomics

Total RNA was extracted and checked for concentration and quality as described in 4.2.2.7. RNA sequencing was performed by the Cologne Center for Genomics. Libraries were prepared from 1 µg total RNA using TruSeq Stranded mRNA kit (Illumina). Sequencing was performed on Illumina NovaSeq6000 PE100. Data analysis was performed as follows: Raw reads were pseudo mapped to GRCh38 Release 95 using kallisto (Bray et al., 2016). The R package DESeq2 was used to calculate the differential gene expression (Love et al., 2014). Statistical significance was determined by using the Benjamini- Hochberg method. p value $p < 0.1$ was considered as significant.

2.2.5   Metabolomics

Metabolite extraction for Liquid Chromatography mass spectrometry (LC-MS)

For metabolite extraction, HeLa cells from 6-well-plates were washed twice with 1 ml ammonium carbonate (75 mM, pH 7.4) prior to two 10 min incubation steps with 400 µl extraction buffer (40:40:20 (v:v:v) acetonitrile:methanol:water containing 100 ng/ml 13C10 ATP, 250 ng/ml citric acid-2,2,4,4-d4 and 250 ng/ml L phenylalanine-13C9,15N as an internal standard (Sigma)) at -20°C. Cells were collected in the extraction buffer and centrifuged at 16,900 x g for 10 min at 4 °C. Supernatants were transferred to fresh tubes and dried using a speed vac concentrator (Eppendorf).

The cell pellets were used for protein concentration determination. Pellets were resuspended in 40 µl sample buffer (100 mM TRIS-HCl, pH 8.5; 4 % SDS) and sonicated (1 s pulse for 1 min; SonoPlus, Bandelin). Samples were incubated for 30 min at 70°C and 1000 rpm and protein concentration was determined via BCA protein assay kit (Thermo Fisher Scientific) according to the manufacturer's instructions. LC-MS or AEX-MS was performed by the Metabolomics Core Facility at MPI for Biology of Ageing.

2.2.5.1 Semi-targeted liquid chromatography-high-resolution mass spectrometry-based (LC-HRS-MS) analysis of amine-containing metabolites

The LC-HRMS analysis of amine-containing compounds was performed using an adapted benzoylchlorid-based derivatisation method (Wong et al., 2016). In brief: The polar fraction of the metabolite extract was re-suspended in 200 µL of LC-MS-grade water (Optima-Grade, Thermo Fisher Scientific) and incubated at 4 °C for 15 min on a thermomixer. The re-suspended extract was centrifuged for 5 min at 16.000 x g at 4°C and 50 µl of the cleared supernatant were mixed in an auto-sampler vial with a 200 µl glass insert (Chromatography Accessories Trott). The aqueous extract was mixed with 25 µl of 100 mM sodium carbonate (Sigma), followed by the addition of 25 µl 2 % (v/v) benzoylchloride (Sigma) in acetonitrile (Optima-Grade, Thermo Fisher). Samples were vortexed and kept at 20 °C until analysis.

For the LC-HRMS analysis, 1 µl of the derivatized sample was injected onto a 100 x 2.1 mm HSS T3 UPLC column (Waters). The flow rate was set to 150 µl/min using a binary buffer system consisting of buffer A (10 mM ammonium formate (Sigma), 0.15 % (v/v) formic acid (Sigma) in LC-MS-grade water (Optima-Grade, Thermo Fisher). Buffer B consisted solely of acetonitrile (Optima-grade, Thermo Fisher). The column temperature was set to 40°C, while the LC gradient was: 0 % B at 0 min, 0-15 % B 0-0.1min; 15-17 % B 0.1 – 0.5 min; 17-55 % B 5.5-14 min; 55-70 % B 14 – 14.5 min, 70-100 % B 14.5 - 18 min; B 100 % 18 - 19 min; 100-0 % B 19 -19.1 min; 0 % B 19.1-28 min; 0 % B. The mass spectrometer (Q-Exactive HF, Thermo Fisher) was operating in positive ionization mode recording the mass range m/z 100-1000. The heated ESI source settings of the mass spectrometer were: Spray voltage 3.5 kV, capillary temperature 300°C, sheath gas flow 60 AU, aux gas flow 20 AU at a temperature of 340°C and the sweep gas to 2 AU. The S-lens was set to a value of 60 arbitrary units. Semi-targeted data analysis for the samples was performed using the TraceFinder software (Version 4.1, Thermo Fisher). The identity of each compound was validated by authentic reference compounds, which were run before and after every sequence. Peak areas of [M + nBz + H]+ ions were extracted using a mass accuracy (<5 ppm) and a retention time tolerance of <0.05 min. Areas of the cellular pool sizes were normalized to the internal standards (U-15N;U-13C amino acid mix (MSK-A2-1.2), Cambridge Isotope Laboratories), which were added to the extraction buffer, followed by a normalization to the protein content of the analyzed sample.

2.2.5.2   Anion-Exchange Chromatography Mass Spectrometry (AEX-MS) for the analysis of anionic metabolites

Extracted metabolites were re-suspended in 200 µl of Optima LC/MS grade water (Thermo Fisher Scientific), of which 100 µl were transferred to polypropylene autosampler vials (Chromatography Accessories Trott, Germany) before AEX-MS analysis.

The samples were analysed using a Dionex ionchromatography system (ICS500+, Thermo Fisher Scientific) as described previously (Schwaiger et al., 2017). In brief, 5 µL of polar metabolite extract were injected in push partial mode, using an overfill factor of 2, onto a Dionex IonPac AS11-HC column (2 mm × 250 mm, 4 µm particle size, Thermo Fisher Scientific) equipped with a Dionex IonPac AG11-HC guard column (2 mm × 50 mm, 4 µm, Thermo Fisher). The column temperature was held at 30 °C, while the auto sampler was set to 6 °C. A potassium hydroxide gradient was generated using a potassium hydroxide cartridge (Eluent Generator, Thermo Fisher), which was supplied with deionized water. The metabolite separation was carried at a flow rate of 380 µL/min, applying the following gradient conditions: 0-3 min, 10 mM KOH; 3-12 min, 10−50 mM KOH; 12-19 min, 50-100 mM KOH; 19-21 min, 100 mM KOH, 21-22 min, 100-10 mM KOH. The column was re-equilibrated at 10 mM for 8 min.

For the analysis of metabolic pool sizes the eluting compounds were detected in negative ion mode [M-H]- using multiple reaction monitoring (MRM) mode with the following settings: Capillary voltage 2.7 kV, desolvation temperature 550 °C, desolvation gas flow 800 l/h, collision cell gas flow 0.15 ml/min.

The MS data analysis was performed using the TargetLynx Software (Version 4.1, Waters). For data analysis the area of the quantitative transition of each compound was extracted and integrated using a retention time (RT) tolerance of <0.1 min as compared to the independently measured reference compounds. Areas of the cellular pool sizes were normalized to the internal standards (citric acid D4), which were added to the extraction buffer, followed by a normalization to the protein content of the analyzed sample.

3 Results

3.1 SLP2 is a mitochondrial interaction platform

To define the role of SLP2 as membrane scaffold, we used HeLa *SLP2-/-* cells stably overexpressing SLP2[FLAG] for co-immunoprecipitation experiments. Anti-FLAG agarose beads were used to isolate SLP2[FLAG] and its interaction partners in an enriched mitochondrial fraction. Eluted proteins were measured by mass spectrometry in four replicates. This allowed the identification of 194 putative interactors of SLP2 with a log2 ratio of ≥ 1 and a false discovery rate (FDR) < 5 %. 77 % of these proteins were MitoCarta3.0 associated. 149 of these interactors were localized to the mitochondrial IM (Fig. 6 a). Co-purification led to identification of known SLP2 interactors such as PARL and YME1L as well PHB, PHB2 (Richter-Dennerlein et al., 2014) and TMBIM5, a mitochondrial Ca^{2+}/H^+ exchanger (Patron et al., 2022)(Fig. 6 b). 1D enrichment analysis was performed to classify the interactors and revealed large mean values for GO terms related to protein import into the inner membrane, the MICOS complex, calcium transport and the respiratory chain (Fig. 6 c). Import and MICOS proteins were consistently enriched with a higher log2 ratio (Fig. 7 a) and often all known subunits of a multimeric protein complex were identified, e.g. TIM23, TIM22 and MICOS complexes. Similarly, numerous subunits of OXPHOS proteins were identified (Fig. 7 b). We further found that SLP2 interacted with the proteases AFG3L2 and SPG7, the mitochondrial calcium uniporter (MCU) and 12 solute carrier family 25 proteins. Some of the identified interactors of this study were also identified by recent proximity based methods of other groups and are examined for overlaps and differences in the discussion (Antonicka et al., 2020; Li et al., 2021).

In summary, we identified known and novel interactors of SLP2 which include mitochondrial import and structural proteins as well as OXPHOS components and metabolic carriers. We especially found SLP2 enriched with all subunits of the MICOS complex.
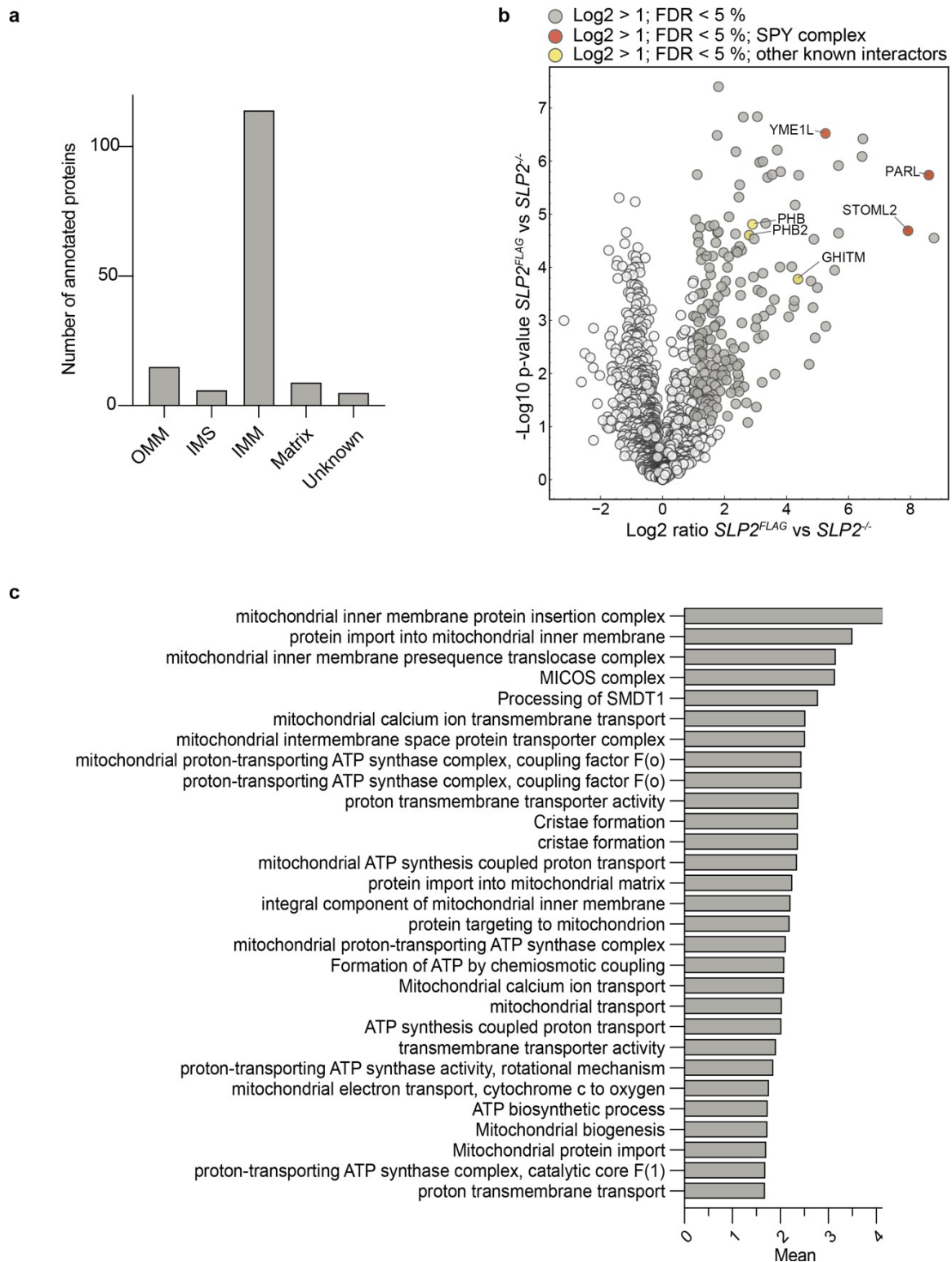
Figure 6: SLP2 forms an interaction platform at the inner mitochondrial membrane

Co-immunoprecipitation of FLAG in an enriched mitochondrial fraction of HeLa *SLP2^{-/-}* vs. *SLP2^{-/-} + SLP2^{FLAG}*, n=4. **(a)** Number of annotated MitoCarta proteins per MitoLocalization as annotated in MitoCarta 3.0. **(b)** Volcano plot of Log2 ratios and -log10 p values of identified proteins; known interactors of SLP2 via IP methods labeled; significant interactors with log2 ratio > 1; FDR < 5 %. **(c)** 1D enrichment analysis of significant interactors for GO terms.

a

b

TIM23 complex			
TIMM23	TIMM17B	TIMM50	TIMM21
TIMM17A			
TIM22 complex			
TIMM29	AGK	TIMM22	
TIM9-TIM10 complex			
TIMM9	TIMM10	TIMM10B	
TIM8-TIM13 complex			
TIMM8B	TIMM8A		
TOM complex			
TOMM40	TOMM22	TOMM5	TOMM6
TOMM7	TOMM70		
SAM complex			
MTX1	MTX2	MTX3	SAMM50
DNAJC11			
PAM			
PAM16	DNAJC19	DNAJC15	
MIA			
CHCHD4	GFER		
MICOS			
APOOL	APOO	QIL1	IMMT
CHCHD6	CHCHD3	MINOS1	

Complex I			
NDUFB5	NDUFB9	NDUFB10	NDUFB4
NDUFC2	NDUFA3	NDUFB8	NDUFA2
NDUFS2	NDUFB11	NDUFS3	NDUFB6
NDUFB3	MT-ND4	NDUFS1	NDUFV1
NDUFA13	NDUFA5		
Complex II			
SDHB	SDHA		
Complex III			
CYC1	UQCRQ	UQCRB	UQCR1
UQCRH	UQCR10		
Complex IV			
COX5A	COX7A2	COX4I1	COX5B
MT-CO2			
Complex V			
ATP5I	ATP5L	ATP5J2	ATP5J
ATP5E	ATP5H	ATP5F1	ATP5A1
ATP5D	ATP5O	ATP5C1	
OXPHOS Assembly and biogenesis			
COX20	COX15	HCCS	COX18
SAMM50	TIMMDC1	COX11	SURF1
NDUFAF3	OXA1L		

Figure 7: SLP2 interacts with import, MICOS and respiratory chain proteins

Co-immunoprecipitation of FLAG in an enriched mitochondrial fraction of HeLa *SLP2^−/−* vs. *SLP2^−/−* + *SLP2^FLAG*, n=4. **(a)** Volcano plot of Log2 ratios and -log10 p values of identified proteins; MICOS, import and OXPHOS proteins labeled; significant interactors with log2 ratio > 1; FDR < 5 %. **(b)** List of significant MICOS, import (upper table) or OXPHOS (lower table) interactors sorted by complex; labeled yellow when all subunits of a complex were identified.

3.2   SLP2 is not required for normal cristae structure

Interactome data for SLP2 generated by co-immunoprecipitation of SLP2^FLAG surprisingly revealed putative interactions of SLP2 with all subunits of the MICOS complex. The MICOS complex is heavily involved in mitochondrial ultrastructure and specifically in cristae maintenance. Cells deficient of functional MICOS complexes display aberrant mitochondrial ultrastructure (Mukherjee et al., 2021; Rampelt et al., 2017; Stephan et al., 2020a). Together with the described role of SLP2 in mitochondrial morphology via SiMH (Tondera et al., 2009) and this novel link to the MICOS complex we sought to investigate the ultrastructure of *SLP2^−/−* mitochondria by EM.

EM images of HeLa *WT* and *SLP2⁻ᐟ⁻* cells were analyzed to assess the size, shape and number of cristae per mitochondrion. Mitochondria of cells lacking SLP2 were significantly smaller and rounder than those of *WT* cells. However, the number of cristae per mitochondrial area was not altered and there was no apparent cristae junction defect (Fig. 8). In summary SLP2 is required for the maintenance of regular and elongated mitochondria but not for the cristae number or junctions under steady-state conditions. This suggests that the interaction of SLP2 and the MICOS complex is not required for the function of MICOS in cristae maintenance.
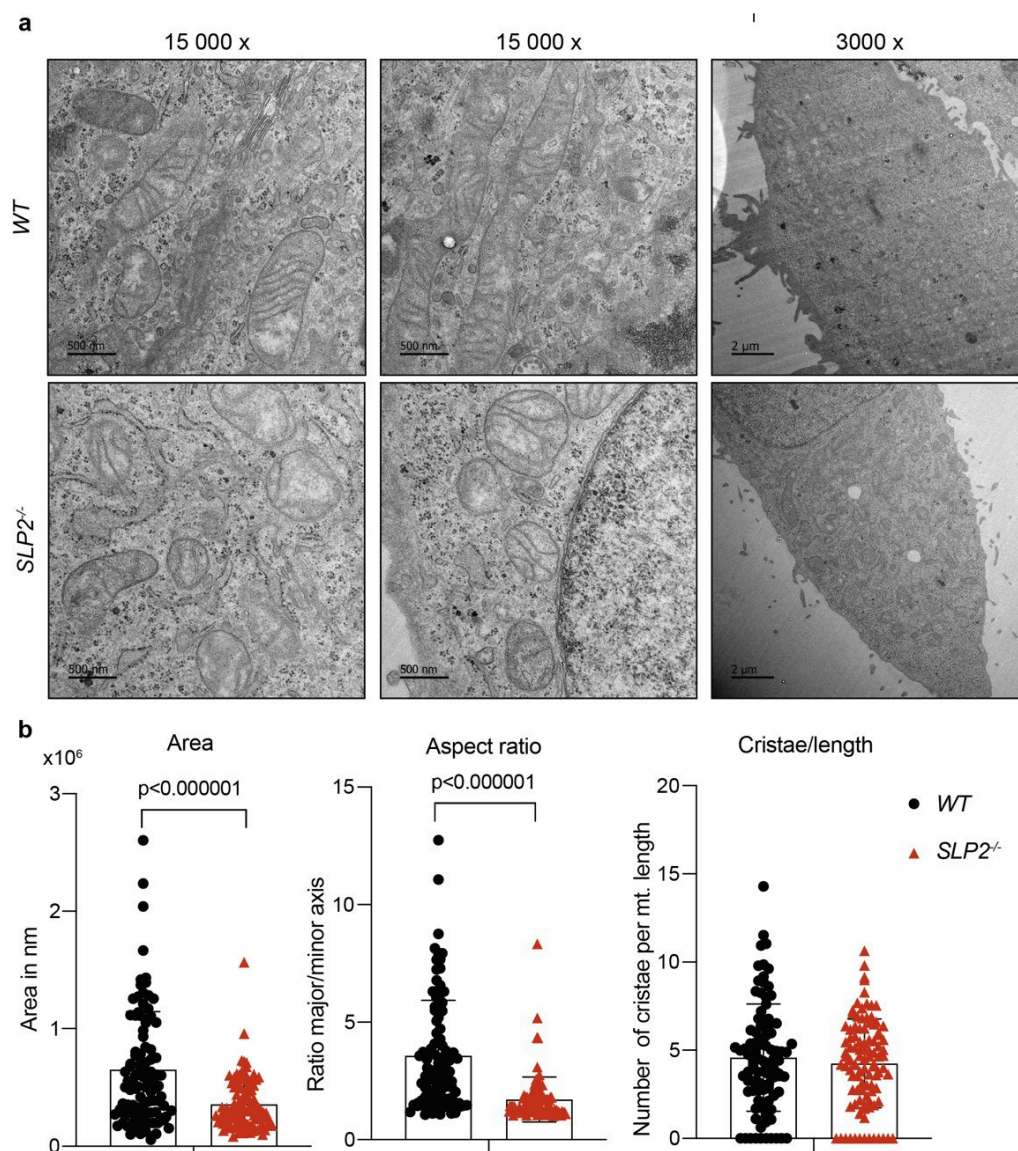
Figure 8: SLP2 does not cause cristae defects
(a) Representative EM images of mitochondria in HeLa *WT* and *SLP2⁻ᐟ⁻*. **(b)** Quantification of mitochondrial area (left), aspect ratio (middle) and cristae/length (right), mitochondria n=100.

3.3 SLP2 deficient cells display respiratory chain defects

The interactome data suggested that SLP2 is connected to mitochondrial processes such as mitochondrial import, cristae organization, OXPHOS and metabolism. To assess these putative roles of SLP2 and characterize *SLP2-/-* cells in an unbiased manner, we performed whole cell proteome analysis of HeLa *WT* and *SLP2-/-* cells. The n=5 experiment identified 6416 proteins in total and 798 of 1136 MitoCarta proteins which equals a 70 % coverage of the mitochondrial proteome. 729 proteins in total and 96 mitochondrial proteins were significantly altered (FDR < 10 %) upon loss of SLP2. The number of significantly downregulated mitochondrial proteins was twice as high as of those upregulated. (Table 7, Fig. 9 a). The 25 % most downregulated MitoCarta proteins included the OXPHOS proteins cytochrome c oxidase subunit 7C (COX7C), complex I assembly factor (TMEM126B), MT-CO3 and ubiquinone biosynthesis monooxygenase (COQ6) as well as the structural and import proteins OPA1, APOO, DNAJC15 and TIMM17B and metabolic proteins and carriers TMBIM5, mitochondrial carrier homolog 1 (MTCH1), pyrroline-5-carboxylate reductase 2 (PYCR2), iron-sulfur cluster assembly 2 homolog (ISCA2), mitochondrial basic amino acids transporter (SLC25A29) and nucleoside diphosphate kinase (NME4). The most upregulated MitoCarta proteins included the metabolic proteins and carriers phosphatidylserine decarboxylase proenzyme (PISD), cytosolic acyl coenzyme A thioester hydrolase (ACOT7), mitochondrial pyruvate carrier 1 (MPC1), lysophospholipase-like protein 1 (LYPLAL1) and zinc transporter 9 (SLC30A9), thioredoxin reductase 1 (TXNRD1) as well as PARL and the complex III assembly factor OCIA domain-containing protein 2 (OCIAD2) (Chojnacka et al., 2022) (Fig. 9 b). The mitochondrial localization of LYPLAL1 and TXNRD1 is however not fully established.

To identify functional clusters of downregulated proteins in *SLP2-/-* cells, we performed String analysis and manual clustering according to protein function. OXPHOS proteins, mostly complex IV (CIV), made up the largest identified cluster which partly overlapped with several proteins involved in TCA cycle metabolism. The second largest cluster contained proteins involved in mitochondrial transcription and translation. Other functional clusters harbored proteins with roles in protein import and structure, mitochondrial carriers, heme and Fe-S cluster synthesis, amino acid metabolism and NAD$^+$ metabolism (Fig. 9 c). Categorical enrichment analysis further strengthened the

finding of CIV being downregulated upon loss of SLP2 as it yielded only the MitoPathway terms for complex IV and its subunits as significant (Fig. 9 d).

Table 7: Number of proteins identified by whole cell proteomics in *WT* and *SLP2⁻ᐟ⁻*

Whole cell proteomics of HeLa *WT* and *SLP2⁻ᐟ⁻* cells, n=5, FDR < 10 %.

	Total	MitoCarta
Down	431	67
Up	298	29

Since many respiratory chain proteins were negatively affected upon loss of SLP2 we further investigated putative effects on OXPHOS assembly and mitochondrial respiration. BN-PAGE of enriched mitochondrial fractions isolated from HeLa *WT* and *SLP2⁻ᐟ⁻* was performed to assess quantity and status of the respiratory chain complexes. For BN-PAGE proteins were extracted by mild lysis conditions using 2 g/g digitonin to preserve respiratory chain supercomplexes. The relative protein amounts of complexes I, II and IV in single complexes and supercomplexes were indeed decreased and thus in line with the proteomic results (Fig. 10 a, b). This also negatively affected complex I and IV activity as measured by in gel activity assay (Fig. 10 c).

To further asses the OXPHOS function we assessed respiration by measurement of the mitochondrial oxygen consumption rate (OCR). The measurement of the oxygen consumption rate of cells in this assay makes use of different inhibitors of the respiratory chain. Oligomycin, a complex V inhibitor, reveals the part of respiration used for ATP synthesis. Addition of FCCP uncouples the oxidative phosphorylation and induces maximal respiration. Lastly rotenone, a complex I inhibitor, and antimycin A, an inhibitor of complex III, completely stop mitochondrial respiration. Seahorse measurements in high glucose media revealed no OCR difference in *SLP2⁻ᐟ⁻* from *WT* cells and a mild decrease in extracellular acidification rate (ECAR) upon loss of SLP2 (Fig. 10 d, e).

In conclusion these findings indicate that SLP2 is required for normal protein and assembled protein levels of respiratory chain complexes I, II and IV but is not needed for total mitochondrial respiration in high glucose conditions of HeLa cells.
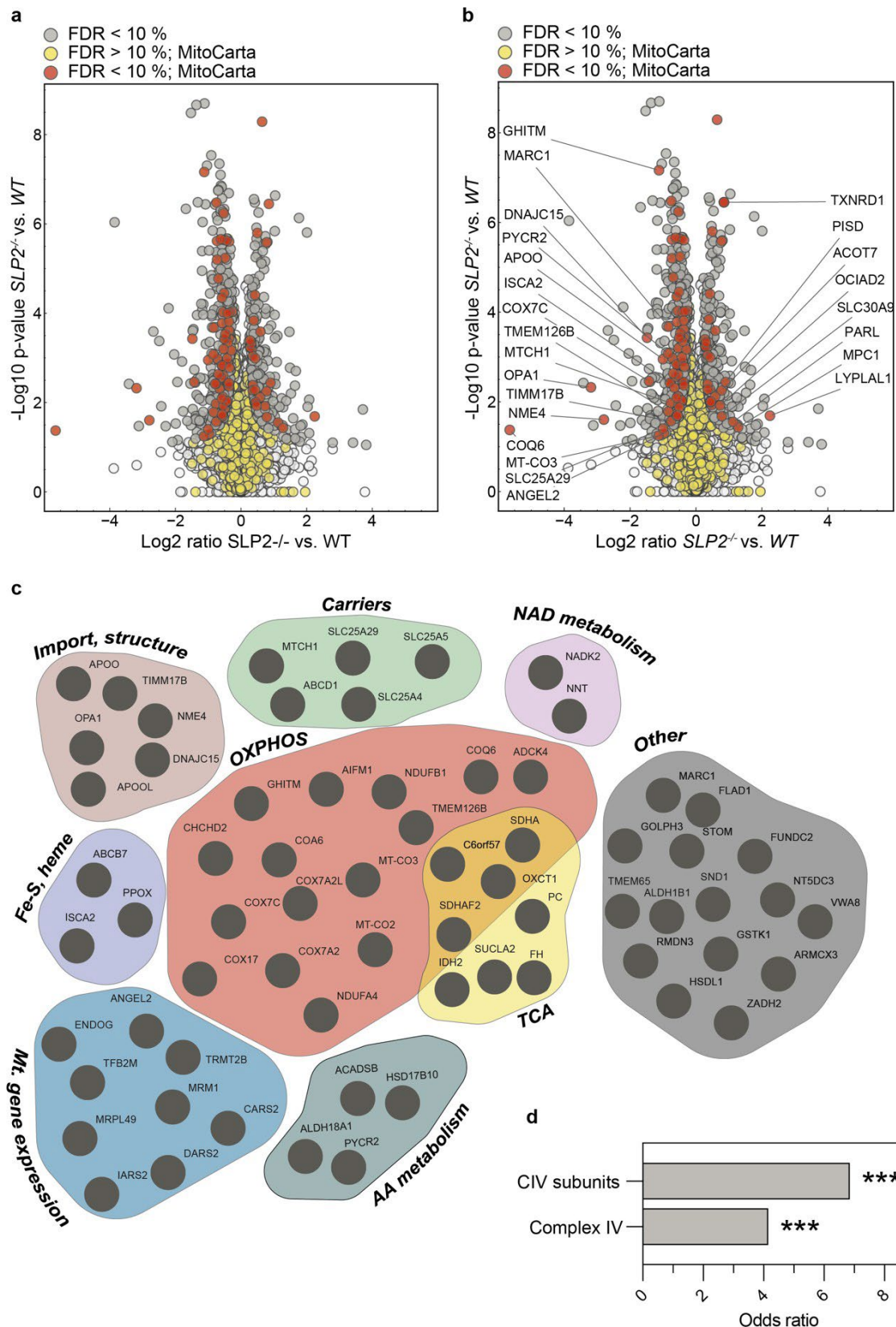
Figure 9: Loss of SLP2 affects respiratory chain proteins among others

Whole cell proteomics of HeLa *WT* and *SLP2^-/-* cells, n=5. **(a)** Volcano plot of Log2 ratios and -log10 p values of identified proteins; MitoCarta proteins highlighted; FDR < 10 %. **(b)** Volcano plot of Log2 ratios and -log10 p values of identified proteins; top 25 % of down- and upregulated MitoCarta proteins labeled; FDR < 10 %. **(c)** String and manual cluster anaylsis of downregulated

MitoCarta proteins; FDR < 10 %; OXPHOS (red), mitochondrial gene expression (blue), TCA cycle (yellow), import and structure (brown), carriers (green), amino acid metabolism (turquoise), Fe-S and heme metabolism (lilac), NAD metabolism (pink). **(d)** Categorical enrichment of significantly downregulated MitoCarta proteins.

45
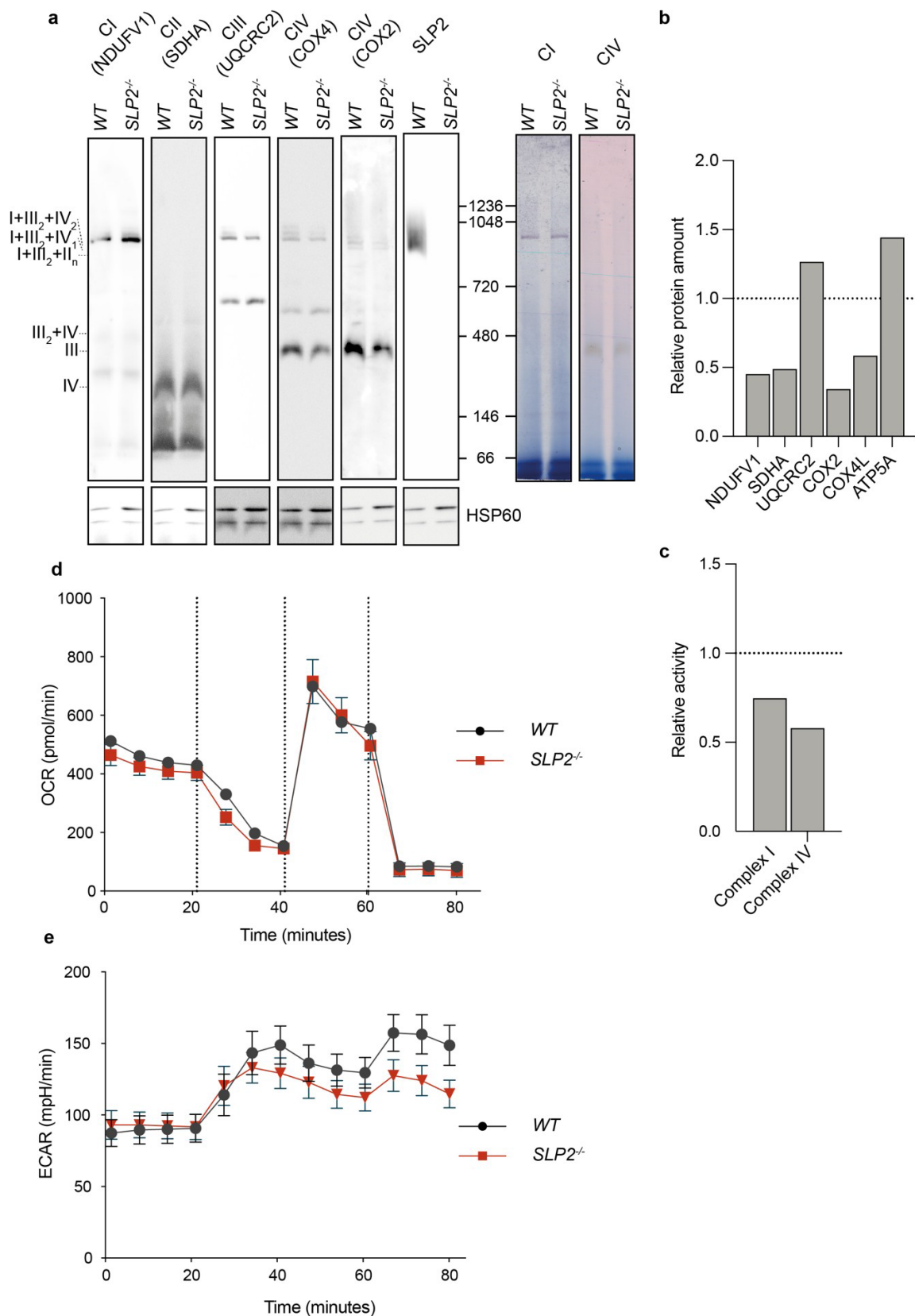
Figure 10: SLP2 supports respiratory chain levels but is not essential for respiration

Enriched mitochondrial fraction of HeLa *WT* and *SLP2$^{-/-}$* subjected to BN PAGE, n=2. **(a)** BN PAGE of respiratory chain complexes and complex I and IV activity assay, n=2. **(b)** Quantification of OXPHOS complexes as seen in (a), normalized to HSP60. **(c)** Quantification complex I and IV activity as seen in (a), n=2. **(d)** OCR and **(e)** ECAR measurement via Seahorse of HeLa *WT* and *SLP2$^{-/-}$* (n=7).

3.4 SLP2 is required to maintain TCA cycle metabolism

In our proteomic analysis of *SLP2$^{-/-}$* cells we found one of the clusters of downregulated proteins to be involved in TCA cycle metabolism. We thus asked whether the decrease of these metabolic enzymes also resulted the levels of TCA cycle intermediates. We analyzed the steady state levels of TCA metabolites and amino acids which are directly linked to TCA metabolism by targeted metabolomics in HeLa *WT* and *SLP2$^{-/-}$* cells. Loss of SLP2 significantly reduced the protein levels of the TCA enzymes isocitrate dehydrogenase (IDH2), succinate--CoA ligase [ADP-forming] subunit beta (SUCLA2), succinate dehydrogenase [ubiquinone] flavoprotein subunit (SDHA), fumarate hydratase (FH) and pyruvate carboxylase (PC) (Fig. 9 a, 11 a). IDH2 is involved in the conversion of isocitrate to α-ketoglutarate, SUCLA2 facilitates the reaction of succinyl CoA to succinate, SDHA allows the oxidation of succinate to fumarate and FH finally catalyzes the hydration of fumarate to malate. PC can carboxylate oxaloacetate from pyruvate that can be fed into the TCA. According to the proteomic findings, measurement of TCA metabolites revealed a significant (p value < 0.05) decrease of citrate, isocitrate, fumarate, malate and PEP while α-ketoglutarate was significantly increased (Fig. 11 a, b).

Most amino acids were overall increased in absence of SLP2 with alanine, asparagine, glycine, histidine, isoleucine, leucine, methionine, phenylalanine, proline, serine, threonine, tryptophane and valine reaching significance (Fig. 11 c). To exclude a role of autophagy in this accumulation of amino acids, we assessed the autophagic flux in HeLa *WT*, *SLP2$^{-/-}$* and *SLP2$^{-/-}$* + *SLP2^{FLAG}* cells. Cells were treated with Bafilomycin A1, an inhibitor of lysosomal degradation, and blotted for the lysosomal marker proteins LC3 and p62. All genotypes displayed similar levels of p62 and LC3-I and -II in untreated conditions and a similar increase of both proteins upon Bafilomycin A1 treatment (Fig. 11 d) indicating that autophagic flux was not altered in *SLP2$^{-/-}$*.

In summary, we found a downregulation of TCA cycle metabolism enzymes and consequently decreased TCA metabolites upon loss of SLP2. We further observed an accumulation of amino acids independently of autophagy in *SLP2⁻ᐟ⁻*.
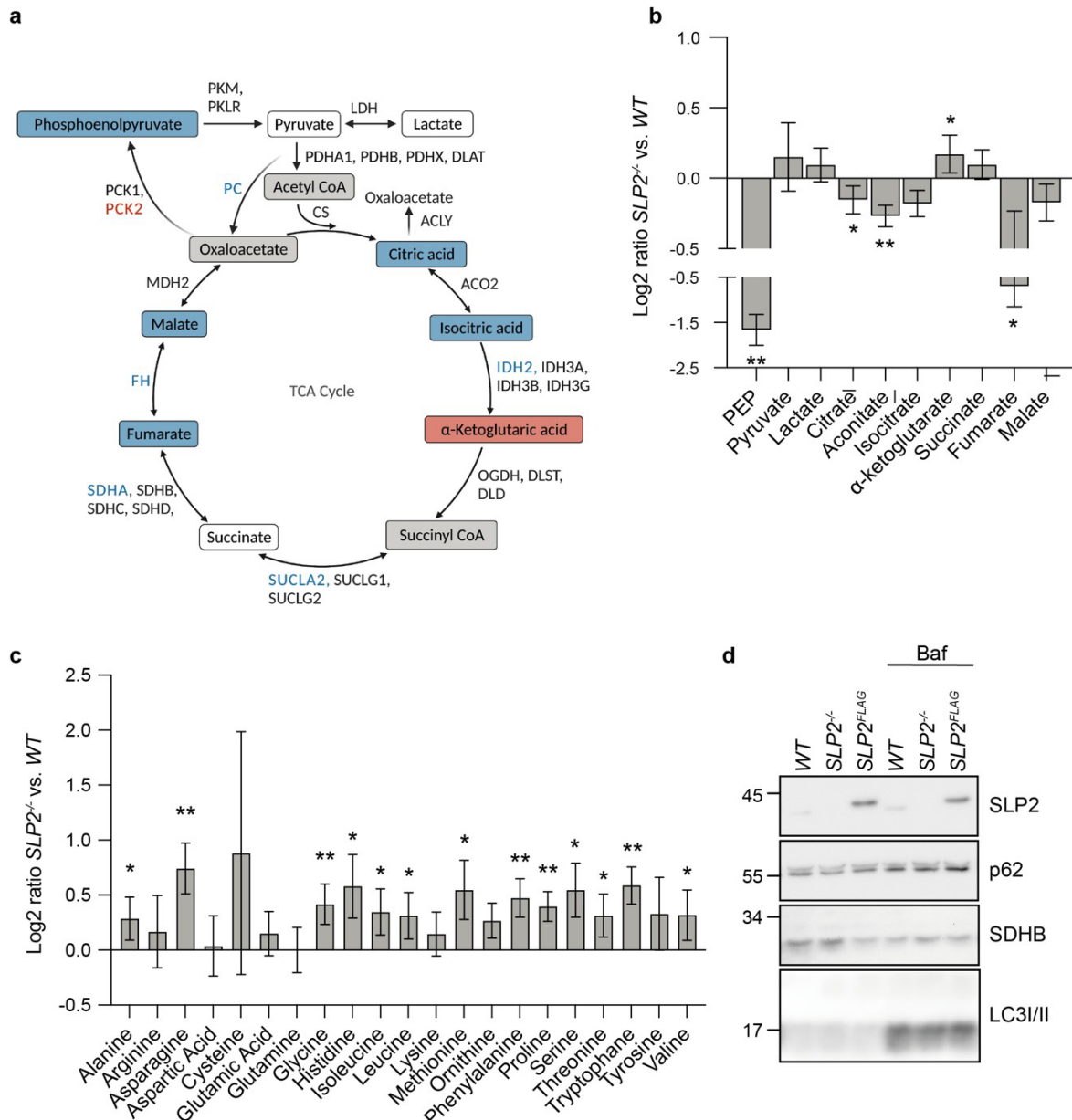
Figure 11: Loss of SLP2 induces TCA cycle defects

(a) TCA cycle schematic indicating results from proteomics for TCA enzymes and metabolites from whole cell metabolomics (n=5); decreased (blue), increased (red), not identified (grey), unchanged (white); proteins FDR < 10 %; metabolites p value < 5 %. **(b)** Log2 ratios of identified TCA cycle metabolites by whole cell metabolomics; n=5. **(c)** Log2 ratios for amino acids from whole cell metabolomics of HeLa *WT* and *SLP2-/-* (n=5). **(d)** Representative WB image of HeLa *WT* , *SLP2⁻ᐟ⁻* and *SLP2⁻ᐟ⁻ + SLP2^{FLAG}* treated with 50 nM Bafilomycin A1 for 2 h; n=3.
p value <0.05 (*), <0.01 (**), <0.001 (***).

3.5   Loss of SLP2 affects proteins post-transcriptionally

Whole cell proteomic analysis of HeLa *WT* and *SLP2⁻/⁻* cells revealed different clusters of downregulated proteins, among them respiratory chain proteins and TCA cycle enzymes which led to defects in OXPHOS assembly and TCA metabolism. We performed RNA sequencing for isolated mRNAs from HeLa *WT* and *SLP2⁻/⁻* in n=3 was applied to further understand if the proteomic changes upon loss of SLP2 were due to transcriptional or post-transcriptional effects. Changes on protein but not on mRNA level could argue for effects on protein stability as described for SLP2 previously (Da Cruz et al., 2008a) or for the involvement of mitochondrial proteases that could be associated with SLP2.

Table 8: Number of MitoCarta proteins and mRNAs identified by whole cell proteomics and RNA sequencing in *WT* and *SLP2⁻/⁻*

HeLa *WT* and *SLP2⁻/⁻* whole cell proteomics, n=5, FDR < 10 %; whole cell RNA sequencing, n=3, adjusted p value > 0.1 (independent) or < 0.1 with opposite log2 ratio to proteomics (opposite).

	Proteomics	Transcriptomics	Independent of mRNA	Opposite to mRNA
Down	67	143	33	2
Up	29	83	23	4

The log2 ratios and significance indicators (FDR, adjusted p value) of both mitochondrial proteins and mRNAs were compared to filter for proteins that were significantly changed on protein but not mRNA level or even altered oppositely to their transcripts. This filtering identified 56 proteins out of 96 significantly altered MitoCarta proteins whose steady state levels changed independently of transcriptional effects. 33 of them displayed decreased protein amounts and 6 proteins even changed in a opposite manner compared to their transcript levels (Table 8). Among them were the interactors DNAJC15, TMBIM5 and APOO which were all decreased in *SLP2⁻/⁻*. Other decreased proteins included respiratory chain proteins of the complexes I, II and IV: TMEM126B and NADH dehydrogenase [ubiquinone] 1 beta subcomplex subunit 1 (NDUFB1), succinate dehydrogenase assembly factor 2 (SDHAF2) and 4 (SDHAF4), cytochrome c oxidase subunit 7A2 (COX7A2), cytochrome c oxidase subunit 7A-related protein (COX7A2L) and cytochrome c oxidase subunit NDUFA4 as well as COQ6 (Fig. 12 b). The complex IV subunit COX7C was decreased despite increased

mRNA levels while superoxide dismutase [Cu-Zn] (SOD1) and superoxide dismutase [Mn] (SOD2) were increased on protein level but decreased on mRNA level.

To examine if the decrease of DNAJC15, TMBIM5 and APOO was due to protein instability HeLa *WT* and *SLP2$^{-/-}$* cells were subjected to a CHX chase for 0, 1, 3, 6 and 9 h to block cytosolic translation and thus observe the degradation of proteins across time (Fig 12 c). TMBIM5, DNAJC15 and APOO were less stable and faster degraded in *SLP2$^{-/-}$* compared to *WT* as quantified by protein amount relative to vinculin indicating role of SLP2 in their post-translational regulation. APOOL, the direct binding partner of APOO which was reduced on protein and mRNA level, stably expressed in these conditions (Fig. 12 c - f).

In conclusion we identified a post-transcriptional regulation of a set of mitochondrial proteins via SLP2 by comparing proteomic and transcriptomic data of *WT* and *SLP2$^{-/-}$* cells. Many of these mRNA independently altered proteins were downregulated upon loss of SLP2. We tested a subset of these proteins and could establish destabilization and increased degradation as the cause of their decreased steady-state levels.
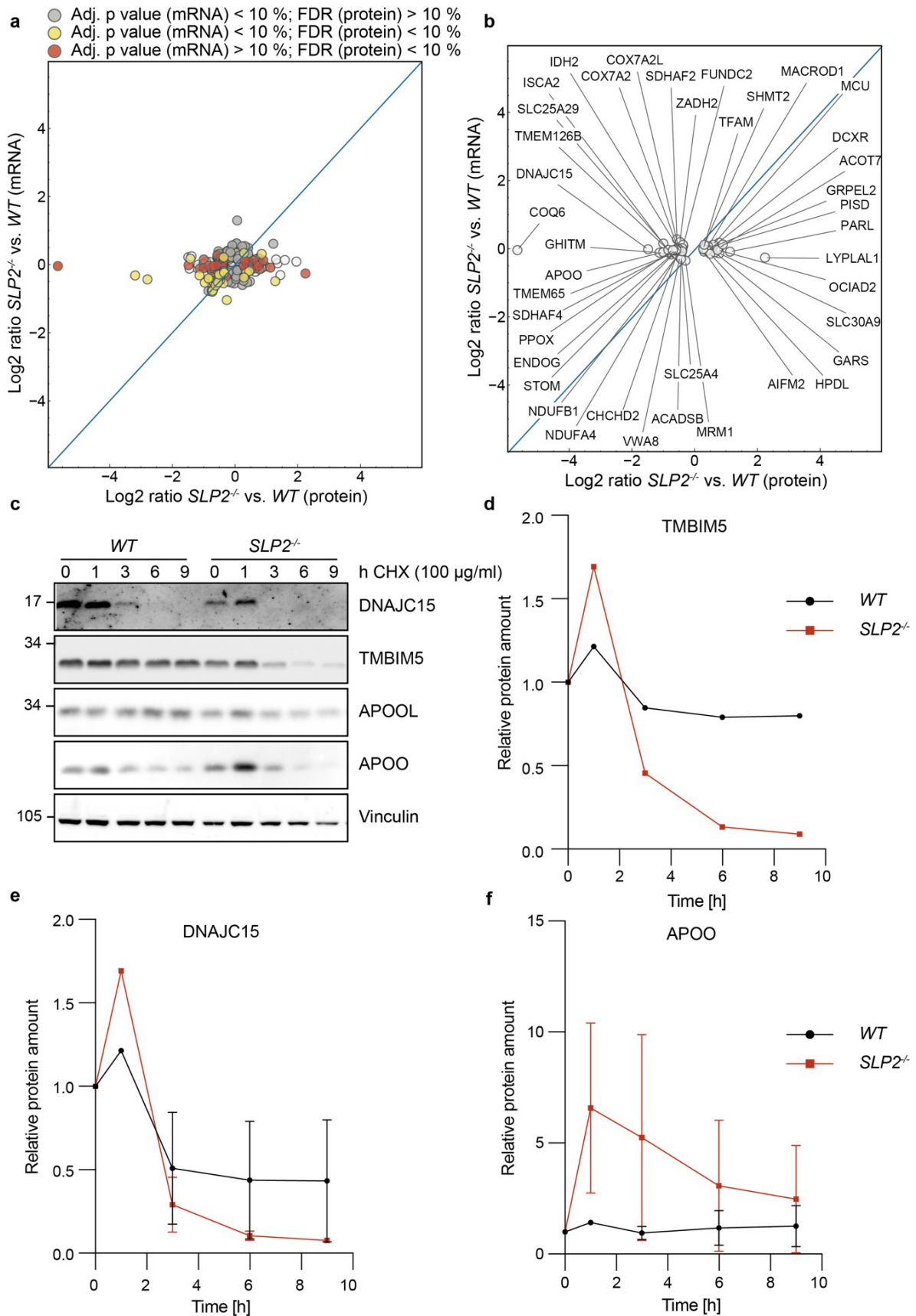
Figure 12: Loss of SLP2 affects proteins post-transcriptionally and alters the turnover of a set of proteins

Whole cell proteomics (n=5) and RNA seq (n=3) of HeLa *WT* and *SLP2⁻/⁻* cells. **(a)** Volcano plot of Log2 ratios of identified MitoCarta proteins and mRNAs; adj. p value (mRNA) and FDR (protein) <

10 % highlighted. **(b)** Volcano plot of Log2 ratios of altered MitoCarta proteins independent of mRNA levels; filtered for adj. p value (mRNA) > 10 % and FDR (protein) < 10 %. **(c)** Representative WB of a CHX chase of HeLa *WT* and *SLP2^-/-* cells with 100 µg/ml CHX for 0, 1, 3, 6, 9 h. **(d)** Quantification of (c), normalized to vinculin and 0 h, n=2.

3.6 SLP2 regulates the turnover of a set of substrates of the *m*-AAA but not the *i*-AAA protease

A combination of proteomics and transcriptomics of *WT* and *SLP2^-/-* cells revealed a post-transcriptional regulation of a set of mitochondrial proteins by SLP2 making them unstable. A post-transcriptional protein level decrease and destabilization could be caused by increased degradation by mitochondrial proteases as introduced in 3.4. Our interactome study of SLP2^FLAG identified an interaction of SLP2 with not only PARL and YME1L of the SPY complex but also with AFG3L2 and SPG7 which make up the *m*-AAA protease. We thus assessed the possible role of these proteases in our newly identified downregulated proteins upon SLP2 loss using transient knockdown experiments.

We compared known YME1L substrates (MacVicar et al., 2019) with the proteomic data of SLP2 and identified OPA1, nucleoside diphosphate kinase (NME4), argininosuccinate synthase (ASS1) and COX2 as putatively SLP2 regulated substrates (Fig. 13 a). The substrates of YME1L, OPA1 and NME4, were altered at mRNA and protein levels, but the decrease in protein levels was significantly greater than the decrease in transcription levels, suggesting that post-transcriptional regulation was likely. The YME1L substrates, complex I assembly factor TMEM126B and cytochrome c oxidase copper chaperone (COX17,) were post-transcriptionally altered but not tested here due to antibody unavailability and low quality results respectively. We hypothesized that substrates that are decreased in *SLP2^-/-* would be rescued to wildtype levels upon *YME1L* knockdown if their turnover was mediated by YME1L and regulated by SLP2. Transient *YME1L* knockdown experiments by siRNA in HeLa *WT* or *SLP2^-/-* followed by WB analysis could however not fully rescue the decrease of COX2 and ASS1 despite proficient knockdown efficiency (Fig. 13 b - f). A protein reduction in *SLP2^-/-* could not be detected for OPA1 which displayed the altered cleavage pattern of OMA1 activation as described upon SLP2 loss (Wai et al., 2016) as well as for the other known YME1L substrates PRELID1 and STARD7 (Fig. 13 g – i). The decrease of NME4 as detected by proteomics was not reproducibly

recapitulated in WB analysis but knockdown of *YME1L* led to its increase. This suggests that the decrease of these YME1L substrates in *SLP2⁻/⁻* was not solely due to an increased turnover by YME1L under these conditions.
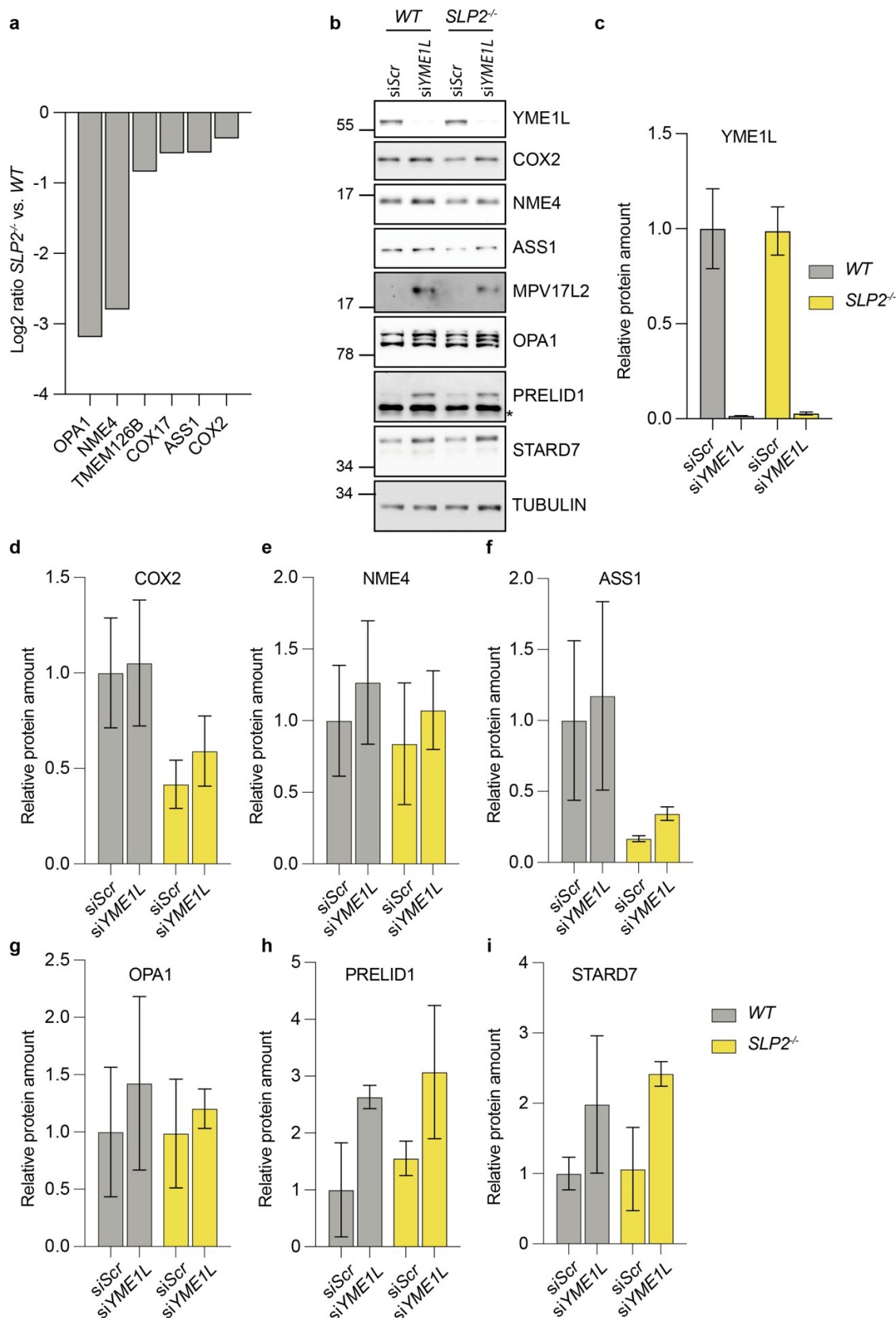
Figure 13: SLP2 does not seem to regulate YME1L mediated proteolysis

(a) Protein log2 ratios of significantly changed (FDR < 10 %) YME1L substrates in *SLP2^-/-^,* whole cell proteome (n=5). **(b)** Representative WB of YME1L substrates upon *YME1L* knockdown in HeLa *WT* and *SLP2^-/-^*, n=3. **(c)-(i)** Quantification of YME1L (c), COX2 (d), NME4 (e), ASS1 (f), OPA1 (g), PRELID1 (h) and STARD7 (i) protein levels upon *YME1L* knockdown normalized to Tubulin.

The same approach was applied for the *m*-AAA protease substrates. Among the putative substrates of *m*-AAA protease identified in the PhD thesis of Yvonne Larsarzewski (unpublished) we found DNAJC15, TMBIM5 and TFB2M decreased in *SLP2^-/-^* cells while ACOT7, OCIAD2, GrpE protein homolog 2 (GRPEL2) and ADP-ribose glycohydrolase MACROD1 were increased. This differential regulation implies that the loss of SLP2 affected protein levels in a substrate-specific manner but did not affect the activity of the *m*-AAA protease in general. (Fig. 14 a). Because a AFG3L2 knockdown led to a decrease of TMBIM5 instead of an accumulation in some cases we used HeLa *WT* and *AFG3L2^-/-^* cells and transiently downregulated *SLP2* by siRNA. We could assess only DNAJC15 and TMBIM5 by WB because antibodies for the other substrates were either not available or did not render conclusive results. A knockdown of *SLP2* in *WT* cells decreased the relative protein amount of TMBIM5. A knockdown of *SLP2* in *AFG3L2^-/-^* cells however did not decrease TMBIM5 indicating that AFG3L2 is responsible for its turnover (Fig. 14 b, d). The results for DNAJC15 which is cleaved into a long (L-) and short (S-) form were variable and were either still decreased by si*SLP2* also in *AFG3L2^-/-^* or not (Fig. 14 b, e – f). This suggested that SLP2 specifically regulates the proteolysis of TMBIM5 and of DNAJC15 in some conditions by the *m*-AAA protease.

In conclusion the loss of SLP2 did not generally lead to a hyperactivation of the *i*- and *m*-AAA protease. With the exception of TMBIM5 the decreased substrate proteins upon complete or partial loss of SLP2 could not be rescued by removal of the protease by knockdown or knockout under these conditions. However TMBIM5 seemed to be subject to increased degradation by the *m*-AAA protease in the absence of SLP2.
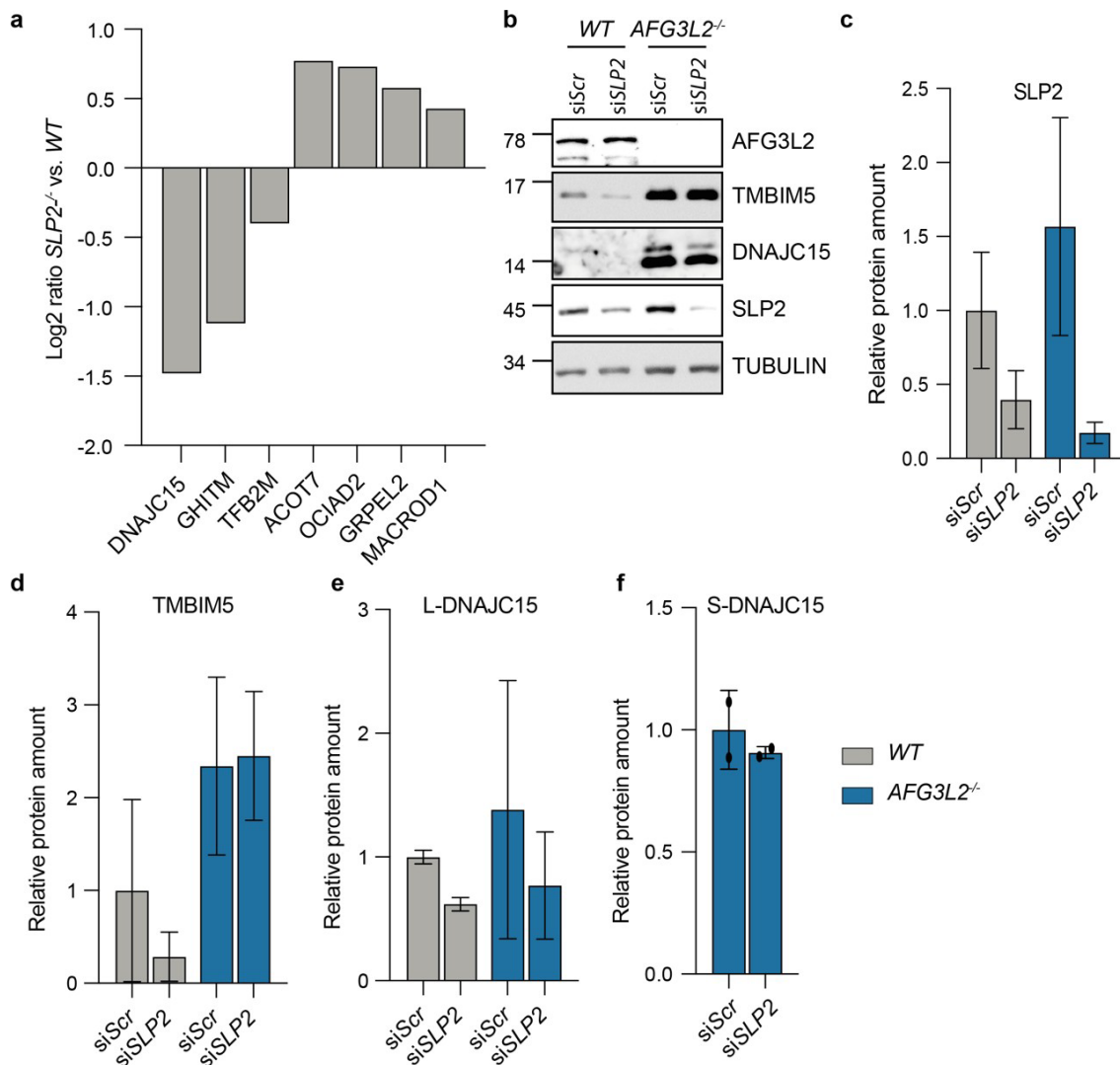
Figure 14: SLP2 regulates TMBIM5 proteolysis by the *m*-AAA protease

(a) Protein log2 ratios of significantly changed (FDR < 10 %) AFG3L2 substrates in *SLP2$^{-/-}$*, whole cell proteome (n=5). **(b)** Representative WB of AFG3L2 substrates upon *SLP2* knockdown in HeLa *WT* and *AFG3L2$^{-/-}$*, n=3. **(c)-(f)** Quantification of SLP2 (c), TMBIM5 (d), L-DNAJC15 (e) and S-DNAJC15 (f) protein levels upon *SLP2* knockdown normalized to Tubulin.

3.7 SLP2 deficiency activates the integrated stress response (ISR)

HeLa cells lacking SLP2 displayed changes of proteins in the respiratory chain, TCA cycle and other mitochondrial processes. This also led to defects in respiratory chain complex activity and TCA metabolism. We asked whether the effect on mitochondrial metabolic pathways *SLP2$^{-/-}$* possibly activates stress induced transcriptional responses. The ISR has been shown to respond to for example mitochondrial dysfunction and amino acid deficiency and to activate pro-survival responses (Pakos-Zebrucka et al., 2016).

We compared the proteome and RNA sequencing data of *SLP2⁻ᐟ⁻* cells with a list of genes activated during classical ISR (Torrence et al., 2021) and found several of them significantly upregulated on protein or mRNA level. This included mRNAs and proteins involved in amino acid metabolism such as the cystine/glutamate transporter SLC7A11, the asparagine synthetase ASNS or the phosphoserine aminotransferase PSAT1 but also the mRNAs of the transcription factors Cyclic AMP-dependent transcription factor ATF3 and ATF4 (Fig. 15 a, b). Phosphorylation of eukaryotic translation initiation factor 2 (EIF2α) is the main effector of the ISR and is responsible for its downstream effects via activating ATF4. WB analysis indeed revealed increased levels of pEIF2α in *SLP2⁻ᐟ⁻* cells compared to *WT* (Fig. 15 c, d).

These results indicate that loss of SLP2 and its consequences such as respiratory chain defects activate the ISR.
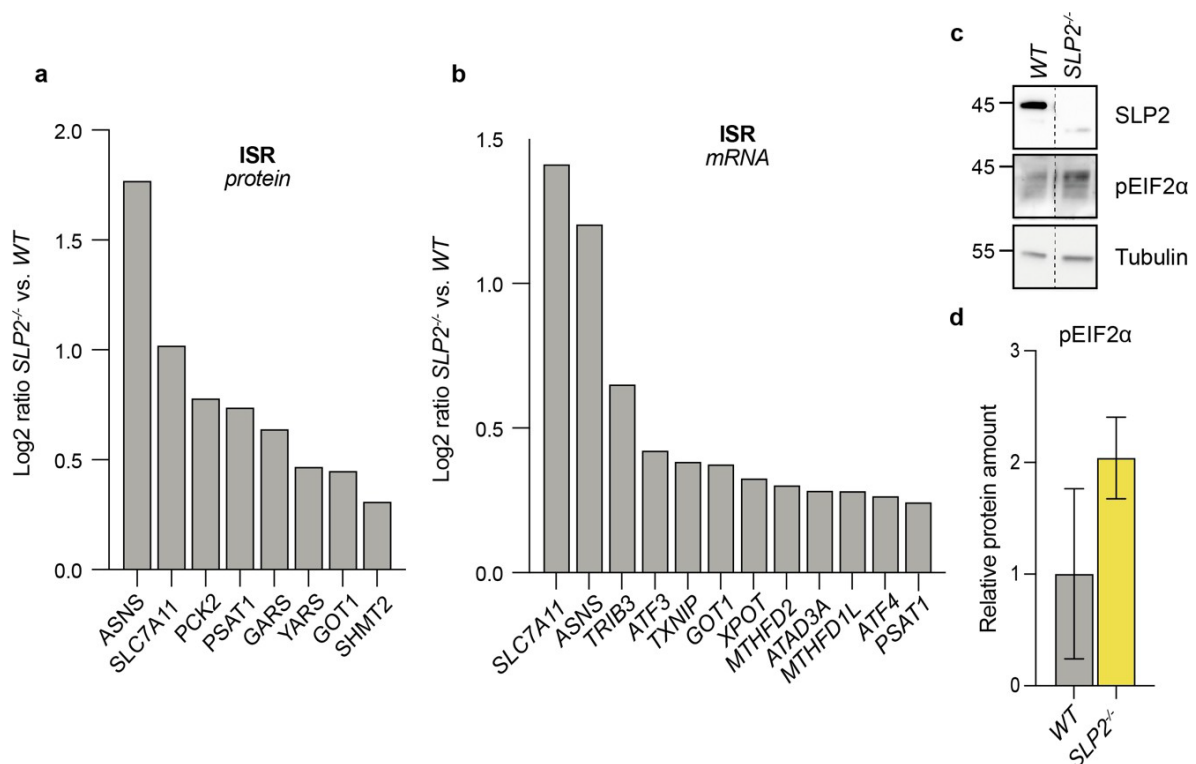
Figure 15: Knockout of SLP2 induces an integrated stress response

Whole cell proteomics (n=5) and RNA seq (n=3) of HeLa *WT* and *SLP2⁻ᐟ⁻* cells. **(a)** Protein log2 ratios of a set of significantly increased (FDR < 10 %) ISR genes in *SLP2⁻ᐟ⁻*. **(b)** mRNA log2 ratios of a set of significantly increased (adj. p value < 10 %) ISR genes in *SLP2⁻ᐟ⁻*. **(c)** Representative WB of pEIF2α in HeLa *WT* and *SLP2⁻ᐟ⁻* and **(d)** quantification, n=3.

3.8 Loss of SLP2 specifically increases mitochondrial small ribosomal subunit turnover

The study of protein stability by CHX experiments revealed that TMBIM5, DNAJC15 and APOO are destabilized in *SLP2^-/-^* and consequently decreased in protein abundance (Fig. 12 c). Various other proteins were also reduced upon loss of SLP2 independent of their mRNA levels as assessed by comparison of proteomic and transcriptomic data in *WT* and *SLP2^-/-^* HeLa cells (Fig. 12 b, table 8). Thus, we asked whether SLP2 has broader effects on mitochondrial protein stability and in this way regulates their protein abundance by using SILAC labeling.

A SILAC pulse-chase experiment which makes use of an initial incorporation of stable heavy isotopes $^{13}C_6{}^{15}N_4$ arginine (Arg10) and $^{13}C_6{}^{15}N_2$ lysine (Lys8) followed by a time chase with light isotopes $^{12}C_6{}^{15}N_4$ arginine (Arg0) and $^{12}C_6{}^{15}N_2$ lysine (Lys0) is an unbiased method to assess protein turnover. The ratio of heavy to light SILAC, hereafter remaining fraction (lnRF), thus indicates protein turnover and was used to calculate the slopes as rates of protein turnover in *WT* and *SLP2^-/-^* (Fig. 16 a).

The turnover slopes of *WT* and *SLP2^-/-^* proteins were plotted against each other and after filtering for MitoCarta3.0, the 10 most differently turned over proteins were labeled. A faster turnover was observed for DNAJC15, TMBIM5 and APOO which further validates the results of the CHX chase (Fig. 16 c). Other proteins with a faster turnover upon loss of SLP2 included the complex IV proteins NDUFA4 and cytochrome c oxidase assembly protein COX16 homolog (COX16), ferritin (FTH1), MRM2 for 16S RNA as well as the mitochondrial small ribosome subunits coiled-coil-helix-coiled-coil-helix domain-containing protein 1 (CHCHD1), MRPS11 and MRPS18C. Among the proteins that were turned over slower in *SLP2^-/-^* were the mitochondrial fission and transport proteins unconventional myosin-XIX (MYO19), mitochondrial cardiolipin hydrolase (PLD6) and mitochondrial ubiquitin ligase activator of NFKB 1 (MUL1) as well as MRPL34 and MRPL51. Other proteins with decreased turnover included the transcription factor Coiled-coil-helix-coiled-coil-helix domain-containing protein 2 (CHCHD2), endonuclease G (ENDOG), succinate dehydrogenase cytochrome b560 subunit (SDHC) and threonylcarbamoyl-AMP synthase (YRDC) which participates in tRNA modifications (Lin et al., 2018).
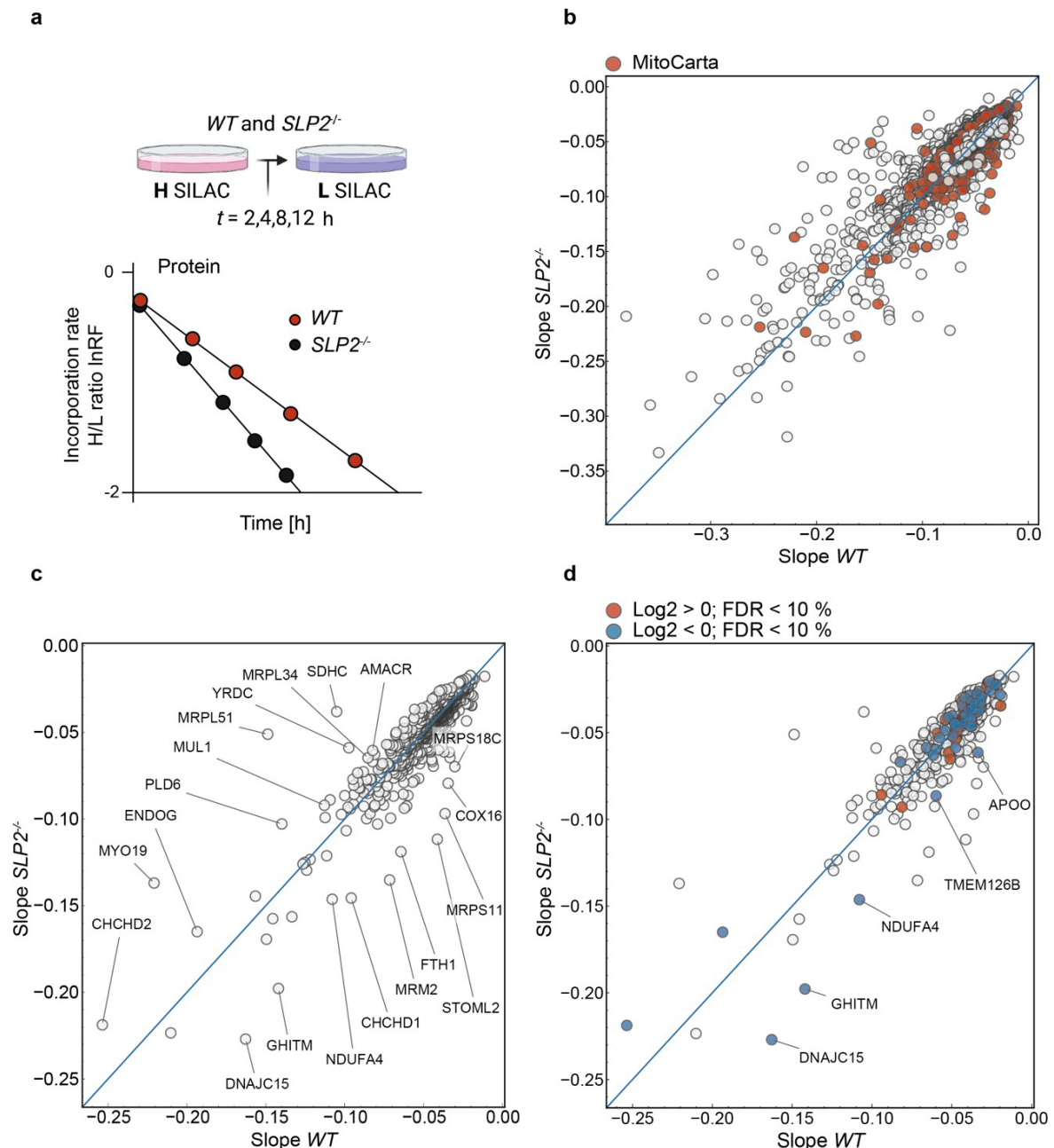
Figure 16: SLP2 affects the turnover of a set of mitochondrial proteins

SILAC pulse-chase experiment of HeLa *WT* and *SLP2*$^{-/-}$ enriched mitochondrial fraction, n=1. **(a)** Schematic workflow of the SILAC pulse-chase experiment, H (heavy), L (light). **(b)** Scatter plot of *WT* and *SLP2*$^{-/-}$ slope values of identified proteins; MitoCarta proteins highlighted. **(c)** Scatter plot of *WT* and *SLP2*$^{-/-}$ slope values of identified MitoCarta proteins; top 10 proteins with faster and slower turnover labeled. **(d)** Scatter plot of *WT* and *SLP2*$^{-/-}$ slope values of identified MitoCarta proteins; proteins with significant log2 ratios in whole cell proteomics highlighted; top 5 proteins with faster turnover and significantly decreased protein level in *SLP2*$^{-/-}$ labeled.

To see if the turnover rates of proteins in absence of SLP2 correlated with their steady state levels we looked at significantly up- and downregulated proteins. The decreased protein levels of DNAJC15, TMBIM5, NDUFA4, TMEM126B and APOO correlated with an increased turnover rate despite no transcriptional change (Fig. 16 d). The same trend for increased turnover was seen for the post-transcriptionally decreased proteins NDUFB1, SDHAF2 and SDHAF4. However, there was no clear relation between turnover and protein abundance in most cases.

To identify groups of proteins that were turned over faster in *SLP2^-/-^*, we performed categorical enrichment analysis of the highest and lowest 5 % of proteins which differ in their turnover rates (i.e. slope difference). The top 5 % of proteins with a faster turnover rate in the absence of SLP2 significantly enriched GO and MitoPathway terms for mitochondrial translation, in particular small ribosome subunit, structural constituent of ribosome, mitochondrial translational elongation and mitochondrial ribosome (Fig. 17 a). Only the term metal ion binding was enriched among proteins exhibiting slower turnover rates in *SLP2^-/-^* only enriched with (Fig. 17 b).

Indeed, the turnover of many small ribosomal subunits was decreased in *SLP2^-/-^* compared to *WT*. The 10 subunits with the most increased turnover in absence of SLP2 were MRPS11, CHCHD1, MRPS18C, MRPS24, AURKAIP1, MRPS12, MRPS14, MRPS10, MRPS35, MRPS15 (Fig. 18 a). This effect of increased ribosome turnover was specific to the small ribosomal subunit as evident in a boxplot for slope difference of the 28S and 39S subunit. Here the slope differences of 28S subunit proteins were significantly increased compared to all MitoCarta3.0 proteins while this was not the case for 39S subunit proteins (Fig. 18 b). Single plots of protein turnover rates, for example for 28S proteins, further strengthened this finding and displayed a faster declining slope in *SLP2^-/-^* (Fig. 18 c - g)*.

In conclusion we found that SLP2 selectively regulates the turnover of a set proteins but does not play a general role in mitochondrial protein turnover. In the case of DNAJC15, TMBIM5, NDUFA4, TMEM126B, APOO and less pronounced for NDUFB1, SDHAF2 and SDHAF4 this increased turnover upon loss of SLP2 consequently led to a significant decrease in protein abundance without effects on mRNA levels. We could not find a general destabilization of the respiratory chain and most other post-transcriptionally altered proteins in *SLP2^-/-^*. Instead, this experiment revealed that SLP2 specifically mediates mitochondrial small ribosomal subunit turnover.

a

b
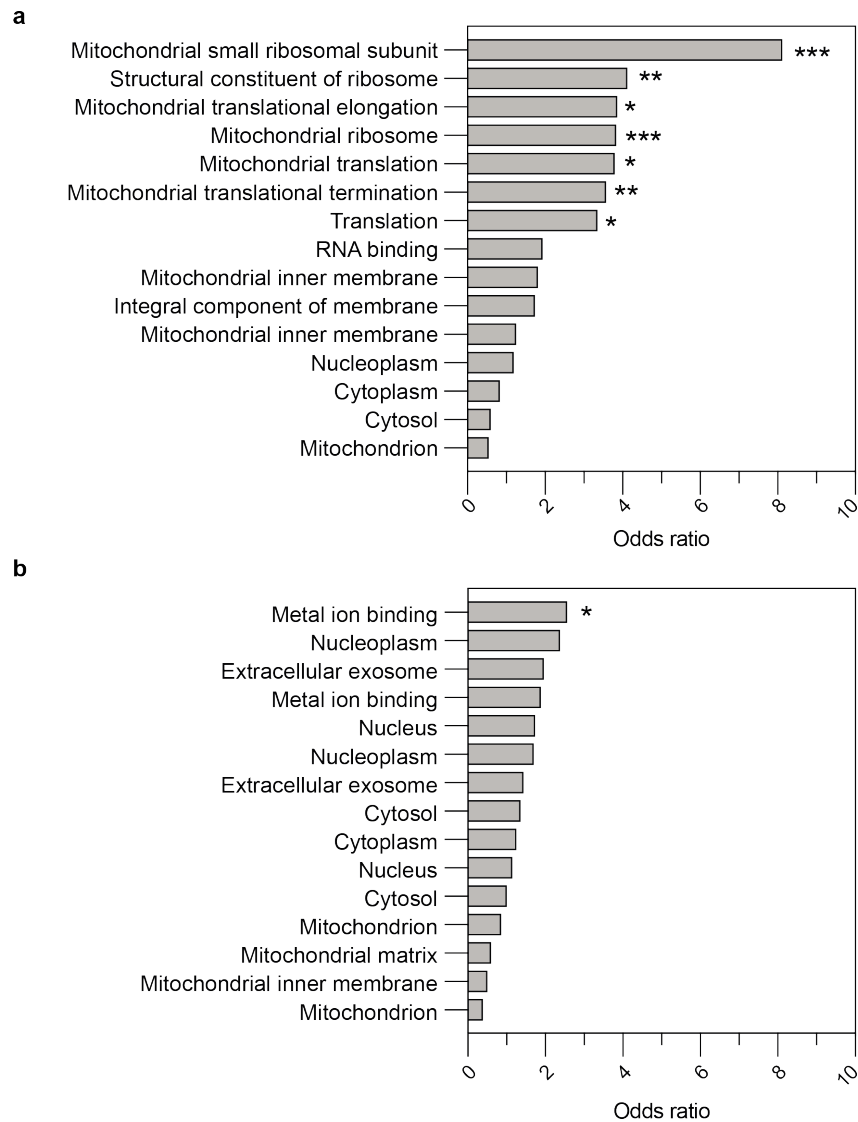
Figure 17: SLP2 regulates mitochondrial small ribosomal subunit turnover

SILAC pulse-chase experiment of HeLa *WT* and *SLP2^-/-* enriched mitochondrial fraction, n=1. **(a)** Categorical enrichment of GO terms of the top 5 % of proteins with faster turnover in *SLP2^-/-*. **(b)** Categorical enrichment of GO terms of the top 5 % of proteins with slower turnover in *SLP2^-/-*. P value <0.05 (*), <0.01 (**), <0.001 (***).
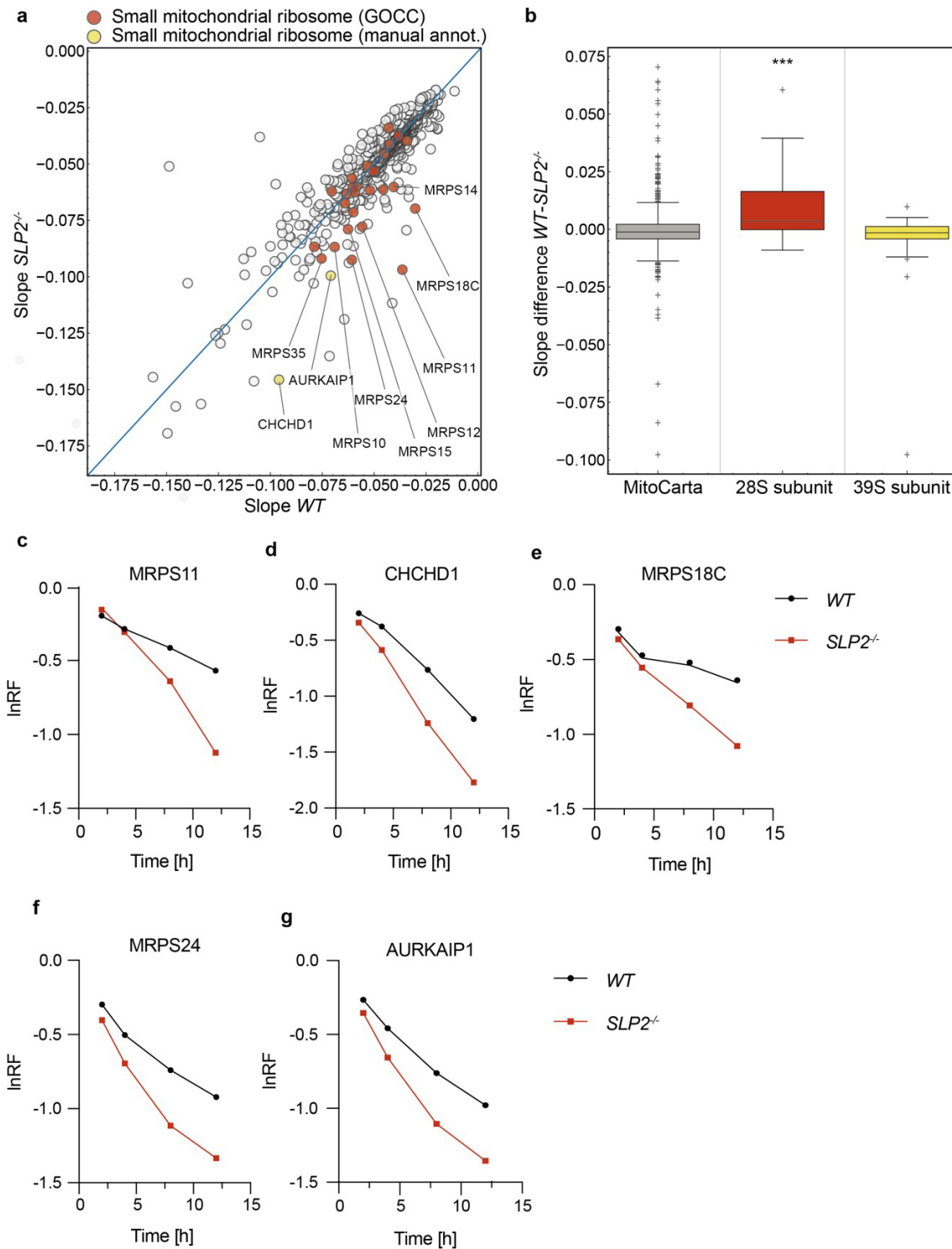
Figure 18: SLP2 regulates the turnover of ribosomal 28S but not 39S subunits

SILAC pulse-chase experiment of HeLa *WT* and *SLP2⁻/⁻* enriched mitochondrial fraction, n=1. **(a)** Scatter plot of *WT* and *SLP2⁻/⁻* slope values of identified MitoCarta proteins; top 10 small ribosomal subunit proteins labeled. **(b)** Box plot of slope differences in *WT* and *SLP2⁻/⁻* of identified MitoCarta, 28S and 39S proteins; p value <0.001 (***). **(d)-(g)** lnRF values of the top 5 28S proteins across time in HeLa *WT* and *SLP2⁻/⁻*.

3.9   SLP2 is required for efficient mitochondrial gene expression

A pulse-chase SILAC experiment in *WT* and *SLP2*^{-/-} cells revealed a role of SLP2 in the turnover of the mitochondrial small ribosomal subunit. Thus, we further investigated effects on mitochondrial gene expression in *SLP2*^{-/-} cells*.

A connection between SLP2 and the mitochondrial gene expression machinery was strengthened by a computational approach using genetic co-essentiality analysis via the FIREWORKS platform (Amici et al., 2021). Genes which display a similar fitness or essentiality in terms of cell growth are predicted to function in the same biological processes. Comparison of the cell growth upon deletion of single genes in various cancer cell lines revealed that SLP2 clearly correlated positively with genes involved in mitochondrial gene expression. 13 out of the 30 top ranked primary coessential genes have been linked to mitochondrial translation while 4 were involved in gene expression at another level (Fig. 19).
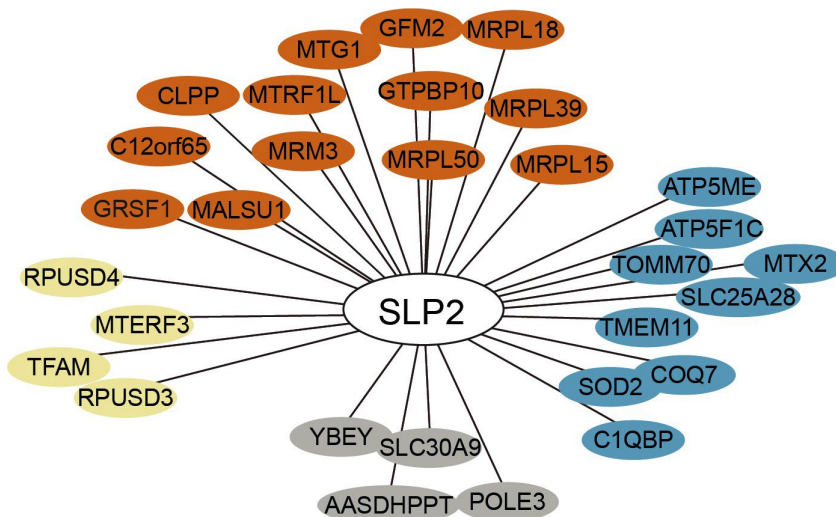
Figure 19: SLP2 positively correlates with mitochondrial translation factors
Coessentiality analysis of SLP2 via Fireworks app, top 30 positively correlating genes, sorted by function; mitochondrial translation (red) and gene expression (yellow), other mitochondrial function (blue), non-MitoCarta (grey).

We hypothesized that SLP2 might function in the assembly of the ribosome causing increased turnover in the absence of SLP2. To monitor ribosome assembly, we performed sucrose gradient ultracentrifugation of an enriched mitochondrial fraction of HeLa *WT* and *SLP2*^{-/-} cells. During gradient centrifugation molecules and complexes will sediment according to their size, shape and density. Thus, the 28S, 39S and 55S ribosome can be separated and visualized. This analysis did not reveal any apparent

differences in the abundance or composition of the 28S and 39S subunits or 55S monosome between WT and *SLP2^(-/-)* cells (Fig. 20 a).
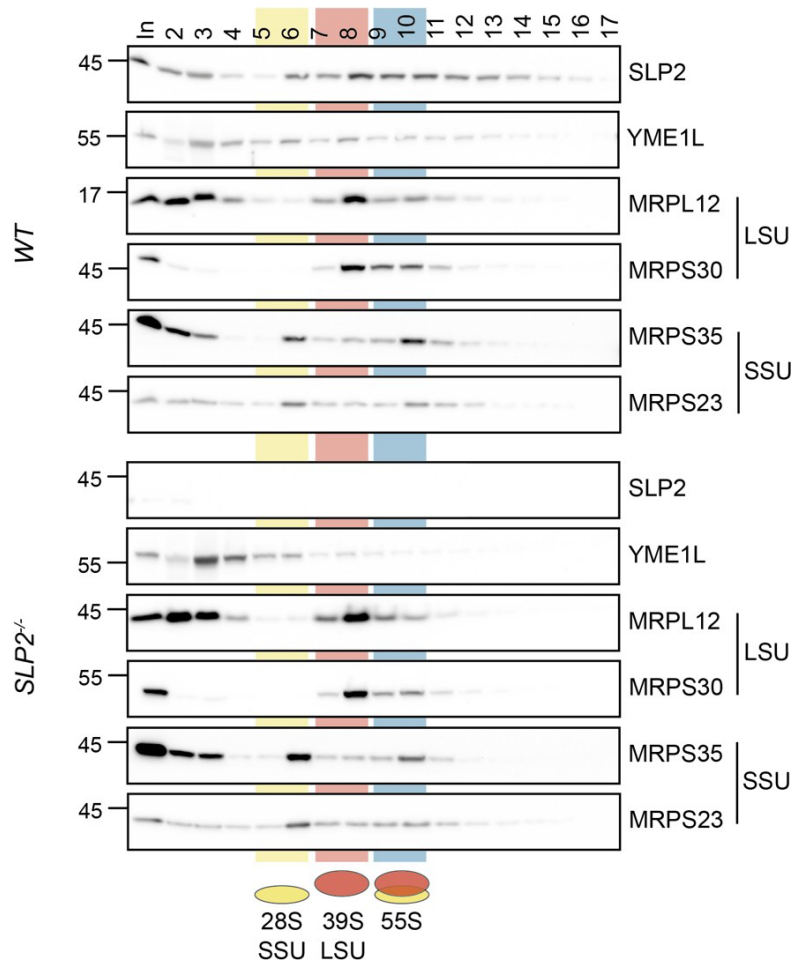
Figure 20: SLP2 does not affect mitoribosome assembly

Representative WB of sucrose gradients of HeLa *WT* and *SLP2^(-/-)*, n=2.

We next analyzed mitochondrial translation with ^{35}S methionine/cysteine pulse labeling. For this experiment cells were first starved of methionine and cysteine and cytosolic translation was blocked by emetine. [35]S methionine/cysteine was then added to the cells to be incorporated into newly synthesized mitochondrial proteins (Fig. 21 c). The method revealed a significant reduction in *SLP2^(-/-)* or upon transient knockdown of *SLP2* via siRNA in HeLa cells. This reduction affected all mitochondrial proteins and was not specific for one of the respiratory chain complexes (Fig. 21 a, b, d, e).

Reduced mitochondrial translation resulted in decreased protein levels of mitochondrially encoded proteins as measured by whole cell proteomics, significantly in the case of the complex IV subunits MT-CO2 and MT-CO3 (Fig. 22 a). To control

whether the reduction of mitochondrial proteins was post-transcriptional we further quantified their mRNA levels by qPCR and found most of them decreased. Most of mtDNA encoded transcripts were decreased and the effect was significant for *MT-ND3, MT-ND5, MT-CYB, MT-CO1-3, MT-ATP6* and *MT-ATP8*. The mRNAs of *MT-ND1* and *MT-ND2* were significantly accumulated compared to *WT* (Fig. 22 b). The decrease of mitochondrially encoded mRNAs was not due to decreased mtDNA which was surprisingly increased in *SLP2^{-/-}* as assessed by qPCR using different mtDNA primers (Fig. 22 c). We further measured 16S and 12S RNA amounts by qPCR which are known to be essential for mitochondrial translation (De Silva et al., 2015) but again found them to be significantly accumulated upon SLP2 loss (Fig. 22 d).

Mitochondrial protein synthesis can appear reduced when the stability of newly synthesized mitochondrial proteins is affected rather than translation itself. We therefore assessed the stability of newly synthesized mitochondrial proteins in a ^{35}S pulse-chase experiment. The method is essentially identical to the pulse experiment described above but ^{35}S methionine is removed after the initial pulse to chase the loss of incorporated ^{35}S and thus assess the turnover of newly synthesized mitochondrial proteins. We found that the decrease in mitochondrial translation was not due to instability of these newly synthesized proteins (Fig. 23 a, b). We also asked whether the assembly of newly synthesized mitochondrial proteins into respiratory complexes was altered using the same ^{35}S pulse-chase approach followed by BN-PAGE analysis. With this method we could assess the complex formation and turnover of newly synthesized mitochondrial proteins over time. While it was difficult to identify specific complexes via this method, we observed the same overall decrease in translation but no further difference in complex stability (Fig. 23 c - e).

In summary we found that SLP2 is required for efficient mitochondrial translation. Loss of SLP2 leads to decreased translation despite fully assembled ribosomes and thus respiratory chain defects as seen by BN-PAGE and activity assays. The SILAC data further shows that this translation defect is either caused by or causes an increased turnover of the small ribosomal subunit.
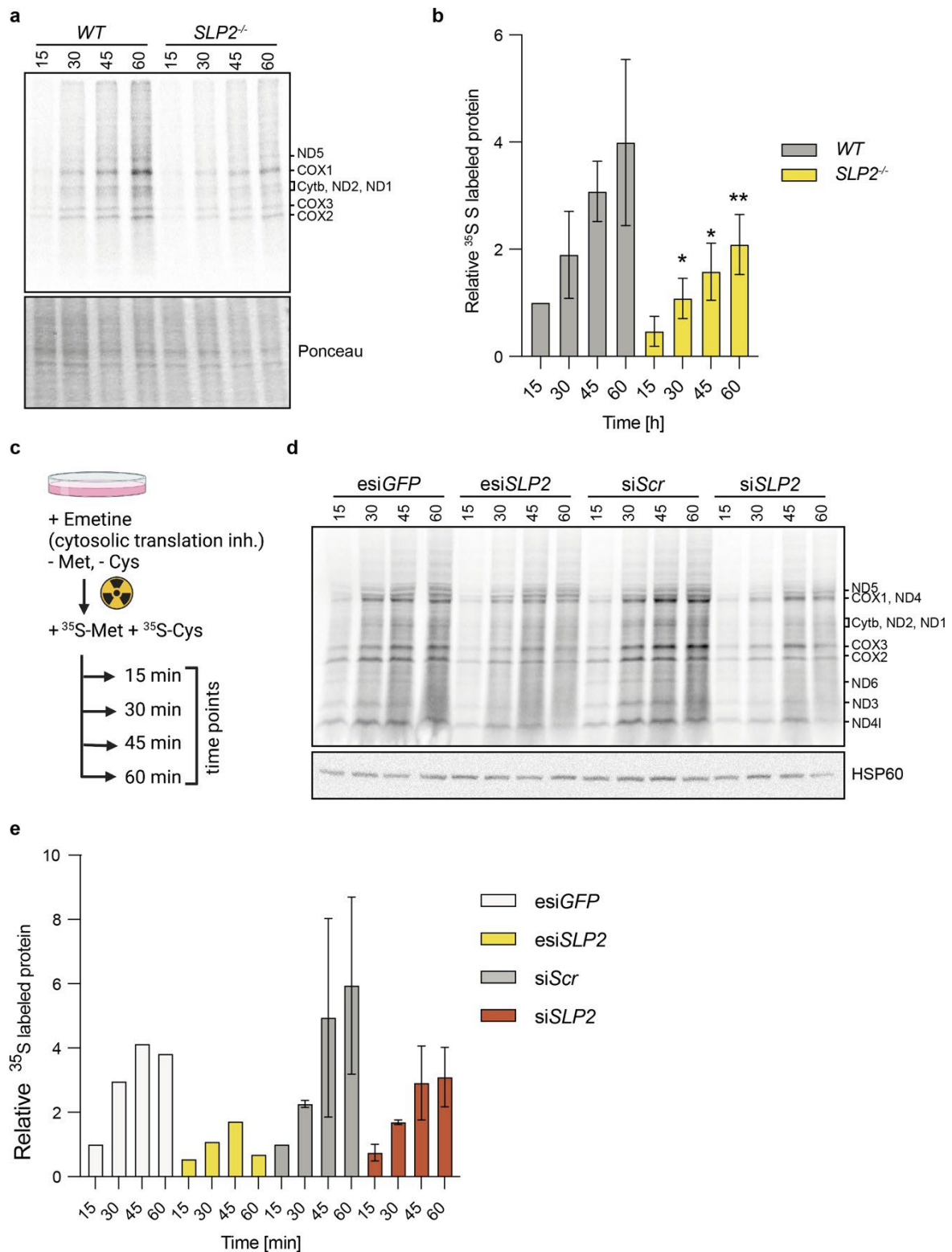
Figure 21: SLP2 is required for efficient mitochondrial translation

^{35}S methionine/cysteine translation assay. **(a)** Representative image of ^{35}S incorporation in HeLa *WT* and *SLP2$^{-/-}$* cells after 15, 30, 45 and 60 min. **(b)** Quantification of (a); n=3; p value <0.05 (*), <0.01 (**), <0.001 (***). **(c)** Schematic workflow of ^{35}S translation assays. **(d)** Representative image of ^{35}S incorporation in HeLa *WT* cells upon knockdown of SLP2 with esiRNA (n=1) or siRNA (n=2) after 15, 30, 45 and 60 min. **(e)** Quantification of (d).
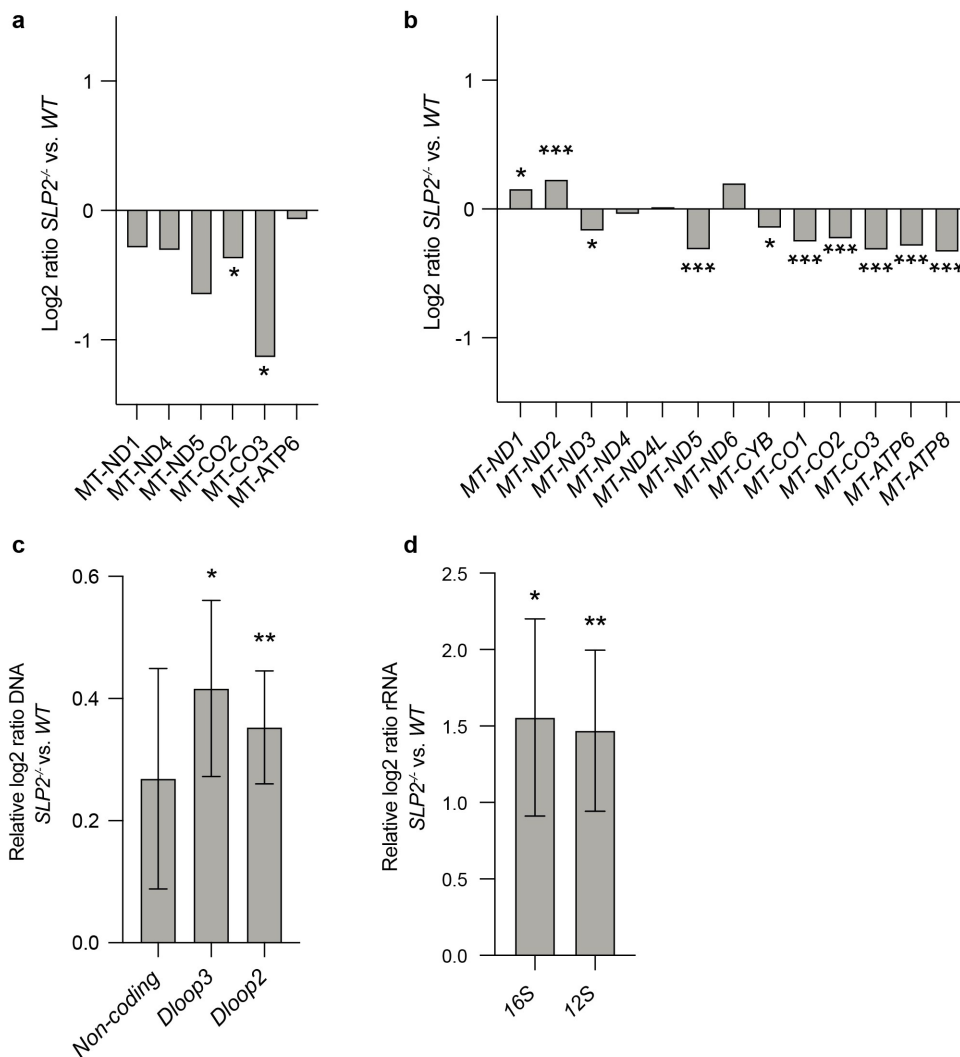
Figure 22: *SLP2-/-* cells display decreased protein and mRNA levels of OXPHOS proteins independent of mtDNA levels

(a) Protein log2 ratios of mitochondrially encoded proteins in HeLa *WT* and *SLP2-/-* as measured by whole cell proteomics, n=5; FDR < 10 % (*). **(b)** mRNA log2 ratios of mitochondrially encoded mRNAs in HeLa *WT* and *SLP2-/-* as measured by whole cell RNA seq, n=5; adj. p value <0.05 (*), <0.01 (**), <0.001 (***). **(c)** Relative log2 ratio of mtDNA as measured by qPCR in HeLa *WT* and *SLP2-/-*, n=3; p value <0.05 (*), <0.01 (**), <0.001 (***). **(d)** Relative log2 ratio of mtDNA as measured by qPCR in HeLa *WT* and *SLP2-/-*, n=3; p value <0.05 (*), <0.01 (**), <0.001 (***).
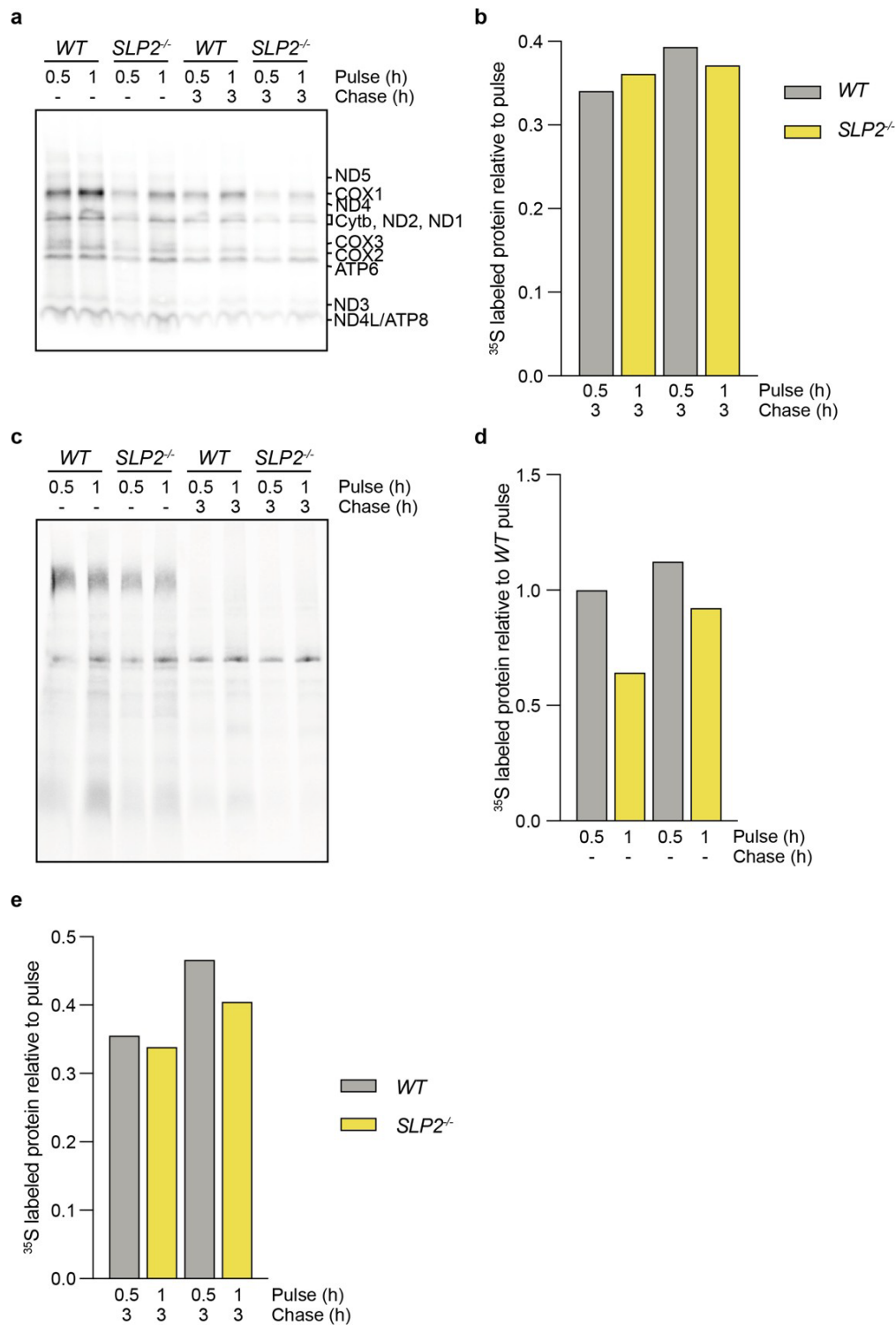
Figure 23: SLP2 does not affect the stability or assembly of newly translated mitochondrial proteins

(a) ^{35}S methionine pulse-chase translation assay with 0.5 and 1 h pulse and 3 h chase in enriched mitochondrial fraction of HeLa *WT* and *SLP2-/-*; n=1. **(b)** Quantification of (a), only chase normalized to respective pulse. **(c)** ^{35}S methionine pulse-chase translation assay with 0.5 and 1 h pulse and 3 h chase in an enriched mitochondrial fraction of HeLa *WT* and *SLP2$^{-/-}$* on BN PAGE; n=1. **(d)** Quantification of (c), only pulse normalized to WT 0.5 h pulse. **(e)** Quantification of (c), only chase normalized to respective pulse.

4   Discussion

SLP2 is one of two mitochondrial scaffold proteins in mitochondria where it forms the SPY complex (Wai et al., 2016). SLP2 has been shown to regulate the respiratory chain (Da Cruz et al., 2008b; Mitsopoulos et al., 2015b, 2015a), calcium handling (Da Cruz et al., 2010) and cardiolipin metabolism (Christie et al., 2011a) but an in-depth analysis of the role of SLP2 in overall mitochondrial function has been missing thus far. By using a vast range of unbiased as well as more targeted biochemical approaches such as mass spectrometry, RNA sequencing, electron microscopy and *in vitro* translation assays we identified SLP2 as a 1) mitochondrial interaction platform with connections to the import machinery, MICOS complex and the respiratory chain, 2) a regulator of OXPHOS complexes with an effect on TCA metabolism and 3) a supporting factor in mitochondrial gene expression by enabling efficient translation.

4.1   SLP2 is a mitochondrial interaction platform
•
While interaction studies have been performed for the neighboring mitochondrial scaffold prohibitin (Richter-Dennerlein et al., 2014), only the prohibitins and proteases PARL and YME1L have been published to interact with SLP2 (Da Cruz et al., 2008a; Wai et al., 2016). With SLP2 being a scaffold, we hypothesized that it also must interact with other proteins and sought to define its interactome by co-immunoprecipitation via anti-FLAG beads in HeLa *WT* vs. *SLP2$^{-/-}$+SLP2^{FLAG}* cells followed by mass spectrometry. Accordingly, we found 194 significant interactors of SLP2 by this method, 149 of them associated with the IM. This result fortifies the tight attachment of SLP2 to the inner membrane despite its matrix localization and the lack of a transmembrane region. A palmitoylation site like in stomatin has been suggested as a mechanism for membrane attachment (Lapatsina et al., 2012). In our hands the disruption of a palmitoylation site in SLP2 however did not alter its localization in our hands (data not shown). Co-immunoprecipitation of SLP2 resulted in enrichment of the published interactors such as PARL and YME1L, as well as a novel unpublished interactor TMBIM5, identified also previously in our group. TMBIM5 functions as a mitochondrial Ca^{2+}/H^+ exchanger allowing mitochondrial Ca^{2+} efflux, similar to the mitochondrial Na^+/Ca^{2+} exchanger NCLX (Palty et al., 2010). In addition to TMBIM5 we identified the calcium channel MCU as well the *m*-AAA protease with AFG3L2 and SPG7. SLP2 has previously been described to regulate mitochondrial calcium

homeostasis as its knockdown increased Ca^{2+} efflux from mitochondria (Da Cruz et al., 2010). The authors hypothesized that the effect might be due to increased activity of NCLX because CGP-37157, an inhibitor of the sodium-calcium exchanger, brought the maximum efflux rate back to wildtype levels in HeLa cells. NCLX can at least partly compensate for loss of TMBIM5 (Patron et al., 2022). This thesis work suggests that the SLP2 effect on calcium metabolism might act via TMBIM5, thus this should be investigated further. The interaction of SLP2 with a calcium exchanger and MCU is reminiscent of stomatin and STOML3 which associate and modulate acid-sensing ion channels in neurons by an unknown mechanism (Price et al., 2004b).

Surprisingly, we found many subunits as well as complete complexes of the mitochondrial import machinery and MICOS as interactors of SLP2. All subunits of the complexes of TIM22, SAM, MIA and MICOS were identified as significantly enriched at high fold change ratios, except for ROMO1 which was not identified at all by mass spectrometry, possibly due to its small size. All subunits of the TIM23 complexes were enriched as well. This suggests a previously unknown link for SLP2 to mitochondrial carrier, presequence and cys motif import as well as cristae organization via MICOS. The interaction with the MICOS complex and changes in subunit levels as described in 4.3 however did not affect cristae morphology. Loss of SLP2 led only to mild ultrastructural defects in mitochondria. Mitochondrial appeared smaller and rounder but did not display gross cristae abnormalities. This finding rather suggested a fragmentation of mitochondria in *SLP2*$^{-/-}$ cells which is in line with the detected destabilization of L-OPA1 and the increased cleavage of OMA1-mediated cleavage of OPA1 in absence of SLP2 as seen also in our experiments (Wai et al., 2016). Other top interactors in the IM were TIMM29 and AGK which are subunits of the TIM22 translocase with mitochondrial carriers as the main import substrates. This could further explain the enrichment of various mitochondrial SLC25 carriers with SLP2. SLP2 is localized in the matrix with tight association to the inner membrane (Wai et al., 2016). Based on this localization it seems likely that the outer membrane and IMS complexes TOM, SAM and MIA were indirect interaction partners via the inner membrane translocases or MICOS. It is also conceivable that the interaction to the TIM23 translocase is in part via the prohibitin complex which has been shown to interact with DNAJC19, TIMM23 and TIMM22 (Richter-Dennerlein et al., 2014). SLP2 may play more general role in the import machinery platform since most of the import factors were predicted to be interactors. OXA1L and SURF1 which are part of the

MITRAC complex that allows for co-translational insertion of mtDNA encoded proteins were also identified as putative interactors but other MITRAC proteins were not found in the experiment. The role of SLP2 in the assembly and expression of mitochondrially encoded proteins is explored in 4.2 and 4.4 respectively.

In addition, SLP2 enriched with subunits and assembly factors of every respiratory chain complex but many of them clustered close to the cut off and could thus be considered more indirect or transient interaction partners. Cytochrome c oxidase assembly protein COX20, a chaperone for COX2, however enriched with a very high log2 ratio and could be more directly involved with SLP2. Further connections of SLP2 to the respiratory chain will be discussed later.

An uniting aspect of many of the putative interactors of SLP2 identified in this experiment is their described association with cardiolipin. TOM, SAM, TIM22, TIM23 and PAM have been shown to structurally rely on CL while AGK catalyzes the conversion of DAG to PA, a precursor of CL. DNAJC19 was shown to influence CL acylation. Two proteins of the MICOS complex APOO and APOOL are related to apolipoproteins and the latter was found to directly bind CL to assemble into the MICOS complex. OPA1, another SLP2 interactor, binds to CL and is needed for SiMH, a process also reliant on SLP2. Cardiolipin was further described to be involved in the regulation of the integrity and activity of all respiratory complexes as well as supercomplexes and was shown to support the structure of mitochondrial carrier proteins (Dudek, 2017). Finally, CL regulates the stability of MCU (Ghosh et al., 2020). One could hypothesize that SLP2 binds or forms membrane domains that are rich in cardiolipin and thus interacts specifically with proteins and complexes reliant on CL. Both the binding of CL and SLP2 and the induction of CL biosynthesis by overexpression of SLP2 have been suggested in the literature supporting the hypothesis (Christie et al., 2011b). The next step to investigate SLP2 membrane domains including both proteins and lipids would be the extraction of native membrane discs via styrene maleic acid copolymer (SMA) or diisobutylene-maleic acid (DIBMA) copolymer as lipid particles. With this method membrane discs would be extracted from mitochondria of WT or SLP2^{FLAG} expressing cells and an IP against FLAG would isolate those particles that contain SLP2^{FLAG}. In combination with the IP data in this thesis such an experiment could reveal direct neighbors of SLP2 that sit within the same membrane domain as well as the surrounding lipids, potentially CL. A

prerequisite is the efficient extraction of SLP2 which in our hands was not successful thus far (data not shown).

While this is the first interactome study of SLP2, other researchers have found it in proximity based assays or even used as bait. Antonicka *et al*. found SLP2 in close proximity to the MICOS subunit APOO, MCU, OXPHOS proteins COX15 and SURF1 as well as the mitochondrial elongation factor Ts (TSFM), required for meiotic nuclear division protein 1 homolog (RMND1) and complement component 1 Q subcomponent-binding protein (C1QBP) which are involved in mitochondrial translation (Janer et al., 2015; S. Pearce, Nezich, & Spinazzola, 2013; Yagi et al., 2012). The study further identified many proteins of the mitochondrial gene expression machinery close to SLP2 which were not enriched in our co-immunoprecipitation, such as mitochondrial initiation factors, translation elongation factors and components of the mitochondrial ribosome (Antonicka et al., 2020). Li *et al*. verified the SLP2 interactors YME1L, PARL, MCU, the MICOS subunit MIC60, mitochondrial import proteins TIMM23, TIMM21, OXA1L and TIMM17B as well some of the OXPHOS proteins and SLC25 carriers. Both studies fortify the links between SLP2, MICOS, OXPHOS, MCU and parts of the import machinery which we also observed albeit with different subunits or to a lesser extent. A surprising aspect however is the close proximity of SLP2 to the mitochondrial ribosome and other components of the gene expression machinery which we did not see in our data. This could be due to the buffer conditions used in our IP which was not suited for ribosomes. However adequate adjustments did not result in enrichment of mitoribosomal proteins with SLP2 but with the control SMIM4 (data not shown) (Dennerlein et al., 2021). This was further supported by IP data using the MitoRibo-tag mouse. IP of the large ribosomal subunit MRPL62 did not enrich SLP2 in normal conditions. Upon loss of MTERF4, which leads to defective ribosome assembly and accumulation of the single small and large subunit, MRPL62 surprisingly precipitates with SLP2 (Busch et al., 2019). This poses the question if SLP2 specifically interacts with subassembled mitoribosomes and thus in healthy conditions cannot be co-immunoprecipitated with the translation machinery. Again, there is a publication that claims mitochondrial ribosomes are attached to OXA1L and thus docking to the inner membrane via CL (Lee et al., 2020b). Recent structural studies have solved the ring structure of SPFH proteins and found that *E.coli* HflK/C forms a cage like complex around the associated protease. Detailed interaction studies for example chemical crosslinking masspectrometory (XLMS) will be required to elucidate how SLP2

interacts with such a variety of proteins including large membrane and matrix protein complexes.

In conclusion, we identify SLP2 as a mitochondrial interaction platform that, possibly by forming CL rich membrane domains, associates with the import machinery, the MICOS complex, the respiratory chain and carrier proteins.

4.2 Loss of SLP2 affects the mitochondrial respiratory chain

We found nearly 200 putative interactors of SLP2 by co-immunoprecipitation experiments and identified previously unknown links to mitochondrial protein import and cristae structure, metabolic carriers and the respiratory chain. We reasoned that loss of SLP2 might induce a drastic change of mitochondrial functionality and the mitochondrial proteome through the lack of these interactions. Using HeLa *WT* and *SLP2^-/-* cells we chose whole cell proteomics analysis to identify proteins affected by SLP2 loss. Depletion of SLP2 led to twice as many significantly decreased than increased mitochondrial proteins which suggested that SLP2 could support their stability. Cluster analysis of these downregulated proteins in *SLP2^-/-* identified subunits of the respiratory chain, TCA cycle, mitochondrial gene expression as well as import and mitochondrial architecture as most affected. Specifically complex IV of the respiratory chain was negatively affected by SLP2 loss also according to categorical enrichment analysis. This is in line with previous publications which linked SLP2 to mitochondrial respiration. In HeLa cells SLP2 was described to influence the stability and protein levels of certain proteins such as PHB, ND6 of complex I and COX4 of complex IV (Da Cruz et al., 2008a). We thus investigated the assembly state of respiratory complexes using BN-PAGE and observed decreased levels of complex I, II and IV in both single complexes and supercomplex arrangements. The activities of complex I and IV were consequently decreased. Despite a clear effect on respiratory chain complex assembly and reduced complex I and IV activity we did not observe a defect in mitochondrial respiration of SLP2^-/- cells as assessed by Seahorse. Others observed a defect in supercomplex formation in MEF and T cells lacking SLP2 rather than of total levels which included a slight increase in ROS production, increased uncoupled respiration, increased reliance on glycolysis and decreased membrane potential (Mitsopoulos et al., 2015a). Previous studies in T cells also did not identify a respiratory defect in absence of SLP2 (Darah A Christie et al., 2012; Mitsopoulos et al., 2015). These studies both found ECAR to be increased which was not the case in

our hands. At this point it is not clear why only complexes I, II and IV but not III or V were affected by loss of SLP2. If SLP2 supports their structural integrity it is conceivable that at least complex V might be out of reach due to its localization at the cristae tip. The published data on the role of SLP2 and mitochondrial respiration in combination with the results described here clearly illustrate that SLP2 is required for optimal function and assembly of the respiratory chain. The extent of this requirement and the severity of the consequences of a loss of SLP2 however seems largely dependent on the conditions of the experiments such as organism, cell type and culture conditions. This is likely the reason why our results differ from those in murine and immune cell lines. Furthermore, all of our experiments were performed under high glucose conditions in which cells do not rely on OXPHOS for ATP production. Measurements in cells adapted to galactose media to enhance the use of OXPHOS, grown at other confluency or in more physiological medium such as plasma-like medium could offer different results. It is also imaginable that cells after transient knockdown of SLP2 could show more severe defects than a stable knockout cell line in which compensatory mechanisms could be activated.

Moreover, at this point it is not clear which defects are primary and which are secondary to SLP2 loss as for instance as an effect of altered lipid microdomains via SLP2. In principle, the compensatory response, in other words the secondary consequences posed by the loss of SLP2 could mask the primary defects. The observed general decrease of the TCA cycle metabolism by transcriptional downregulation of its enzymes might be a response to the OXPHOS defect. This has been shown to be the case in deficiencies for respiratory chain subunits such as COX10 (Ahola et al., 2022), complex II (Lussey-Lepoutre et al., 2015; Ryan et al., 2021) and patient mutations of complexes I, IV and V (Adant et al., 2022). This TCA cycle defect upon loss of SLP2 can thus be attributed to the changes of the respiratory chain. During the metabolic characterization of *SLP2$^{-/-}$* cells we further observed a global accumulation of amino acids independently of autophagic flux which was in line with a mild activation of the ISR. The ISR is activated by different stressors such as ER stress, amino acid or heme deprivation and viral infection and via different regulators leads to phosphorylation of eIF2α. This reduces global translation but supports the translation of specific genes, among them pro-survival genes and activating transcription factor 4 (ATF4) which in turn e.g. alters amino acid metabolism. Mitochondria with defective translation or the respiratory chain were previously shown

to induce ISR (Mick et al., 2020; Pakos-Zebrucka et al., 2016; Sasaki et al., 2020). Recently, OMA1 has been identified to cleave DELE1 which then accumulates in the cytosol and activates the kinase heme-regulated inhibitor (HRI, E2AK1) to phosphorylate eIF2α (Ahola et al., 2022; Fessler et al., 2020; Guo et al., 2020). ISR has been described to promote one carbon metabolism and amino acid accumulation (Bao et al., 2016; Nikkanen et al., 2016). This is line with the increase of 1-C intermediates methionine, serine and glycine in *SLP2$^{-/-}$* cells while accumulated asparagine matches the increase of asparagine synthetase ASNS. The activation of ISR is in line with the respiratory chain defects we observe in *SLP2$^{-/-}$* cells and is further explained by the decreased translation discussed in 4.4. To further investigate the effects on TCA cycle enzymes and amino acid metabolism in *SLP2$^{-/-}$* cells future experiments should be done in low glucose conditions that lack additional amino acid or pyruvate supplementation and flux measurements should be considered. Further characterization of the ISR in *SLP2$^{-/-}$* should include quantification of ATF4 protein levels and identification of the effector kinase such as HRI. A transient knockdown of DELE1 or OMA1 could clarify their involvement in this stress response in absence of SLP2. Treatment of *SLP2$^{-/-}$* cells with integrated stress response inhibitor (ISRIB) and subsequent measurement of amino acids could verify if ISR is the cause of the accumulation.

In combination with the interactome data which revealed the interaction of SLP2 with subunits of all respiratory chain complexes, our data suggests that SLP2 supports the function and assembly of the mitochondrial respiratory chain. These OXPHOS defects likely cause impaired TCA cycle metabolism and an activation of the ISR which consequently results in amino acid accumulation.

4.3 SLP2 regulates a subset of mitochondria proteins post-transcriptionally

We aimed to understand the mechanism of mitochondrial protein regulation by SLP2 as identified by whole cells proteomics. Combination of the proteomic data with RNA sequencing was applied to differentiate transcriptional and post-transcriptional effects. The analysis identified a subset of proteins that were decreased in *SLP2$^{-/-}$* without transcriptional suppression. This included several respiratory chain subunits or assembly factors of complex I (NDUFB1, TMEM126B), II (SDHAF2, SDHAF4) and IV (COX7A2, COX7A2L) which further confirmed the results obtained from BN-PAGE. NDUFB1 and TMEM126B are responsible for the assembly of the distal proton

pumping module P_D (Guerrero-Castillo et al., 2017) and ND2 module (Formosa et al., 2020) respectively. SDHAF2 and SDHAF4 are two of four assembly factors of complex II and were shown to be required for maximal activity (Van Vranken et al., 2014). Interestingly, COX7A2 and COX7A2L (SCAF1) have been suggested to be exchanged to allow for CIII-IV interaction (Cogliati et al., 2016; Lobo-Jarne et al., 2018). SLP2 could be involved in the assembly of CII and CIII-CIV supercomplex by regulating the levels of these proteins.

Other downregulated proteins in *SLP2$^{-/-}$* regardless of mRNA included TMBIM5 which was identified as an interactor in this thesis. NCLX, the Na$^+$/Ca^{2+} exchanger supposedly regulated by SLP2, can partially compensate for loss of TMBIM5 (Patron et al., 2022). TMBIM5 is a substrate and inhibitor of the *m*-AAA protease which also has been linked to calcium metabolism by regulating the gatekeeping of MCU (König et al., 2016). Thus it is imaginable that the strong decrease of TMBIM5 in *SLP2$^{-/-}$* leads to hyperactivation of NCLX and increased calcium extrusion. DNAJC15, part of the TIM23/PAM complex with TIMM17A (translocase A), was also decreased upon loss of SLP2 despite normal mRNA levels and was identified as an interactor in 3.1. Translocase A was shown to be non-essential under normal conditions in contrast to translocase B (DNAJC19 and TIMM17B) (Sinha et al., 2014). The authors observed a decreased respiratory chain complex activity in absence of translocase A but no significant effect on mitochondrial content. This could indicate a specific role in the import of respiration specific import factors. The supportive role in respiratory chain maintenance of SLP2 is in line with this putative supportive role of translocase A. SLP2 could scaffold DNAJC15 to allow for more efficient import and assembly of respiratory chain complex proteins. Import experiments in *WT* and *SLP2$^{-/-}$* conditions that increase OXPHOS reliance such as galactose medium could address this hypothesis.

We discovered APOO of the MICOS complex as an interactor of SLP2 which displayed decreased protein amounts in *SLP2$^{-/-}$* but normal transcript levels. Its direct binding partner APOOL was an interactor of SLP2 that was reduced on both protein and mRNA level. Thus, it is conceivable that the decrease of APOO consequently led to decrease of APOOL as a transcriptional response. However complete loss of APOO in HAP1 cells led to overexpression of APOOL instead. The same publication described that neither APOO or APOOL were required for MICOS assembly and stability but

supported respiratory chain supercomplexes and the ATP synthase. They further found that decrease of APOO also decreased cardiolipin levels (Anand et al., 2020). In HeLa cells loss of APOO displayed largely normal cristae structure and no respiratory chain assembly defects (Stephan et al., 2020b). The lack of a strong cristae phenotype is in line with the EM results of *SLP2*$^{-/-}$ as described in 3.1. As APOO and APOOL are the CL-binding components of the MICOS complex it is possible that their decrease is due to a putative lack of or rearrangement of CL microdomains in *SLP2*$^{-/-}$.

4.3.1 Proteolysis by the *i*- and *m*-AAA protease is regulated by SLP2 in a substrate-specific manner

Post-translationally protein levels are dependent on the stability or turnover of a protein and its degradation by the ubiquitin-proteosome or lysosomal proteolysis pathway as well as by mitochondrial proteases (Cooper, 2000; Doherty and Whitfield, 2014; Krämer et al., 2021). We hypothesized that SLP2 might regulate global mitochondrial protein turnover as described before for subunits of complex I and IV (Da Cruz et al., 2008a). A CHX chase verified our hypothesis for the tested proteins TMBIM5, DNAJC15 and APOO. The diminished protein stability observed in *SLP2*$^{-/-}$ could be rendered by the activation of proteases degrading these proteins. In accordance with this scenario, some of the identified proteins regulated post-transcriptionally, TMEM126B, TMBIM5 and DNAJC15, were indeed substrates of interacting proteases of SLP2. SLP2 closely interacts with YME1L in the SPY complex but so far, no function of this interaction has been identified. We hypothesized that SLP2 could scaffold YME1L to regulate its function. Therefore, we compared YME1L substrates with the proteomic data of SLP2 and found six putative YME1L substrates downregulated. Knockdown of YME1L in *SLP2*$^{-/-}$ however could not rescue the decrease of COX2 and ASS1 observed on WB. YME1L has been described to be heavily involved in mitochondrial metabolism. It is conceivable that while SPY exists also during steady-state conditions its requirement only becomes apparent upon certain stress conditions. Then SLP2 could potentially regulate YME1L to adapt its proteolytic activity to the cellular demand. This would be reminiscent of SiMH during which SLP2 is specifically required in stress conditions (Tondera et al., 2009). In addition, it is imaginable that a complete loss of YME1L could lead to different results compared to a transient knockdown. Substrates of PARL were not addressed in this thesis.

We also identified the *m*-AAA protease enriched with SLP2 and thus hypothesized that SLP2 could play a role in *m*-AAA regulation. Comparison of our proteomic data of *SLP2⁻/⁻* with a list of putative *m*-AAA substrates (Yvonne Lasarzewski, unpublished) resulted in seven proteins that were enriched or decreased upon SLP2 loss, including TMBIM5 and DNAJC15 (Patron et al., 2022). Indeed, TMBIM5 was not decreased anymore upon knockdown of SLP2 in *AFG3L2⁻/⁻* cells. On the other hand, the decrease of DNAJC15 could not be rescued to the same extent. This indicates that the *m*-AAA protease degrades TMBIM5 more upon loss of SLP2 in a substrate-specific manner. We propose that SLP2 specifically scaffolds TMBIM5 and protects it from degradation by the *m*-AAA protease. Double knockout cells for both the *m*-AAA protease and SLP2 could help explain the decrease of DNAJC15 more confidently.

In conclusion we found that SLP2 is not required for overall proteolysis mediated by the *i*- or *m*-AAA protease in our experimental conditions. We instead revealed that SLP2 specifically associates with TMBIM5 and protects it from degradation by the *m*-AAA protease. This is reminiscent of the regulation of acid-sensing ion channels by other stomatins (Price et al., 2004a). The reason for the association with YME1L in the SPY complex should be investigated further in the future.

4.3.2   SLP2 plays a role in 28S turnover

Based on our positive results on TMBIM5, DNAJC15, and APOO, we aimed to investigate the role of SLP2 on mitochondrial proteome turnover rates using an unbiased pulse-chase SILAC approach. This experiment verified the increased turnover of the above mentioned proteins and further revealed increased turnover rates of NDUFA4, TMEM126B, NDUFB1, SDHAF2, and SDHAF4 in *SLP2⁻/⁻*. These results strengthen the link of SLP2 to calcium homeostasis, import, cristae organization, and the respiratory chain but do not explain all of the major proteome changes observed in our whole cell proteome measurement. Instead, we surprisingly identified a new role of SLP2 in the turnover of the mitochondrial small ribosome as the pre-dominant group of regulated proteins. Several 28S proteins were turned over faster upon loss of SLP2 while 39S proteins remained unaffected. This could for example be due to ribosome assembly issues or 12S rRNA defects which will be discussed in 4.4. It is also imaginable that the effect is much more downstream and the consequence of impaired translation (see 4.4). The reason for the differential effect on the 28S and 39S ribosome

is however not clear. Our pulse-chase SILAC turnover approach does not match the expected results suggested by whole cell proteome data in combination with RNA sequencing for 28S proteins and the majority of other proteins. This means that not all decreased proteins that were independent from mRNA levels were turned over faster. The increased turnover of the 28S ribosome did not correlate with a change in steady-state protein or transcript levels. Possible explanations for this discrepancy will be explored in 4.3.2.1.

4.3.2.1   Technical limitations of the pulse-chase SILAC experiment

Protein turnover is the results of protein synthesis and degradation. Increased turnover can be caused by increased synthesis or degradation. Decreased turnover is accordingly a decrease in synthesis or degradation. The hypothesis is that a protein that is decreased on steady-state level but not on mRNA level should be the target of increased turnover by means of increased degradation. However, there are several limits to our approach that may explain the discrepancy between the hypothesis stated above and the observed protein turnover.

First, we compare steady-state protein level, mRNA level, and protein turnover but the experiments were not performed using the same cells batches and were performed on different days. Depending on the cell cycle and overall status of the cells the results could have been different. Moreover, the pulse-SILAC approach was also performed on an enriched mitochondrial fraction instead of total cell lysate. Additionally, limitations arise from the chase duration of 12 h for the pulse-SILAC chase. Some proteins which are rapidly turned over in *SLP2*$^{-/-}$ within that time and thus display decreased protein levels tended to display plateau lnRF values at later trial time points indicating that the first model kinetic assumption might be violated. This could for example be due to delayed mitochondrial import or label reutilization. Hence, the duration of the chase was restricted to 12 h but it is likely that proteins that are turned over at slower rates are not quantifiable in the assessed time frame and might be affected by the protein import capabilities of the cell under tested conditions. Thus, it is possible that post-transcriptionally or post-translationally regulated proteins in *SLP2*$^{-/-}$ would indeed show increased turnover in later time points. The opposite is imaginable for proteins that we identify as turned over faster but which do not show decreased protein levels despite unaltered mRNA. In this case, later time points might reveal that the turnover kinetic is faster at first but slows down with time. Additionally, studies have shown that newly

synthesized proteins are actually more likely to be degraded than older molecules (Schubert et al., 2000; Wheatley et al., 1980). This is especially true for proteins of the mitochondrial ribosome. When comparing the stability of mitoribosomal proteins in mitochondria vs. in mitoribosomes Bogenhagen *et al*. found that most mitoribosomal proteins are synthesized in excess and degraded if not assembled (Daniel Bogenhagen et al., 2018), which could explain the first-order kinetic discrepancy. This reveals another limitation of our study which cannot recognize the difference of free ribosomal proteins and those integrated into the ribosome. Therefore, it is possible that unassembled 28S proteins are rapidly turned over in *SLP2*$^{-/-}$ while assembled proteins are more stable which could mask an overall effect on assembly. Ribosomal assembly will be discussed in section 4.4.

In sum, we identified a novel role of SLP2 in the regulation of 28S turnover. Our experimental setup did not reveal a general effect on mitochondrial of SLP2 which could explain the various post-transcriptionally decreased proteins. However, our SILAC approach verified the proteomic results for TMBIM5, DNAJC15, and APOO and further revealed increased turnover rates of NDUFA4, TMEM126B, NDUFB1, SDHAF2, and SDHAF4 which lead to their destabilization. Adaptation of the conditions of our approach with simultaneous measurement of steady-state protein level, mRNA, and turnover over a longer time in n=3 could shed light on the remaining questions and strengthen the existing results.

4.4 SLP2 is required for efficient mitochondrial gene expression

Our finding of increased 28S ribosome turnover upon loss of SLP2 was supported by *in silico* gene essentiality analysis. The FIREWORKS platform found *SLP2* positively correlating with various genes involved in mitochondrial gene expression and especially translation. Most genes were related to ribosome assembly, maturation, termination or translation overall. We hypothesized that the destabilization of 28S proteins could be either cause or consequence of defective mitoribosome assembly. Instability of the mitochondrial ribosome or other alterations have been observed upon loss of many assembly cofactors. It was reported that mitoribosomes failed to assemble properly e.g. upon loss of Mpv17-like protein 2 (MPV17L2) (Dalla Rosa et al., 2014), TFB1M (Metodiev et al., 2009b) or ERAL1 (Uchiumi et al., 2010). Sucrose gradient ultracentrifugation however revealed no differences in the assembly of 28S, 39S or 55S ribosome in *SLP2*$^{-/-}$. Despite fully assembled ribosomes mitochondrial

translation of all proteins was decreased upon stable or transient loss of SLP2 and resulted in decreased levels of mitochondrial proteins, especially MT-CO2 and MT-CO3. This was not due to destabilization of newly translated proteins or a decrease of mtDNA or ribosomal RNA. In fact, mtDNA levels and the amount of the ribosomal RNAs *12S* and *16S* were increased in absence of SLP2. The increase in mtDNA was in line with significantly accumulated TFAM protein levels which have been shown to correlate with mtDNA amounts (Ekstrand et al., 2004). This was probably a compensatory mechanism due to the decrease in mitochondrial translation. Interestingly the mitochondrial mRNA transcript levels were decreased with exception of *MT-ND1, MT-ND2* and *MT-ND6*. The accumulation of *12S* and *16S* RNA proves that mitochondrial transcription itself works in *SLP2$^{-/-}$*. However, it is striking that the accumulated transcripts *12S*, *16S, MT-ND1* and *MT-ND2* on the heavy strand as well as *MT-ND6* on the light strand are all the first transcribed genes and all others after are decreased. The levels of mt-tRNAs are not altered. This suggests that transcription and tRNA excision is actually not affected but instead there might be a defect in either mRNA maturation and processing, stability or a feedback from decreased translation (Yeo et al., 2015). The increase of *12S*, *16S, MT-ND1*, *MT-ND2* and *MT-ND6* could suggest that mtDNA is transcribed but the products are degraded thus the first transcribed mRNAs still accumulate. The levels of mitochondrial RNA granule (MRG) proteins such as LRPPRC are not changed in *SLP2$^{-/-}$* but an effect of SLP2 on MRG organization is possible. MRGs are centers for mitochondrial RNA metabolism and ribosome assembly and have been observed in contact with the inner membrane (Antonicka and Shoubridge, 2015; Rey et al., 2020), presumably via MRPL45 as the membrane anchor together with OXA1L (Jourdain et al., 2016). The membrane association of the mitochondrial ribosome and thus perhaps also RNA granules has been suggested to be facilitated via CL as loss of CL led to a decreased interaction of OXA1L and the mitoribosome (Lee et al., 2020b). This raises the question if the effect of SLP2 on mitochondrial gene expression is due to its suggested role in mitochondrial CL compartmentalization (Christie et al., 2011a). Interestingly loss of SLP2 induced the transcriptional downregulation of several amino-acyl tRNA synthetases including DARS2 and EARS2 which have been implicated in diseases (Dogan et al., 2014; Rumyantseva et al., 2020; Talim et al., 2013). Their downregulated could be a consequence of inefficient translation but the aminoacylation status of tRNAs in *SLP2$^{-/-}$* was not investigated. Insufficient levels of aminoacyl-tRNA were shown to lead to

ribosome pausing which could further reduce translation efficiency (Ayyub et al., 2020). Another study identified an effect of SLP2 on mitochondrial gene expression in *SLP2*-/- T-cells which is in line with our results. They also did not observe differences in ribosome assembly but saw reduced translation and no effects on transcription (Mitsopoulos et al., 2017).
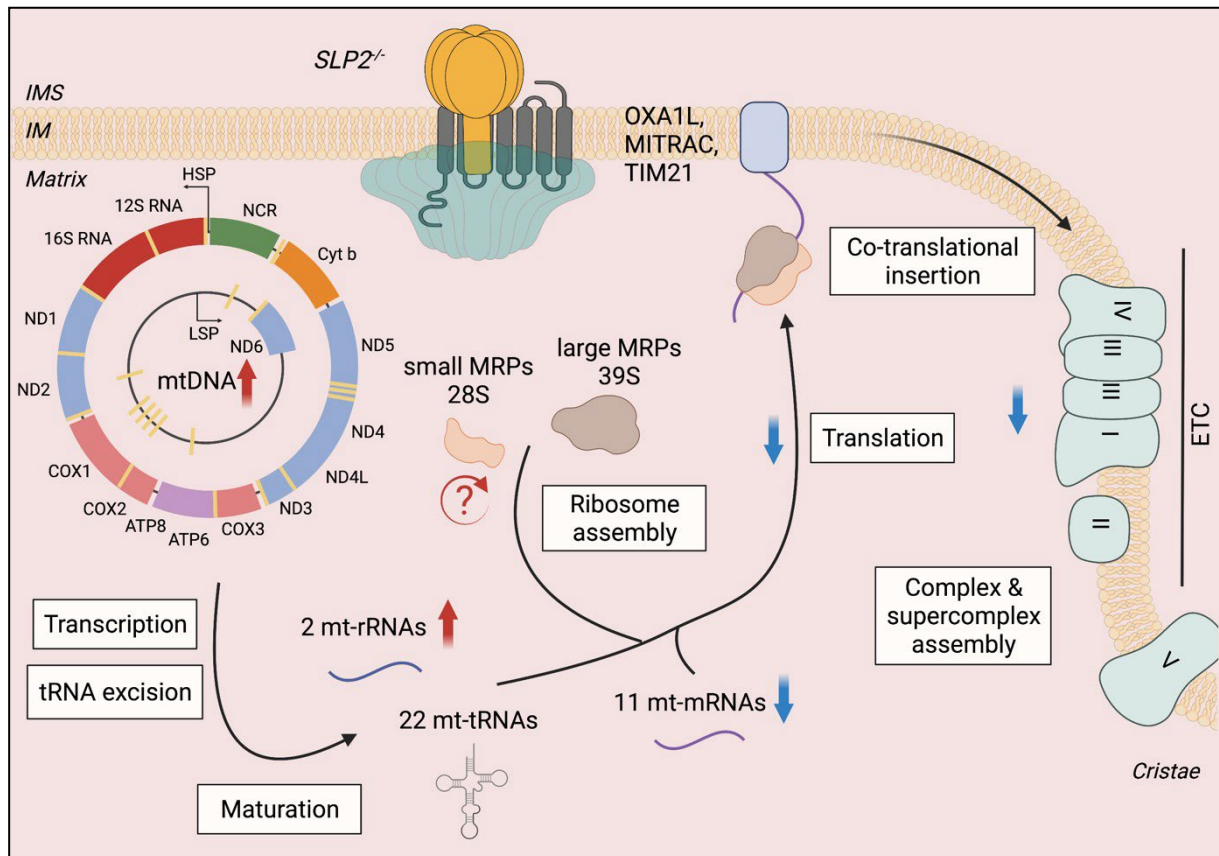
Figure 24: SLP2 is required for efficient mitochondrial gene expression
Schematic illustration of the effects on mitochondrial gene expression in *SLP2*-/-. Cells lacking SLP2 display a translation defect, increased 28S turnover and consequently reduced OXPHOS subunit proteins as well as transcript levels. The levels of mtDNA and rRNAs were increased.

Future experiments should explore the mechanism by which SLP2 affects mitochondrial gene expression. *In vitro* transcription and mRNA stability assays could elucidate whether SLP2 plays a role in transcription or mRNA processing. Co-localization by immunofluorescence microscopy could assess the organization of nucleoids, RNA granules and translating ribosomes (Zorkau et al., 2021) in absence of SLP2. Co-immunoprecipitation of OXA1L in *SLP2*-/- could reveal if membrane association of the mitochondrial ribosome is disturbed. Pulse-chase SILAC and subsequent sucrose gradient ultracentrifugation could offer more insights into the kinetics of mitochondrial ribosome assembly upon loss of SLP2. From our experiments

and those of other authors we know that SLP2 does not interact with mitoribosomes under normal conditions (3.1) but is in close proximity to them and other translation components (Antonicka et al., 2020; Li et al., 2021) and specifically interacts with sub-assembled or defective ribosomes (Busch et al., 2019). It would thus be interesting to find other conditions in which SLP2 binds to the ribosome or to catch a transient interaction e.g. during assembly by using cross-linking agents.

In conclusion we identified a novel role of SLP2 in mitochondrial gene expression. Loss of SLP2 led to decreased translation, mitochondrially encoded transcripts and proteins despite fully assembled ribosomes. We hypothesize that SLP2 supports efficient mitochondrial translation by an unknown mechanism and thus its absence affects mitochondrial small subunit turnover.
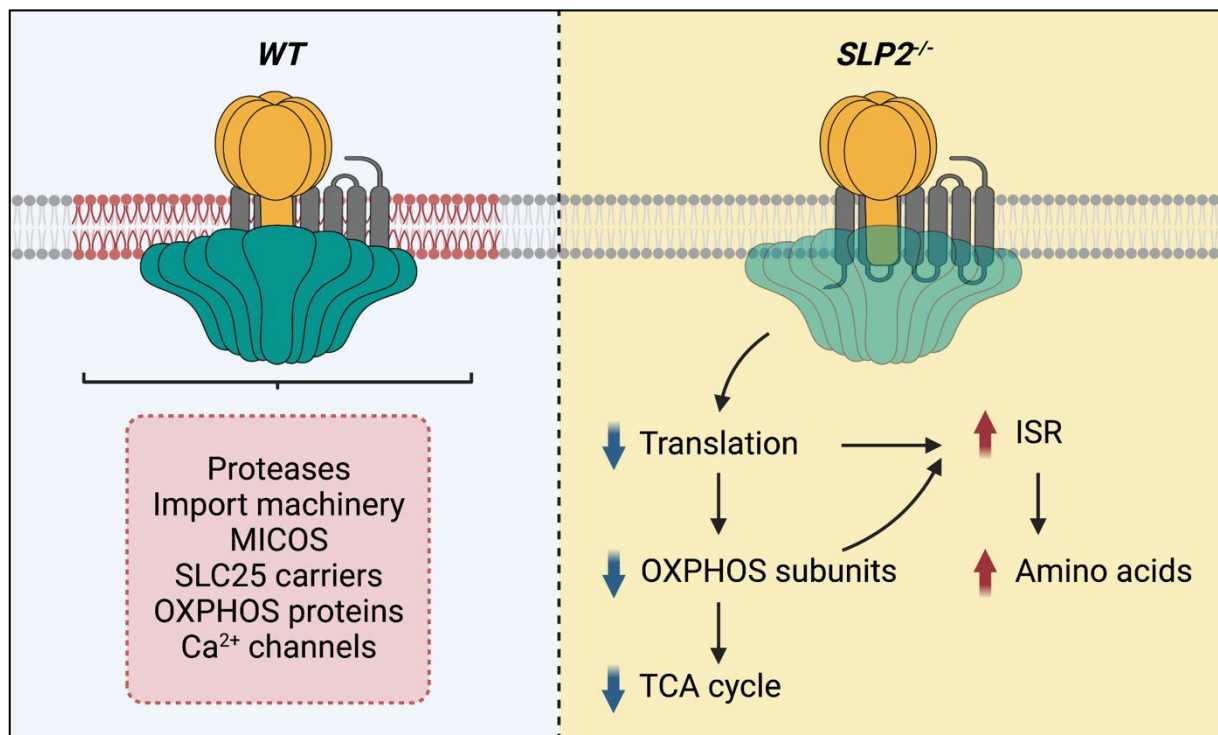
Figure 25: The functions of SLP2

Schematic illustration of the functions of SLP2 as identified in this thesis. SLP2 is a mitochondrial interaction platform and is required for efficient mitochondrial gene expression and thus the maintenance of OXPHOS protein levels. This mitochondrial dysfunction leads to a defective TCA cycle and an activation of the ISR. The red membrane patch indicates a CL domain and CL dependent proteins and complexes associated with SLP2.

4.5   Concluding remarks

This thesis identified SLP2 as an interaction platform in mitochondria with a novel role in mitochondrial gene expression. We found that SLP2 regulates the mitochondrial respiratory chain and its respiratory activity by supporting efficient mitochondrial translation. Remarkably, the mitochondrial dysfunction upon loss of SLP2 induces the integrated stress response as a secondary effect. We further identified a novel stabilizing role of SLP2 on several mitochondrial proteins as well as the 28S ribosome. In summary, our work connects SLP2 to essential aspects of mitochondrial function including previously unknown links to mitochondrial import, calcium maintenance and the MICOS complex and further elucidates its diverse scaffolding network. Future work should focus on the mechanism by which SLP2 regulates mitochondrial gene expression and investigate the role of cardiolipin in these phenotypes.

5   Appendix

Appendix Table 1: Putative interactors of SLP2

List of significantly (FDR < 5 %) enriched proteins in a co-immunoprecipitation experiment of HeLa *SLP2^{-/-}+SLP2^{FLAG}* vs. *SLP2^{-/-}*, n=4.

Gene name	Log2 ratio	-Log10 p value	MitoCarta3.0	MitoCarta3.0 Sublocalization
HAX1	8.76	4.55		
PARL	8.59	5.74	+	MIM
STOML2	7.92	4.69	+	MIM
TMEM160	6.46	6.42		
C19orf52	6.44	6.09	+	MIM
COX20	5.68	4.64	+	MIM
SFXN3	5.67	5.91	+	MIM
AGK	5.55	3.94	+	MIM
APOOL	5.27	2.89	+	MIM
YME1L1	5.25	6.52	+	MIM
SFXN1	4.99	3.61	+	MIM
STOML2	4.92	2.67		
TIMM23	4.88	4.53	+	MIM
APOO	4.85	3.24	+	MIM
MCU	4.79	3.74	+	MIM
TIMM17B	4.73	2.17	+	MIM
CLPB	4.39	5.73		
GHITM	4.37	3.77	+	MIM
TIMM9	4.28	5.17	+	MIM
OCIAD2	4.25	3.37	+	unknown
SDHB	4.24	3.26	+	MIM
TIMM22	4.17	4.01	+	MIM
COX15	4.07	3.07	+	MIM
HCCS	3.81	5.80	+	IMS
TIMM17A	3.79	4.00	+	MIM
TIMM10	3.70	6.21	+	MIM
QIL1	3.62	1.99	+	MIM
ATP5I	3.61	3.39	+	MIM
MPV17L2	3.54	5.74	+	MIM
ATP5L	3.49	3.19	+	MIM
CLPB	3.39	5.69	+	IMS
MTX2	3.32	4.83	+	MOM
TMEM126A	3.27	3.08	+	MIM
SLC25A24	3.26	2.72	+	MIM
DNAJC11	3.24	3.89	+	MOM
SLC25A3	3.23	5.99	+	MIM

Gene name	Log2 ratio	-Log10 p value	MitoCarta3.0	MitoCarta3.0 Sublocalization
ULK4	3.21	1.83		
SLC25A12	3.20	3.53	+	MIM
TIMM50	3.14	5.97	+	MIM
TIMM10B	3.09	2.66	+	MIM
SLC25A11	3.07	3.57	+	MIM
TIMM21	3.06	6.84	+	MIM
DNAJC30	3.05	3.03	+	MIM
PER2	3.03	1.37		
ATP5J2	3.01	2.87	+	MIM
TPRG1L	2.95	4.53		
SLC25A13	2.93	3.82	+	MIM
PHB	2.90	4.81	+	MIM
PHB2	2.80	4.60	+	MIM
PLGRKT	2.75	1.08	+	Membrane
ATPIF1	2.71	1.45	+	Matrix
TMEM65	2.63	1.75	+	MIM
SLC35A4	2.63	2.50		
IMMT	2.60	6.83	+	MIM
COX18	2.56	2.95	+	MIM
MTX1	2.55	4.32	+	MOM
C9orf89	2.52	3.47		
SLC25A10	2.52	3.72	+	MIM
GPD2	2.49	5.55	+	MIM
CHCHD2	2.48	4.39	+	IMS
LACTB	2.48	2.19	+	IMS
GSR	2.47	1.66	+	Matrix
SAMM50	2.46	5.32	+	MOM
CHCHD6	2.46	1.90	+	MIM
ATP5J	2.44	1.77	+	MIM
DNAJC15	2.43	2.00	+	MIM
IMMT	2.42	4.28		
CCSMST1	2.41	2.15	+	IMS
SLC25A1	2.37	4.31	+	MIM
CHCHD3	2.36	6.18	+	MIM
ATP5E	2.36	1.43	+	MIM
MT-CO2	2.35	4.63	+	MIM
MINOS1	2.32	1.71	+	MIM
PSIP1	2.30	2.47		
RAB13	2.24	2.26		
NCOA2	2.22	2.57		
CCDC127	2.20	1.64	+	Membrane
TOMM40	2.15	2.27	+	MOM

Gene name	Log2 ratio	-Log10 p value	MitoCarta3.0	MitoCarta3.0 Sublocalization
SLC25A5	2.14	4.95	+	MIM
HTRA2	2.14	2.13	+	MIM
SEPT6	2.13	4.20		
DNAJC19	2.10	1.20	+	MIM
ATP5H	2.09	4.00	+	MIM
CHCHD4	2.07	2.18	+	IMS
GRIA2	2.06	1.87		
PET100	2.04	3.74	+	MIM
CD55	2.04	2.24		
FAM162A	2.02	1.98	+	MIM
TIMMDC1	2.02	3.54	+	MIM
SQRDL	1.99	2.36	+	MIM
OCIAD1	1.97	4.28	+	MOM
RMND1	1.94	2.06	+	MIM
COX11	1.93	1.87	+	MIM
FAM210A	1.91	1.97	+	MIM
SLC25A6	1.90	3.64	+	MIM
MTX3	1.90	2.74	+	MOM
SPG7	1.88	2.01	+	MIM
RAB5A	1.86	1.67		
NDUFB5	1.85	2.99	+	MIM
RAB5C	1.80	7.40		
ATP5F1	1.80	4.67	+	MIM
ATP5B	1.80	3.44	+	MIM
AIFM1	1.77	4.66	+	MIM
NDUFB4	1.77	2.28	+	MIM
TMEM177	1.77	1.94	+	MIM
CYC1	1.76	6.48		
PDIA4	1.75	1.36		
ABCB10	1.73	1.98	+	MIM
LGALS1	1.73	1.51		
SURF1	1.72	2.10	+	MIM
ATP5A1	1.72	4.46	+	MIM
UQCRQ	1.71	2.45	+	MIM
GLRX5	1.70	1.78	+	Matrix
COX5A	1.69	2.90	+	MIM
C1QBP	1.67	2.88	+	Matrix
PAM16	1.67	3.31	+	MIM
ANXA1	1.67	1.97		
PRDX5	1.67	4.79	+	Matrix
ATP5D	1.65	3.19	+	MIM
OPA3	1.63	1.60	+	MOM

Gene name	Log2 ratio	-Log10 p value	MitoCarta3.0	MitoCarta3.0 Sublocalization
ABCB7	1.62	1.41	+	MIM
ATP5O	1.62	4.21	+	MIM
ALDOC	1.61	1.21		
TOMM22	1.59	3.14	+	MOM
COX7A2	1.58	2.15	+	MIM
SQSTM1	1.57	1.83		
EHHADH	1.56	2.37	+	unknown
TIMM8B	1.56	3.86	+	MIM
CTSB	1.56	1.11		
NNT	1.55	2.64	+	MIM
IGHG2	1.53	1.57		
COX4I1	1.52	4.77	+	MIM
RAB14	1.51	3.99		
RSL1D1	1.51	1.51		
LARP4	1.49	1.50		
HIBADH	1.48	1.30	+	Matrix
ATP5C1	1.47	3.31	+	MIM
COX5B	1.47	2.64	+	MIM
SLC1A5	1.46	1.42		
NDUFB8	1.46	2.81	+	MIM
EXOG	1.43	1.69	+	MIM
TSFM	1.43	1.52	+	Matrix
MYO19	1.42	4.21	+	MOM
RPLP1	1.40	1.48		
C2orf47	1.39	3.68	+	Matrix
IGKV	1.39	1.86		
TIMM8A	1.35	2.19	+	MIM
RAB1B	1.35	2.01		
PISD	1.33	1.36	+	MIM
NDUFAF3	1.31	1.55	+	MIM
PGK1	1.30	1.49		
NDUFB11	1.29	3.52	+	MIM
NDUFB3	1.28	2.34	+	MIM
OXA1L	1.28	1.51	+	MIM
NDUFV1	1.28	2.52	+	MIM
ARMC1	1.28	2.77		
UQCRB	1.28	3.21	+	MIM
MTCH2	1.27	2.41	+	MOM
ALDOA	1.27	1.48		
SMIM8	1.26	1.80	+	MOM
NDUFB9	1.26	4.27	+	MIM
RAB9A	1.26	2.37		

Gene name	Log2 ratio	-Log10 p value	MitoCarta3.0	MitoCarta3.0 Sublocalization
NDUFC2	1.26	2.60	+	MIM
AFG3L2	1.25	4.14	+	MIM
SF3B1	1.23	1.23		
NDUFA2	1.23	2.14	+	MIM
NDUFS3	1.22	3.04	+	MIM
SDHA	1.21	4.75	+	MIM
MT-ND4	1.20	3.50	+	MIM
NDUFA13	1.19	2.74	+	MIM
CYB5B	1.18	1.84	+	MOM
RAB10	1.18	2.55		
PGAM5	1.17	2.44	+	MOM
TMEM11	1.17	2.97	+	MIM
ADCK5	1.17	2.67	+	unknown
NDUFB10	1.16	4.47	+	MIM
NDUFA3	1.16	1.25	+	MIM
SLC25A19	1.16	1.63	+	MIM
NDUFS2	1.14	4.59	+	MIM
TRIP6	1.13	1.63		
MARCH5	1.12	1.19	+	MOM
UQCRC1	1.12	5.74	+	MIM
NDUFB6	1.11	1.96	+	MIM
UQCRH	1.11	2.69	+	MIM
OPA1	1.08	3.07	+	MIM
NDUFS1	1.07	4.90	+	MIM
ACO2	1.06	1.27	+	Matrix
AHCY	1.05	1.85		
HMGN1	1.05	1.25		
EIF5A	1.04	1.66		
RAB2A	1.03	2.26		
DSG2	1.02	1.22		
UQCR10	1.01	1.64	+	MIM
NDUFA5	1.00	3.08	+	MIM

Appendix Table 2: Proteome and transcriptome changes upon loss of SLP2

List of significantly (FDR < 10 %) altered mitochondrial proteins in a whole cell proteome experiment of HeLa *WT* vs. *SLP2*$^{-/-}$, n=5. Comparison with whole cell RNA sequencing data, HeLa *WT* vs. *SLP2*$^{-/-}$, n=3. Labeled as mRNA independent if the adjusted p value of transcriptome data was either < 0.1 or opposite to the proteome data.

	Proteomics		Transcriptomics		
Proteins	Log2 ratio	-Log10 p value	Log2 ratio	-Log10 Adj. P value	mRNA independent
COQ6	-5.65	1.37	-0.04	0.05	+
OPA1	-3.19	2.32	-0.32	2.83	-
NME4	-2.80	1.60	-0.44	3.26	-
DNAJC15	-1.48	3.43	-0.02	0.02	+
COX7C	-1.43	2.46	0.17	1.24	+
MT-CO3	-1.13	1.25	-0.32	12.68	-
GHITM	-1.12	7.16	-0.12	0.79	+
APOO	-1.00	2.95	-0.10	0.16	+
SLC25A29	-1.00	1.40	0.15	0.47	+
ANGEL2	-0.97	1.30	-0.53	2.10	-
PYCR2	-0.84	3.08	-0.41	3.25	-
TMEM126B	-0.84	1.78	-0.04	0.06	+
MARC1	-0.84	3.68	-0.44	8.35	-
ISCA2	-0.79	2.42	-0.11	0.15	+
MTCH1	-0.76	1.97	-0.56	30.58	-
TMEM65	-0.76	2.42	-0.17	0.51	+
TIMM17B	-0.76	1.57	-0.55	4.08	-
ABCD1	-0.75	6.48	-0.76	15.58	-
CARS2	-0.73	5.62	-0.47	6.54	-
NNT	-0.73	5.20	-0.80	20.22	-
APOOL	-0.72	2.98	-0.77	4.90	-
PPOX	-0.69	2.64	-0.04	0.05	+
AIFM1	-0.69	4.78	-0.71	16.28	-
ENDOG	-0.65	2.31	-0.12	0.19	+
SUCLA2	-0.62	5.66	-0.61	3.32	-
SLC25A5	-0.61	2.56	-0.46	16.57	-
SDHAF4	-0.59	2.84	-0.06	0.10	+
COA6	-0.59	2.09	-0.02	0.03	+
NT5DC3	-0.59	4.35	-0.54	2.30	-
HSDL1	-0.58	1.68	-0.08	0.12	+
COX17	-0.58	1.73	-0.03	0.03	+
ABCB7	-0.58	3.78	-0.52	4.00	-
SDHAF2	-0.56	2.83	0.28	0.60	+
COQ8B	-0.55	1.70	-0.04	0.05	+
NDUFA4	-0.55	2.13	-0.19	0.75	+

Proteins	Proteomics		Transcriptomics		
	Log2 ratio	-Log10 p value	Log2 ratio	-Log10 Adj. P value	mRNA independent
STOM	-0.55	4.03	-0.04	0.17	+
TRMT2B	-0.54	2.60	-0.52	2.75	-
COX7A2	-0.54	1.93	0.03	0.05	+
CHCHD2	-0.53	3.20	-0.08	0.52	+
IARS2	-0.53	6.24	-0.42	10.33	-
HSD17B10	-0.52	5.64	-0.43	6.42	-
ARMCX3	-0.51	4.45	-0.35	2.52	-
NADK2	-0.51	3.43	-0.29	1.66	-
COX7A2L	-0.50	1.87	-0.01	0.02	+
SDHA	-0.48	5.24	-0.33	10.48	-
FLAD1	-0.48	3.53	-0.46	2.74	-
VWA8	-0.47	3.45	-0.25	0.60	+
ZADH2	-0.47	2.01	0.19	0.75	+
IDH2	-0.45	5.63	-0.10	0.34	+
ACADSB	-0.43	2.03	-0.30	0.73	+
SLC25A4	-0.42	2.02	-0.24	0.51	+
GSTK1	-0.42	4.00	-0.22	1.04	+
DARS2	-0.42	2.99	-0.26	1.57	-
RMDN3	-0.41	2.44	-0.07	0.13	+
TFB2M	-0.40	3.34	-0.08	0.13	+
SND1	-0.40	2.89	0.02	0.05	+
NDUFB1	-0.40	2.39	-0.04	0.05	+
MRPL49	-0.37	2.44	0.12	0.29	+
OXCT1	-0.37	3.81	-0.19	2.13	-
FH	-0.37	3.62	-0.55	10.30	-
MT-CO2	-0.37	2.36	-0.23	4.80	-
FUNDC2	-0.36	3.43	0.09	0.22	+
PC	-0.36	5.61	0.21	1.02	+
ALDH18A1	-0.35	4.02	-0.20	1.71	-
GOLPH3	-0.35	2.78	-0.24	2.82	-
MRM1	-0.29	3.17	-0.35	1.00	+
ALDH1B1	-0.27	4.03	-1.04	29.90	-
TFAM	0.27	3.39	-0.01	0.02	+
AK4	0.28	3.24	-0.38	1.70	+
ALDH3A2	0.29	3.32	0.34	1.84	-
AIFM2	0.30	3.23	-0.08	0.15	+
SHMT2	0.31	3.33	0.12	0.68	+
AKR7A2	0.33	3.20	-0.01	0.02	+
SOD2	0.36	3.04	-0.24	1.59	+
MTFP1	0.36	2.27	-0.01	0.01	+
HINT1	0.36	2.39	0.07	0.26	+

Proteins	Proteomics		Transcriptomics		
	Log2 ratio	-Log10 p value	Log2 ratio	-Log10 Adj. P value	mRNA independent
ECHDC1	0.39	3.84	-0.05	0.09	+
GLS	0.42	4.41	-0.02	0.02	+
DCXR	0.43	2.28	-0.05	0.08	+
MACROD1	0.43	2.99	0.07	0.10	+
RPIA	0.43	1.99	-0.03	0.04	+
SOD1	0.45	2.00	-0.19	1.76	+
MRPS17	0.47	1.93	-0.01	0.01	+
HPDL	0.50	5.80	-0.15	0.29	+
GRPEL2	0.58	2.12	0.05	0.06	+
MCU	0.59	3.59	0.12	0.22	+
GARS	0.64	8.29	-0.11	0.56	+
OCIAD2	0.73	1.92	-0.04	0.04	+
ACOT7	0.77	2.25	0.02	0.03	+
PCK2	0.78	5.59	0.18	0.30	+
SLC30A9	0.78	1.68	-0.14	0.38	+
TXNRD1	0.85	6.45	0.31	6.82	-
PISD	0.90	2.44	0.12	0.25	+
PARL	1.13	1.55	-0.09	0.15	+
MPC1	1.28	1.43	-0.49	1.86	+
LYPLAL1	2.24	1.69	-0.26	0.50	+

Appendix Table 3: Mitochondrial protein turnover upon loss of SLP2

List of the top 40 mitochondrial proteins with increased turnover and the top 40 mitochondrial proteins with decreased turnover in HeLa *WT* vs. *SLP2*$^{-/-}$, n=1. lnRF values and slope difference indicated.

Gene name	Slope difference *WT-SLP2*$^{-/-}$	*WT*				*SLP2*$^{-/-}$			
		lnRF 2 h	lnRF 4 h	lnRF 8 h	lnRF 12 h	lnRF 2 h	lnRF 4 h	lnRF 8 h	lnRF 12 h
STOML2	0.07	-0.07	-0.14	-0.30	-0.48	-0.34	-0.67	-0.78	-1.77
DNAJC15	0.06	-0.36	-0.69	-1.28	-2.00	-0.54	-1.07	-2.07	-2.79
MRM2	0.06	-0.30	-0.49	-0.85	-1.00	-0.29	-0.48	-1.08	-1.60
MRPS11	0.06	-0.20	-0.29	-0.42	-0.57	-0.14	-0.31	-0.64	-1.12
GHITM	0.06	-0.24	-0.50	-1.08	-1.67	-0.52	-1.14	-2.04	-2.47
FTH1	0.05	-0.13	-0.22	-0.49	-0.74	-0.14	-0.35	-0.90	-1.34
CHCHD1	0.05	-0.26	-0.38	-0.76	-1.20	-0.34	-0.59	-1.24	-1.77
COX16	0.04	-0.16	-0.30	-0.48	-0.51	-0.12	-0.35	-0.60	-0.94
MRPS18C	0.04	-0.30	-0.47	-0.52	-0.64	-0.36	-0.55	-0.81	-1.08
NDUFA4	0.04	-0.28	-0.45	-0.91	-1.38	-0.34	-0.62	-1.29	-1.86

Gene name	Slope difference *WT-SLP2⁻ᐟ⁻*	WT				SLP2⁻ᐟ⁻			
		lnRF 2 h	lnRF 4 h	lnRF 8 h	lnRF 12 h	lnRF 2 h	lnRF 4 h	lnRF 8 h	lnRF 12 h
MRPS24	0.03	-0.30	-0.50	-0.74	-0.92	-0.40	-0.69	-1.12	-1.33
RSAD1	0.03	-0.32	-0.64	-1.00	-1.17	-0.31	-0.66	-0.85	-1.44
PCBD2	0.03	-0.32	-0.42	-0.46	-0.69	-0.14	-0.24	-0.50	-0.78
AURKAIP1	0.03	-0.27	-0.46	-0.76	-0.98	-0.35	-0.66	-1.10	-1.35
APOO	0.03	-0.10	-0.14	-0.28	-0.43	-0.11	-0.21	-0.42	-0.71
TMEM126B	0.03	-0.34	-0.42	-0.66	-0.93	-0.44	-0.61	-0.98	-1.30
ATPSCKMT	0.03	-0.20	-0.38	-0.44	-0.68	-0.24	-0.35	-0.64	-0.93
OXSM	0.02	-0.52	-0.59	-0.77	-0.88	-0.22	-0.28	-0.42	-0.85
NDUFA6	0.02	-0.19	-0.39	-0.70	-1.05	-0.25	-0.43	-0.89	-1.27
ATP5MPL	0.02	-0.14	-0.29	-0.55	-0.66	-0.18	-0.42	-0.68	-0.98
PDSS1	0.02	-0.22	-0.44	-1.03	-1.53	-0.27	-0.61	-1.22	-1.85
SLC25A36	0.02	-0.06	-0.19	-0.50	-0.68	-0.04	-0.18	-0.58	-0.87
COX18	0.02	-0.20	-0.25	-0.43	-0.63	-0.12	-0.39	-0.60	-0.83
MRPS12	0.02	-0.20	-0.33	-0.51	-0.77	-0.17	-0.36	-0.63	-0.96
SNAP29	0.02	-0.16	-0.19	-0.49	-0.69	-0.16	-0.27	-0.53	-0.95
NDUFC2	0.02	-0.14	-0.28	-0.47	-0.62	-0.17	-0.34	-0.60	-0.87
CBR4	0.02	-0.24	-0.34	-0.35	-0.50	-0.22	-0.30	-0.47	-0.65
ALKBH1	0.02	-0.18	-0.28	-0.43	-0.51	-0.30	-0.40	-0.67	-0.80
SLC25A44	0.02	-0.05	-0.14	-0.31	-0.43	-0.05	-0.20	-0.41	-0.64
ARMCX2	0.02	-0.33	-0.52	-1.09	-1.81	-0.40	-0.73	-1.37	-2.10
MRPS14	0.02	-0.12	-0.24	-0.36	-0.55	-0.17	-0.32	-0.51	-0.79
MRPS10	0.02	-0.20	-0.36	-0.65	-0.87	-0.23	-0.43	-0.83	-1.10
NDUFA11	0.02	-0.10	-0.18	-0.27	-0.46	-0.14	-0.23	-0.47	-0.65
MRPS35	0.02	-0.23	-0.44	-0.73	-0.97	-0.28	-0.50	-0.87	-1.20
MRPS15	0.02	-0.15	-0.29	-0.56	-0.78	-0.16	-0.38	-0.68	-0.97
MTG2	-0.01	-0.23	-0.60	-1.22	-1.85	-0.23	-0.56	-1.27	-1.68
MIPEP	-0.01	-0.13	-0.21	-0.40	-0.61	-0.09	-0.18	-0.31	-0.54
GPAM	-0.01	-0.14	-0.33	-0.76	-1.04	-0.12	-0.26	-0.65	-0.88
MRPL27	-0.01	-0.12	-0.22	-0.42	-0.68	-0.10	-0.20	-0.41	-0.59
UQCRB	-0.01	-0.21	-0.30	-0.53	-0.69	-0.21	-0.27	-0.44	-0.60
BCKDHB	-0.01	-0.08	-0.08	-0.26	-0.44	-0.04	-0.11	-0.12	-0.32
GADD45GIP1	-0.01	-0.37	-0.46	-0.70	-0.87	-0.30	-0.39	-0.53	-0.68
GRHPR	-0.01	-0.10	-0.18	-0.30	-0.54	-0.09	-0.16	-0.30	-0.38
TIMMDC1	-0.01	-0.22	-0.40	-0.88	-1.34	-0.17	-0.34	-0.74	-1.15
ACAD8	-0.01	-0.14	-0.25	-0.58	-0.68	-0.11	-0.17	-0.30	-0.55

Gene name	Slope difference *WT-SLP2⁻/⁻*	*WT*				*SLP2⁻/⁻*			
		lnRF 2 h	lnRF 4 h	lnRF 8 h	lnRF 12 h	lnRF 2 h	lnRF 4 h	lnRF 8 h	lnRF 12 h
NDUFS6	-0.01	-0.47	-0.71	-1.06	-1.47	-0.59	-0.73	-1.22	-1.55
PTRH1	-0.01	-0.18	-0.25	-0.47	-0.72	-0.06	-0.21	-0.36	-0.52
NDUFA2	-0.01	-0.16	-0.30	-0.58	-1.12	-0.19	-0.31	-0.61	-0.99
NME6	-0.01	-0.08	-0.15	-0.34	-0.51	-0.08	-0.16	-0.23	-0.40
NIT2	-0.01	-0.13	-0.12	-0.23	-0.44	-0.06	-0.09	-0.16	-0.33
PDHA1	-0.01	-0.11	-0.22	-0.43	-0.67	-0.08	-0.15	-0.33	-0.49
PRKACA	-0.01	-0.16	-0.33	-0.46	-0.92	-0.19	-0.26	-0.52	-0.74
QTRT1	-0.01	-0.20	-0.34	-0.51	-0.73	-0.12	-0.31	-0.38	-0.52
TRMT1	-0.02	-0.22	-0.39	-0.61	-0.84	-0.22	-0.43	-0.63	-0.76
STOM	-0.02	-0.15	-0.31	-0.66	-1.00	-0.13	-0.25	-0.53	-0.80
TOP3A	-0.02	-0.26	-0.42	-0.72	-1.15	-0.28	-0.36	-0.69	-0.98
POLG	-0.02	-0.16	-0.31	-0.59	-0.83	-0.18	-0.29	-0.53	-0.71
FASTKD3	-0.02	-0.23	-0.39	-0.66	-1.00	-0.22	-0.41	-0.62	-0.88
NFU1	-0.02	-0.22	-0.36	-0.64	-0.89	-0.24	-0.29	-0.55	-0.71
TOMM20	-0.02	-0.18	-0.39	-0.70	-1.08	-0.13	-0.29	-0.60	-0.87
MTX1	-0.02	-0.11	-0.22	-0.46	-0.73	-0.09	-0.17	-0.35	-0.53
RPUSD4	-0.02	-0.14	-0.27	-0.50	-0.92	-0.14	-0.23	-0.59	-0.77
ISCA1	-0.02	-0.13	-0.26	-0.66	-1.03	-0.12	-0.25	-0.54	-0.84
COA1	-0.02	-0.04	-0.12	-0.42	-0.58	-0.09	-0.11	-0.25	-0.45
COQ5	-0.02	-0.22	-0.48	-0.76	-1.29	-0.17	-0.34	-0.70	-1.05
MRPL34	-0.02	-0.12	-0.20	-0.45	-0.87	-0.12	-0.23	-0.40	-0.78
MUL1	-0.02	-0.31	-0.55	-0.89	-1.48	-0.39	-0.58	-0.92	-1.32
AMACR	-0.02	-0.15	-0.28	-0.70	-0.94	-0.15	-0.29	-0.53	-0.76
ENDOG	-0.03	-0.37	-0.68	-1.58	-2.26	-0.41	-0.75	-1.28	-2.10
CHCHD2	-0.03	-0.98	-1.85	-2.94	-3.57	-1.08	-2.14	-3.06	-3.37
PLD6	-0.04	-0.43	-0.61	-1.31	-1.77	-0.31	-0.52	-1.00	-1.32
YRDC	-0.04	-0.19	-0.31	-0.73	-1.14	-0.27	-0.39	-0.74	-0.83
SDHC	-0.07	-0.10	-0.19	-0.89	-1.05	-0.09	-0.18	-0.31	-0.48
MYO19	-0.08	-0.14	-0.32	-1.02	-2.35	-0.14	-0.23	-0.97	-1.42
MRPL51	-0.10	-0.13	-0.34	-0.44	-1.74	-0.17	-0.37	-0.54	-0.71

6   List of abbreviations

AARS	aminoacyl-tRNA synthetase
ACOT7	cytosolic acyl coenzyme A thioester hydrolase
ADP	adenosine diphosphate
AEX-MS	anion-exchange chromatography mass spectrometry
AFG3L2	AFG3-like protein 2
AGK	acylglycerol Kinase
ANT1/SLC25A4	ADP/ATP translocase 1
APOO	MICOS complex subunit MIC26
APOOL	MICOS complex subunit MIC27
ASIC	acid-sensing ion channel
ASNS	asparagine synthetase
ASS1	argininosuccinate synthase
ATF3, ATF4	cyclic AMP-dependent transcription factor 3, 4
ATP	adenosine triphosphate
BN-PAGE	blue native polyacrylamide gel electrophoresis
C12ORF65/MTFR	mitochondrial translation release factor in rescue
C1QBP	complement component 1 Q subcomponent-binding protein
CHCHD1	coiled-coil-helix-coiled-coil-helix domain-containing protein 1
CHCHD2	coiled-coil-helix-coiled-coil-helix domain-containing protein 2
CHX	cycloheximide
CL	cardiolipin
CLPP	caseinolytic peptidase subunit P
CLPX	caseinolytic peptidase subunit X
COA3/MITRAC12	cytochrome c oxidase assembly factor 3 homolog
CODAS	cerebral, ocular, dental, auricular, skeletal anomalies
COQ6	ubiquinone biosynthesis monooxygenase
COX16	cytochrome c oxidase assembly protein COX16 homolog
COX7A2	cytochrome c oxidase subunit 7A2
COX7A2L	cytochrome c oxidase subunit 7A-related protein
COX7C	cytochrome c oxidase subunit 7C
CRLS1/CLS1	cardiolipin synthase
DDX28	probable ATP-dependent RNA helicase DDX28
DELE1	DAP3 Binding Cell Death Enhancer 1
DHX30	ATP-dependent RNA helicase DHX30
DIABLO/SMAC	diablo IAP-binding mitochondrial protein
DIBMA	diisobutylene-maleic acid
DNAJC15	DnaJ homolog subfamily C member 15
DNAJC19	DnaJ homolog subfamily C member 19
DRP1/DNM1L	Dynamin-related protein 1
ECAR	extracellular acidification rate
EIF2α	eukaryotic translation initiation factor 2
ELAC2/RNase Z	elaC ribonuclease Z 2
EM	electron microscopy
EMRE	essential MCU regulator
ENDOG	endonuclease G
ER	endoplasmic reticulum
ERAL1	GTPase Era
FASTK	FAST kinase domain-containing protein
FCS	fetal calf serum
FDR	false discovery rate
FH	fumarate hydratase
FLOT1/2	flotillin
FTH1	ferritin
FtsH	ATP-dependent zinc metalloprotease

GRPEL2	GrpE protein homolog 2
GTPBP5/6/7/10	mitochondrial ribosome-associated GTPase 2
H	heavy
HRI	heme-regulated inhibitor
HSD17B10/MRPP2	hydroxysteroid 17-beta dehydrogenase 10
HSP	hereditary spastic paraplegia
HSP	heavy-strand promoter
HSP7	hereditary spastic paraplegia
HTRA2	high temperature requirement mitochondrial serine protease A2)/Omi
IBM	Inner boundary membrane
ICT1	peptidyl-tRNA hydrolase ICT1
IDH2	isocitrate dehydrogenase
IF2/3	initiation factor 2/3
IM	inner mitochondrial membrane
IMMP	inner membrane protease
IMS	intermembrane space
IP3	inositol 1,4,5-trisphosphate
ISCA2	iron-sulfur cluster assembly 2 homolog
ISR	integrated stress response
L	light
LACTB	β-lactamase-like protein
LC3	microtubule-associated proteins 1A/1B light chain 3C
LHON	Leber's hereditary optic neuropathy
LONP1	Lon protease homolog
LRPPRC	leucine-rich penticopeptiderich domain containing protein
LSP	light-strand promoter
LYPLAL1	lysophospholipase-like protein 1
MCU	mitochondrial calcium uniporter
MEC2	mechanosensory protein 2
MELAS	mitochondrial Encephalopathy, Lactic Acidosis, and Stroke-like episodes
MEP	microsomal endopeptidase
MFN1, 2	mitofusin 1, 2
MIA	mitochondrial IMS import and assembly
MIC60/25/19/10/13	MICOS complex subunit 60/25/19/10/13
MICOS	mitochondrial contact site and cristae organizing system
MICU1/2	calcium uptake protein 1/2
MITRAC	mitochondrial translation regulation assembly intermediate of cytochrome c oxidase
MPC1	mitochondrial pyruvate carrier 1
MPC1/2	mitochondrial carrier proteins like pyruvate carrier
MPP	mitochondrial processing peptidase
MPV17L2	Mpv17-like protein 2
MRM1/2/3	rRNA methyltransferase 1/2/3
mRNA	messenger RNA
MRPL32	39S ribosomal protein L32
MTCH1	mitochondrial carrier homolog 1
mtDNA	mitochondrial DNA
MTERF1	transcription termination factor 1
mtLSU	39S mitochondrial large ribosomal subunit
MTPAP	mitochondrial poly(A) polymerase
MTRF1	peptide chain release factor 1
mtSSU	28S mitochondrial small ribosomal subunit
MUL1	mitochondrial ubiquitin ligase activator of NFKB 1
MYO19	unconventional myosin-XIX

NCLX	mitochondrial Na+/Ca2+ exchanger
NDUFB1	NADH dehydrogenase [ubiquinone] 1 beta subcomplex subunit 1
NME4	nucleoside diphosphate kinase
NSUN4	5-methylcytosine rRNA methyltransferase NSUN4
OCIAD2	complex III assembly factor OCIA domain-containing protein 2
OCR	oxygen consumption rate
OM	outer mitochondrial membrane
OMA1	metalloendopeptidase OMA1
OPA1	optic atrophy protein 1
OXPHOS	oxidative phosphorylation
p62	ubiquitin-binding protein p62
PA	phosphatidic acid
PAM	presequence translocase-associated motor
PARL	presenilin-associated rhomboid-like protease
PBS	phosphate buffered saline
PC	phosphatidylcholine
PC	pyruvate carboxylase
PE	phosphatidylethanolamine
PG	phosphatidylglycerol
PGAM5	phosphoglycerate mutase 5
PGS1	phosphatidylglycerol phosphate synthase
PHB1/2	prohibitin 1/2
PI	phosphatidylinositol
PINK1	PTEN induced putative kinase 1
PISD	phosphatidylserine decarboxylase proenzyme
PITRM1	pitrilysin metallopeptidase 1
PLD6	mitochondrial cardiolipin hydrolase
PNPT1	polynucleotide phosphorylase
POLG	DNA polymerase γ
POLRMT	DNA-directed RNA polymerase
PRELID1	PRELI domain-containing protein 1
PRORP	protein-only RNase P catalytic subunit
PS	phosphatidylserine
PSAT1	phosphoserine aminotransferase
PTPMT1	protein-tyrosine phosphatase mitochondrial 1
PVDF	polyvinylidene fluoride
PYCR2	pyrroline-5-carboxylate reductase 2
RMND1	required for meiotic nuclear division protein 1 homolog
ROS	reactive oxygen species
RPUSD4	pseudouridylate synthase
rRNA	ribosomal RNA
SAM	sorting and assembly machinery
SCA28	spinocerebellar ataxia
SDHA	succinate dehydrogenase [ubiquinone] flavoprotein subunit
SDHAF2	succinate dehydrogenase assembly factor 2
SDHAF4	succinate dehydrogenase assembly factor 4
SDHC	succinate dehydrogenase cytochrome b560
SDS-PAGE	sodium dodecyl sulfate polyacrylamide gel electrophoresis
SiMH	stress-induced mitochondrial hyperfusion
SLC25A29	mitochondrial basic amino acids transporter
SLC30A9	zinc transporter 9
SLC7A11	cystine/glutamate transporter
SLIRP	stem–loop interacting RNA-binding protein
SLP2	stomatin-like protein 2

SMA	styrene maleic acid copolymer
SOD1	superoxide dismutase [Cu-Zn]
SOD2	superoxide dismutase [Mn]
SPFH	stomatin/prohibitin/flotillin/HflK/C
SPG7	paraplegin
SSBP	single-stranded DNA-binding protein
STARD7	steroidogenic acute regulatory protein (StAR)-related lipid transfer protein 7
SUCLA2	succinate--CoA ligase [ADP-forming] subunit beta
SURF1	surfeit locus protein 1
SUV3	ATP-dependent RNA helicase SUPV3L1
TAMM41	phosphatidate cytidylyltransferase
TAZ	tafazzin
TCA	tricarboxylic acid cycle
TCA	trichloroacetic acid
TEFM	transcription elongation factor
TFAM	transcription factor A
TFB1M	dimethyladenosine transferase 1
TFB2M	mitochondrial transcription factor B2
TIM22	translocase of the inner membrane 22
TIM23	translocase of the inner membrane 23
TIMM17A	mitochondrial import inner membrane translocase subunit Tim17-A
TIMM21	translocase of the inner mitochondrial membrane 21
TMBIM5	transmembrane BAX inhibitor motif-containing protein 5
TMEM126B	complex I assembly factor
TOM	translocase of outer membrane
TRM2B	tRNA (uracil-5-)-methyltransferase homolog B
TRM61B	tRNA (adenine(58)-N(1))-methyltransferase
TRMT10C/MRPP1	tRNA methyltransferase 10C
tRNA	transfer RNA
TRNT1	tRNA nucleotidyl transferase 1
TSFM	mitochondrial elongation factor Ts
TTC19	tetratricopeptide repeat protein 19
TWNK	Twinkle mtDNA helicase
TXNRD1	thioredoxin reductase 1
YME1L	ATP-dependent zinc metalloprotease YME1L1
YRDC	threonylcarbamoyl-AMP synthase

7   Zusammenfassung

Mitochondrien sind essenzielle Organellen, die diverse Funktionen in eukaryotischen Zellen ausführen. Sie besitzen eine komplexe Ultrastruktur mit zwei Membranen und mehreren Kompartimenten, in denen mitochondrial- und nukleär-kodierte Proteine die mitochondriale Funktion organisiert sicherstellen. Diese Organisation innerhalb der Mitochondrien wird durch verschiedene Proteine, Proteinkomplexe und Lipide gewährleistet, z.B. durch die ATP Synthase, Atmungsketten(super)komplexe, den MICOS-Komplex, die GTPase OPA1, das Lipid Cardiolipin und die Strukturproteine PHB, PHB2 und SLP2.

Im Gegensatz zum essenziellen Prohibitin-Komplex ist wenig über die Funktionen von SLP2 bekannt. Zusammen mit den Proteasen PARL und YME1L bildet SLP2 den sogenannten SPY-Komplex an der inneren Membran der Mitochondrien und beeinflusst die Superkomplexbildung der Atmungskette, den mitochondrialen Calciumhaushalt sowie die stressbedingte Hyperfusion von Mitochondrien.

Um die Funktion von SLP2 in Mitochondrien zu verstehen, wurden Immunpräzipitationsexperimente von SLP2 sowie verschiedene Omics-Ansätze und biochemische Versuche in humanen *SLP2* defizienten Zellen durchgeführt. Dabei fanden wir heraus, dass SLP2 mit einer Vielzahl von mitochondrialen Proteinen interagiert und somit fest mit dem mitochondrialen Netzwerk verknüpft ist. Ein Verlust von SLP2 führte zu einer globalen Beeinträchtigung der mitochondrialen Genexpression und einem gesteigerten Umsatz der kleinen mitochondrialen ribosomalen Untereinheit sowie der Interaktoren TMBIM5, DNAJC15 und APOO. Dieser Genexpressionsdefekt führte zu Defiziten der Atmungskette und sekundär zu einer Beeinträchtigung des Krebszyklus sowie einer Stressreaktion der Zelle, der integrierten Stressantwort.

Insgesamt zeigen wir in dieser Arbeit, dass SLP2 für die optimale Funktion von Mitochondrien mittels der Genexpression benötigt wird. Des Weiteren decken wir zuvor unbekannte Zusammenhänge von SLP2 im Bereich der Proteinimportmachinerie, des MICOS-Komplex und der Atmungskette auf und entdecken proteinspezifische Effekte von SLP2 auf den Umsatz von Proteinen. Somit zeigen wir mit den Ergebnissen dieser Arbeit, dass SLP2 ein wichtiges Strukturprotein mit diversen Einflüssen auf die mitochondriale Funktion ist.

9   Eidesstattliche Erklärung

Erklärung zur Dissertation
gemäß der Promotionsordnung vom 12. März 2020

Diese Erklärung muss in der Dissertation enthalten sein.
(*This version must be included in the doctoral thesis*)

„Hiermit versichere ich an Eides statt, dass ich die vorliegende Dissertation selbstständig und ohne die Benutzung anderer als der angegebenen Hilfsmittel und Literatur angefertigt habe. Alle Stellen, die wörtlich oder sinngemäß aus veröffentlichten und nicht veröffentlichten Werken dem Wortlaut oder dem Sinn nach entnommen wurden, sind als solche kenntlich gemacht. Ich versichere an Eides statt, dass diese Dissertation noch keiner anderen Fakultät oder Universität zur Prüfung vorgelegen hat; dass sie - abgesehen von unten angegebenen Teilpublikationen und eingebundenen Artikeln und Manuskripten - noch nicht veröffentlicht worden ist sowie, dass ich eine Veröffentlichung der Dissertation vor Abschluss der Promotion nicht ohne Genehmigung des Promotionsausschusses vornehmen werde. Die Bestimmungen dieser Ordnung sind mir bekannt. Darüber hinaus erkläre ich hiermit, dass ich die Ordnung zur Sicherung guter wissenschaftlicher Praxis und zum Umgang mit wissenschaftlichem Fehlverhalten der Universität zu Köln gelesen und sie bei der Durchführung der Dissertation zugrundeliegenden Arbeiten und der schriftlich verfassten Dissertation beachtet habe und verpflichte mich hiermit, die dort genannten Vorgaben bei allen wissenschaftlichen Tätigkeiten zu beachten und umzusetzen. Ich versichere, dass die eingereichte elektronische Fassung der eingereichten Druckfassung vollständig entspricht."

Teilpublikationen:

Datum, Name und Unterschrift

25.08.2022, Britta Ingrid Gudrun Thewes

11 References

Acín-Pérez, R., Fernández-Silva, P., Peleato, M.L., Pérez-Martos, A., and Enriquez, J.A. (2008). Respiratory active mitochondrial supercomplexes. Mol. Cell *32*, 529–539. https://doi.org/10.1016/J.MOLCEL.2008.10.021.

Adant, I., Bird, M., Decru, B., Windmolders, P., Wallays, M., de Witte, P., Rymen, D., Witters, P., Vermeersch, P., Cassiman, D., et al. (2022). Pyruvate and uridine rescue the metabolic profile of OXPHOS dysfunction. Mol. Metab. *63*, 101537. https://doi.org/10.1016/J.MOLMET.2022.101537.

Ahola, S., Mejías, P.R., Hermans, S., Chandragiri, S., Giavalisco, P., Nolte, H., and Langer, T. (2022). OMA1-mediated integrated stress response protects against ferroptosis in mitochondrial cardiomyopathy. Cell Metab. *0*. https://doi.org/10.1016/J.CMET.2022.08.017.

Ahting, U., Thieffry, M., Engelhardt, H., Hegerl, R., Neupert, W., and Nussberger, S. (2001). Tom40, the pore-forming component of the protein-conducting TOM channel in the outer membrane of mitochondria. J. Cell Biol. *153*, 1151–1160. https://doi.org/10.1083/JCB.153.6.1151.

Akepati, V.R., Müller, E.C., Otto, A., Strauss, H.M., Portwich, M., and Alexander, C. (2008). Characterization of OPA1 isoforms isolated from mouse tissues. J. Neurochem. *106*, 372–383. https://doi.org/10.1111/J.1471-4159.2008.05401.X.

Aloni, Y., and Attardi, G. (1971). Expression of the mitochondrial genome in HeLa cells. II. Evidence for complete transcription of mitochondrial DNA. J. Mol. Biol. *55*, 251–267. https://doi.org/10.1016/0022-2836(71)90195-1.

Amici, D.R., Jackson, J.M., Truica, M.I., Smith, R.S., Abdulkadir, S.A., and Mendillo, M.L. (2021). FIREWORKS: a bottom-up approach to integrative coessentiality network analysis. Life Sci. Alliance *4*. https://doi.org/10.26508/LSA.202000882.

Anand, R., Wai, T., Baker, M.J., Kladt, N., Schauss, A.C., Rugarli, E., and Langer, T. (2014). The i-AAA protease YME1L and OMA1 cleave OPA1 to balance mitochondrial fusion and fission. J. Cell Biol. *204*, 919–929. https://doi.org/10.1083/JCB.201308006.

Anand, R., Kondadi, A.K., Meisterknecht, J., Golombek, M., Nortmann, O., Riedel, J., Peifer-Weiß, L., Brocke-Ahmadinejad, N., Schlütermann, D., Stork, B., et al. (2020). MIC26 and MIC27 cooperate to regulate cardiolipin levels and the landscape of OXPHOS complexes. Life Sci. Alliance *3*. https://doi.org/10.26508/LSA.202000711.

Ande, S.R., Nguyen, K.H., Grégoire Nyomba, B.L., and Mishra, S. (2016). Prohibitin-induced, obesity-associated insulin resistance and accompanying low-grade

inflammation causes NASH and HCC. Sci. Rep. https://doi.org/10.1038/srep23608.

Anderson, S., Bankier, A.T., Barrell, B.G., De Bruijn, M.H.L., Coulson, A.R., Drouin, J., Eperon, I.C., Nierlich, D.P., Roe, B.A., Sanger, F., et al. (1981). Sequence and organization of the human mitochondrial genome. Nature *290*, 457–465. https://doi.org/10.1038/290457A0.

Antonicka, H., and Shoubridge, E.A. (2015). Mitochondrial RNA Granules Are Centers for Posttranscriptional RNA Processing and Ribosome Biogenesis. Cell Rep. *10*, 920–932. https://doi.org/10.1016/J.CELREP.2015.01.030.

Antonicka, H., Choquet, K., Lin, Z., Gingras, A., Kleinman, C.L., and Shoubridge, E.A. (2017). A pseudouridine synthase module is essential for mitochondrial protein synthesis and cell viability. EMBO Rep. *18*, 28–38. https://doi.org/10.15252/EMBR.201643391.

Antonicka, H., Lin, Z.Y., Janer, A., Aaltonen, M.J., Weraarpachai, W., Gingras, A.C., and Shoubridge, E.A. (2020). A High-Density Human Mitochondrial Proximity Interaction Network. Cell Metab. *32*, 479-497.e9. https://doi.org/10.1016/J.CMET.2020.07.017.

Ayyub, S.A., Gao, F., Lightowlers, R.N., and Chrzanowska-Lightowlers, Z.M. (2020). Rescuing stalled mammalian mitoribosomes - What can we learn from bacteria? J. Cell Sci. *133*. https://doi.org/10.1242/JCS.231811/224718.

Backes, S., Hess, S., Boos, F., Woellhaf, M.W., Gödel, S., Jung, M., Mühlhaus, T., and Herrmann, J.M. (2018). Tom70 enhances mitochondrial preprotein import efficiency by binding to internal targeting sequences. J. Cell Biol. *217*, 1369–1382. https://doi.org/10.1083/JCB.201708044.

Baker, T.A., and Sauer, R.T. (2012). ClpXP, an ATP-powered unfolding and protein-degradation machine. Biochim. Biophys. Acta *1823*, 15–28. https://doi.org/10.1016/J.BBAMCR.2011.06.007.

Banci, L., Bertini, I., Cefaro, C., Ciofi-Baffoni, S., Gallo, A., Martinelli, M., Sideris, D.P., Katrakili, N., and Tokatlidis, K. (2009). MIA40 is an oxidoreductase that catalyzes oxidative protein folding in mitochondria. Nat. Struct. Mol. Biol. 2009 162 *16*, 198–206. https://doi.org/10.1038/nsmb.1553.

Bao, X.R., Ong, S.E., Goldberger, O., Peng, J., Sharma, R., Thompson, D.A., Vafai, S.B., Cox, A.G., Marutani, E., Ichinose, F., et al. (2016). Mitochondrial dysfunction remodels one-carbon metabolism in human cells. Elife *5*. https://doi.org/10.7554/ELIFE.10575.

Bar-Yaacov, D., Frumkin, I., Yashiro, Y., Chujo, T., Ishigami, Y., Chemla, Y., Blumberg, A., Schlesinger, O., Bieri, P., Greber, B., et al. (2016). Mitochondrial 16S rRNA Is Methylated by tRNA Methyltransferase TRMT61B in All Vertebrates. PLoS Biol. *14*. https://doi.org/10.1371/JOURNAL.PBIO.1002557.

Berger, K.H., and Yaffe, M.P. (1998). Prohibitin family members interact genetically with mitochondrial inheritance components in Saccharomyces cerevisiae. Mol. Cell. Biol. *18*, 4043–4052. .

Bhattacharyya, T., Karnezis, A.N., Murphy, S.P., Hoang, T., Freeman, B.C., Phillips, B., and Morimoto, R.I. (1995). Cloning and subcellular localization of human mitochondrial hsp70. J. Biol. Chem. *270*, 1705–1710. https://doi.org/10.1074/JBC.270.4.1705.

Blanchi, C., Genova, M.L., Castelli, G.P., and Lenaz, G. (2004). The mitochondrial respiratory chain is partially organized in a supercomplex assembly: kinetic evidence using flux control analysis. J. Biol. Chem. *279*, 36562–36569. https://doi.org/10.1074/JBC.M405135200.

Blum, T.B., Hahn, A., Meier, T., Davies, K.M., and Kühlbrandt, W. (2019). Dimers of mitochondrial ATP synthase induce membrane curvature and self-assemble into rows. Proc. Natl. Acad. Sci. U. S. A. *116*, 4250–4255. https://doi.org/10.1073/PNAS.1816556116/SUPPL_FILE/PNAS.1816556116.SM02. MP4.

Boczonadi, V., and Horvath, R. (2014). Mitochondria: Impaired mitochondrial translation in human disease. Int. J. Biochem. Cell Biol. *48*, 77. https://doi.org/10.1016/J.BIOCEL.2013.12.011.

Bonn, F., Tatsuta, T., Petrungaro, C., Riemer, J., and Langer, T. (2011). Presequence-dependent folding ensures MrpL32 processing by the m-AAA protease in mitochondria. EMBO J. *30*, 2545–2556. https://doi.org/10.1038/EMBOJ.2011.169.

Borges, J.C., Fischer, H., Craievich, A.F., Hansen, L.D., and Ramos, C.H.I. (2003). Free Human Mitochondrial GrpE Is a Symmetric Dimer in Solution *. J. Biol. Chem. *278*, 35337–35344. https://doi.org/10.1074/JBC.M305083200.

Borowski, L.S., Dziembowski, A., Hejnowicz, M.S., Stepien, P.P., and Szczesny, R.J. (2013). Human mitochondrial RNA decay mediated by PNPase-hSuv3 complex takes place in distinct foci. Nucleic Acids Res. *41*, 1223–1240. https://doi.org/10.1093/NAR/GKS1130.

Bota, D.A., and Davies, K.J.A. (2016). Mitochondrial Lon protease in human disease

and aging: Including an etiologic classification of Lon-related diseases and disorders. Free Radic. Biol. Med. *100*, 188–198. https://doi.org/10.1016/J.FREERADBIOMED.2016.06.031.

Brandt, T., Mourier, A., Tain, L.S., Partridge, L., Larsson, N.G., and Kühlbrandt, W. (2017). Changes of mitochondrial ultrastructure and function during ageing in mice and Drosophila. Elife *6*. https://doi.org/10.7554/ELIFE.24662.

Bray, N.L., Pimentel, H., Melsted, P., and Pachter, L. (2016). Near-optimal probabilistic RNA-seq quantification. Nat. Biotechnol. *34*, 525–527. https://doi.org/10.1038/NBT.3519.

Browman, D.T., Hoegg, M.B., and Robbins, S.M. (2007). The SPFH domain-containing proteins: more than lipid raft markers. Trends Cell Biol. https://doi.org/10.1016/j.tcb.2007.06.005.

Brown, A., Amunts, A., Bai, X.C., Sugimoto, Y., Edwards, P.C., Murshudov, G., Scheres, S.H.W., and Ramakrishnan, V. (2014). Structure of the large ribosomal subunit from human mitochondria. Science *346*, 718–722. https://doi.org/10.1126/SCIENCE.1258026.

Bruderer, R., Bernhardt, O.M., Gandhi, T., Miladinović, S.M., Cheng, L.Y., Messner, S., Ehrenberger, T., Zanotelli, V., Butscheid, Y., Escher, C., et al. (2015). Extending the limits of quantitative proteome profiling with data-independent acquisition and application to acetaminophen-treated three-dimensional liver microtissues. Mol. Cell. Proteomics *14*, 1400–1410. https://doi.org/10.1074/MCP.M114.044305.

Busch, J.D., Cipullo, M., Atanassov, I., Bratic, A., Silva Ramos, E., Schöndorf, T., Li, X., Pearce, S.F., Milenkovic, D., Rorbach, J., et al. (2019). MitoRibo-Tag Mice Provide a Tool for In Vivo Studies of Mitoribosome Composition. Cell Rep. *29*, 1728-1738.e9. https://doi.org/10.1016/J.CELREP.2019.09.080.

Cao, W., Zhang, B., Liu, Y., Li, H., Zhang, S., Fu, L., Niu, Y., Ning, L., Cao, X., Liu,Z., et al. (2007). High-level SLP-2 expression and HER-2/neu protein expression are associated with decreased breast cancer patient survival. Am. J. Clin. Pathol. *128*, 430–436. https://doi.org/10.1309/C6X54HRB580EP2NQ.

Cao, W., Zhang, B., Ding, F., Zhang, W., Sun, B., and Liu, Z. (2013). Expression of SLP-2 Was Associated with Invasion of Esophageal Squamous Cell Carcinoma. PLoS One https://doi.org/10.1371/journal.pone.0063890.

Cardenas-Rodriguez, M., Chatzi, A., and Tokatlidis, K. (2018). Iron-sulfur clusters: from metals through mitochondria biogenesis to disease. J. Biol. Inorg. Chem. *23*, 509–

520. https://doi.org/10.1007/S00775-018-1548-6.

Carlile, T.M., Rojas-Duran, M.F., Zinshteyn, B., Shin, H., Bartoli, K.M., and Gilbert, W. V. (2014). Pseudouridine profiling reveals regulated mRNA pseudouridylation in yeast and human cells. Nature *515*, 143–146. https://doi.org/10.1038/NATURE13802.

Casari, G., De Fusco, M., Ciarmatori, S., Zeviani, M., Mora, M., Fernandez, P., De Michele, G., Filla, A., Cocozza, S., Marconi, R., et al. (1998). Spastic paraplegia and OXPHOS impairment caused by mutations in paraplegin, a nuclear-encoded mitochondrial metalloprotease. Cell *93*, 973–983. https://doi.org/10.1016/S0092-8674(00)81203-9.

Chacinska, A., Koehler, C.M., Milenkovic, D., Lithgow, T., and Pfanner, N. (2009). Importing Mitochondrial Proteins: Machineries and Mechanisms. Cell *138*, 628–644. https://doi.org/10.1016/J.CELL.2009.08.005.

Chance, B., Estabrook, R.W., and Lee, C.P. (1963). Electron Transport in the Oxysome. Science *140*, 379–380. https://doi.org/10.1126/SCIENCE.140.3565.379-C.

Chen, H.-W., Rainey, R.N., Balatoni, C.E., Dawson, D.W., Troke, J.J., Wasiak, S., Hong, J.S., McBride, H.M., Koehler, C.M., Teitell, M.A., et al. (2006). Mammalian polynucleotide phosphorylase is an intermembrane space RNase that maintains mitochondrial homeostasis. Mol. Cell. Biol. *26*, 8475–8487. https://doi.org/10.1128/MCB.01002-06.

Chojnacka, K.J., Elancheliyan, P., Mussulini, B.H.M., Mohanraj, K., Callegari, S., Gosk, A., Banach, T., Góral, T., Szczepanowska, K., Rehling, P., et al. (2022). Ovarian carcinoma immunoreactive antigen-like protein 2 (OCIAD2) is a novel complex III-specific assembly factor in mitochondria. Mol. Biol. Cell *33*, ar29. https://doi.org/10.1091/MBC.E21-03-0143/ASSET/IMAGES/LARGE/MBC-33-AR29-G006.JPEG.

Christie, D.A., Lemke, C.D., Elias, I.M., Chau, L.A., Kirchhof, M.G., Li, B., Ball, E.H., Dunn, S.D., Hatch, G.M., and Madrenas, J. (2011a). Stomatin-Like Protein 2 Binds Cardiolipin and Regulates Mitochondrial Biogenesis and Function. Mol. Cell. Biol. https://doi.org/10.1128/mcb.05393-11.

Christie, D.A., Lemke, C.D., Elias, I.M., Chau, L.A., Kirchhof, M.G., Li, B., Ball, E.H., Dunn, S.D., Hatch, G.M., and Madrenas, J. (2011b). Stomatin-Like Protein 2 Binds Cardiolipin and Regulates Mitochondrial Biogenesis and Function. Mol. Cell. Biol. https://doi.org/10.1128/MCB.05393-11.

Cipullo, M., Pearce, S.F., Lopez Sanchez, I.G., Gopalakrishna, S., Krüger, A.,

Schober, F., Busch, J.D., Li, X., Wredenberg, A., Atanassov, I., et al. (2021). Human GTPBP5 is involved in the late stage of mitoribosome large subunit assembly. Nucleic Acids Res. *49*, 354–370. https://doi.org/10.1093/NAR/GKAA1131.

Cogliati, S., Calvo, E., Loureiro, M., Guaras, A.M., Nieto-Arellano, R., Garcia-Poyatos, C., Ezkurdia, I., Mercader, N., Vázquez, J., and Enriquez, J.A. (2016). Mechanism of super-assembly of respiratory complexes III and IV. Nat. 2016 5397630 *539*, 579–582. https://doi.org/10.1038/nature20157.

Cooper, G.M. (2000). Protein Degradation. In The Cell: A Molecular Approach. 2nd Edition., (Sinauer Associates), p.

Cox, J., and Mann, M. (2008). MaxQuant enables high peptide identification rates, individualized p.p.b.-range mass accuracies and proteome-wide protein quantification. Nat. Biotechnol. *26*, 1367–1372. https://doi.org/10.1038/NBT.1511.

Cox, J., Neuhauser, N., Michalski, A., Scheltema, R.A., Olsen, J. V., and Mann, M. (2011). Andromeda: a peptide search engine integrated into the MaxQuant environment. J. Proteome Res. *10*, 1794–1805. https://doi.org/10.1021/PR101065J.

Da Cruz, S., Parone, P.A., Gonzalo, P., Bienvenut, W. V., Tondera, D., Jourdain, A., Quadroni, M., and Martinou, J.C. (2008a). SLP-2 interacts with prohibitins in the mitochondrial inner membrane and contributes to their stability. Biochim. Biophys. Acta - Mol. Cell Res. *1783*, 904–911. https://doi.org/10.1016/J.BBAMCR.2008.02.006.

Da Cruz, S., Parone, P.A., Gonzalo, P., Bienvenut, W. V., Tondera, D., Jourdain, A., Quadroni, M., and Martinou, J.C. (2008b). SLP-2 interacts with prohibitins in the mitochondrial inner membrane and contributes to their stability. Biochim. Biophys. Acta - Mol. Cell Res. *1783*, 904–911. https://doi.org/10.1016/j.bbamcr.2008.02.006.

Da Cruz, S., De Marchi, U., Frieden, M., Parone, P.A., Martinou, J.C., and Demaurex, N. (2010). SLP-2 negatively modulates mitochondrial sodium-calcium exchange. Cell Calcium https://doi.org/10.1016/j.ceca.2009.10.005.

D'Souza, A.R., and Minczuk, M. (2018). Mitochondrial transcription and translation: overview. Essays Biochem. *62*, 309. https://doi.org/10.1042/EBC20170102.

Dalla Rosa, I., Durigon, R., Pearce, S.F., Rorbach, J., Hirst, E.M.A., Vidoni, S., Reyes, A., Brea-Calvo, G., Minczuk, M., Woellhaf, M.W., et al. (2014). MPV17L2 is required for ribosome assembly in mitochondria. Nucleic Acids Res. *42*, 8500–8515. https://doi.org/10.1093/NAR/GKU513.

Daniel Bogenhagen, A.F., Ostermeyer-Fay, A.G., Haley, J.D., and Garcia-Diaz Correspondence, M. (2018). Kinetics and Mechanism of Mammalian Mitochondrial

Ribosome Assembly. CellReports *22*, 1935–1944. https://doi.org/10.1016/j.celrep.2018.01.066.

Darshi, M., Mendiola, V.L., Mackey, M.R., Murphy, A.N., Koller, A., Perkins, G.A., Ellisman, M.H., and Taylor, S.S. (2011). ChChd3, an inner mitochondrial membrane protein, is essential for maintaining Crista integrity and mitochondrial function. J. Biol. Chem. *286*, 2918–2932. https://doi.org/10.1074/JBC.M110.171975/ATTACHMENT/9CED306E-AF4F-42C2-B71B-22ECA6627B3A/MMC1.PDF.

Daumke, O., and Lewin, G.R. (2022). SPFH protein cage — one ring to rule them all. Cell Res. *32*, 117–118. https://doi.org/10.1038/S41422-021-00605-7.

Dekker, P.J.T., Keil, P., Rassow, J., Maarse, A.C., Pfanner, N., and Meijer, M. (1993). Identification of MIM23, a putative component of the protein import machinery of the mitochondrial inner membrane. FEBS Lett. *330*, 66–70. https://doi.org/10.1016/0014-5793(93)80921-G.

Delettre, C., Lenaers, G., Griffoin, J.M., Gigarel, N., Lorenzo, C., Belenguer, P., Pelloquin, L., Grosgeorge, J., Turc-Carel, C., Perret, E., et al. (2000). Nuclear gene OPA1, encoding a mitochondrial dynamin-related protein, is mutated in dominant optic atrophy. Nat. Genet. *26*, 207–210. https://doi.org/10.1038/79936.

Dennerlein, S., Rozanska, A., Wydro, M., Chrzanowska-Lightowlers, Z.M.A., and Lightowlers, R.N. (2010). Human ERAL1 is a mitochondrial RNA chaperone involved in the assembly of the 28S small mitochondrial ribosomal subunit. Biochem. J. *430*, 551. https://doi.org/10.1042/BJ20100757.

Dennerlein, S., Poerschke, S., Oeljeklaus, S., Wang, C., Richter-Dennerlein, R., Sattmann, J., Bauermeister, D., Hanitsch, E., Stoldt, S., Langer, T., et al. (2021). Defining the interactome of the human mitochondrial ribosome identifies SMIM4 and TMEM223 as respiratory chain assembly factors. Elife *10*. https://doi.org/10.7554/ELIFE.68213.

Deshwal, S., Fiedler, K.U., Langer, T., Langer, T., and Langer, T. (2020). Mitochondrial Proteases: Multifaceted Regulators of Mitochondrial Plasticity. Https://Doi.Org/10.1146/Annurev-Biochem-062917-012739 *89*, 501–528. https://doi.org/10.1146/ANNUREV-BIOCHEM-062917-012739.

Dogan, S.A., Pujol, C., Maiti, P., Kukat, A., Wang, S., Hermans, S., Senft, K., Wibom, R., Rugarli, E.I., and Trifunovic, A. (2014). Tissue-Specific Loss of DARS2 Activates Stress Responses Independently of Respiratory Chain Deficiency in the Heart. Cell

Metab. *19*, 458–469. https://doi.org/10.1016/J.CMET.2014.02.004.

Doherty, M.K., and Whitfield, P.D. (2014). Proteomics moves from expression to turnover: update and future perspective. Http://Dx.Doi.Org/10.1586/Epr.11.19 *8*, 325–334. https://doi.org/10.1586/EPR.11.19.

Dudek, J. (2017). Role of cardiolipin in mitochondrial signaling pathways. Front. Cell Dev. Biol. *5*, 90. https://doi.org/10.3389/FCELL.2017.00090/BIBTEX.

Dutta, D., Ali, N., Banerjee, E., Singh, R., Naskar, A., Paidi, R.K., and Mohanakumar, K.P. (2018). Low Levels of Prohibitin in Substantia Nigra Makes Dopaminergic Neurons Vulnerable in Parkinson's Disease. Mol. Neurobiol. *55*, 804–821. https://doi.org/10.1007/S12035-016-0328-Y.

Eiyama, A., Aaltonen, M.J., Nolte, H., Tatsuta, T., and Langer, T. (2021). Disturbed intramitochondrial phosphatidic acid transport impairs cellular stress signaling. J. Biol. Chem. *296*. https://doi.org/10.1016/J.JBC.2021.100335/ATTACHMENT/C9797456-4170-45B9-BCEC-CD0963D0CE16/MMC5.XLSX.

Ekstrand, M.I., Falkenberg, M., Rantanen, A., Park, C.B., Gaspari, M., Hultenby, K., Rustin, P., Gustafsson, C.M., and Larsson, N.G. (2004). Mitochondrial transcription factor A regulates mtDNA copy number in mammals. Hum. Mol. Genet. *13*, 935–944. https://doi.org/10.1093/HMG/DDH109.

Fernández-Silva, P., Enriquez, J.A., and Montoya, J. (2003). Replication and transcription of mammalian mitochondrial DNA. Exp. Physiol. *88*, 41–56. https://doi.org/10.1113/EPH8802514.

Fessler, E., Eckl, E.M., Schmitt, S., Mancilla, I.A., Meyer-Bender, M.F., Hanf, M., Philippou-Massier, J., Krebs, S., Zischka, H., and Jae, L.T. (2020). A pathway coordinated by DELE1 relays mitochondrial stress to the cytosol. Nature *579*, 433. https://doi.org/10.1038/S41586-020-2076-4.

Formosa, L.E., Muellner-Wong, L., Reljic, B., Sharpe, A.J., Jackson, T.D., Beilharz, T.H., Stojanovski, D., Lazarou, M., Stroud, D.A., and Ryan, M.T. (2020). Dissecting the Roles of Mitochondrial Complex I Intermediate Assembly Complex Factors in the Biogenesis of Complex I. Cell Rep. *31*, 107541. https://doi.org/10.1016/J.CELREP.2020.107541.

Freya, T.G., and Mannellab, C.A. (2000). The internal structure of mitochondria. Trends Biochem. Sci. *25*, 319–324. https://doi.org/10.1016/S0968-0004(00)01609-1.

Ghosh, S., Ball, W.B., Madaris, T.R., Srikantan, S., Madesh, M., Mootha, V.K., and Gohil, V.M. (2020). An essential role for cardiolipin in the stability and function of the

mitochondrial calcium uniporter. Proc. Natl. Acad. Sci. U. S. A. *117*, 16383–16390. https://doi.org/10.1073/PNAS.2000640117/SUPPL_FILE/PNAS.2000640117.SAPP.PDF.

Gray, H., and Wongs, T.W. (1992). Purification and Identification of Subunit Structure of the Human Mitochondrial DNA Polymerase. J. Biol. Chem. *267*, 5835–5841. https://doi.org/10.1016/S0021-9258(18)42629-4.

Greber, B.J., Boehringer, D., Leibundgut, M., Bieri, P., Leitner, A., Schmitz, N., Aebersold, R., and Ban, N. (2014). The complete structure of the large subunit of the mammalian mitochondrial ribosome. Nature *515*, 283–286. https://doi.org/10.1038/NATURE13895.

Greber, B.J., Bieri, P., Leibundgut, M., Leitner, A., Aebersold, R., Boehringer, D., and Ban, N. (2015). Ribosome. The complete structure of the 55S mammalian mitochondrial ribosome. Science *348*, 303–308. https://doi.org/10.1126/SCIENCE.AAA3872.

Guerrero-Castillo, S., Baertling, F., Kownatzki, D., Wessels, H.J., Arnold, S., Brandt, U., and Nijtmans, L. (2017). The Assembly Pathway of Mitochondrial Respiratory Chain Complex I. Cell Metab. *25*, 128–139. https://doi.org/10.1016/J.CMET.2016.09.002.

Guo, X., Aviles, G., Liu, Y., Tian, R., Unger, B.A., Lin, Y.H.T., Wiita, A.P., Xu, K., Correia, M.A., and Kampmann, M. (2020). Mitochondrial stress is relayed to the cytosol by an OMA1-DELE1-HRI pathway. Nature *579*, 427. https://doi.org/10.1038/S41586-020-2078-2.

Guo, Y., Cheong, N.E., Zhang, Z.J., De Rose, R., Deng, Y., Farber, S.A., Fernandes-Alnemri, T., and Alnemri, E.S. (2004). Tim50, a component of the mitochondrial translocator, regulates mitochondrial integrity and cell death. J. Biol. Chem. *279*, 24813–24825. https://doi.org/10.1074/JBC.M402049200.

Gustafsson, C.M., Falkenberg, M., and Larsson, N.-G. (2016). Maintenance and Expression of Mammalian Mitochondrial DNA. Annu. Rev. Biochem. *85*, 133–160. https://doi.org/10.1146/annurev-biochem-060815-014402.

Hammarsund, M., Wilson, W., Corcoran, M., Merup, M., Einhorn, S., Grandér, D., and Sangfelt, O. (2001). Identification and characterization of two novel human mitochondrial elongation factor genes, hEFG2 and hEFG1, phylogenetically conserved through evolution. Hum. Genet. *109*, 542–550. https://doi.org/10.1007/S00439-001-0610-5.

Harner, M., Körner, C., Walther, D., Mokranjac, D., Kaesmacher, J., Welsch, U., Griffith, J., Mann, M., Reggiori, F., and Neupert, W. (2011). The mitochondrial contact site complex, a determinant of mitochondrial architecture. EMBO J. *30*, 4356–4370. https://doi.org/10.1038/EMBOJ.2011.379.

Hartmann, B., Wai, T., Hu, H., MacVicar, T., Musante, L., Fischer-Zirnsak, B., Stenzel, W., Gräf, R., Van Den Heuvel, L., Ropers, H.H., et al. (2016a). Homozygous YME1L1 mutation causes mitochondriopathy with optic atrophy and mitochondrial network fragmentation. Elife *5*. https://doi.org/10.7554/ELIFE.16078.

Hartmann, B., Wai, T., Hu, H., MacVicar, T., Elife, L.M.-, and 2016, U. (2016b). Homozygous YME1L1 mutation causes mitochondriopathy with optic atrophy and mitochondrial network fragmentation. Elife.

He, J., Cooper, H.M., Reyes, A., Di Re, M., Sembongi, H., Gao, J., Neuman, K.C., Fearnley, I.M., Spinazzola, A., Walker, J.E., et al. (2012). Mitochondrial nucleoid interacting proteins support mitochondrial protein synthesis. Nucleic Acids Res. *40*, 6109. https://doi.org/10.1093/NAR/GKS266.

Hilander, T., Jackson, C.B., Robciuc, M., Bashir, T., and Zhao, H. (2021). The roles of assembly factors in mammalian mitoribosome biogenesis. Mitochondrion *60*, 70–84. https://doi.org/10.1016/J.MITO.2021.07.008.

Hillen, H.S., Temiakov, D., and Cramer, P. (2018). Structural basis of mitochondrial transcription. Nat. Struct. Mol. Biol. *25*, 754–765. https://doi.org/10.1038/S41594-018-0122-9.

Holt, I.J., Spinazzola, A., Janssen, M.C.H., and Spelbrink, J.N. (2022). Disorders of Replication, Transcription and Translation of Mitochondrial DNA. Physician's Guid. to Diagnosis, Treat. Follow. Inherit. Metab. Dis. 843–887. https://doi.org/10.1007/978-3-030-67727-5_45.

Holzmann, J., Frank, P., Löffler, E., Bennett, K.L., Gerner, C., and Rossmanith, W. (2008). RNase P without RNA: identification and functional reconstitution of the human mitochondrial tRNA processing enzyme. Cell *135*, 462–474. https://doi.org/10.1016/J.CELL.2008.09.013.

Hoppins, S., Collins, S.R., Cassidy-Stone, A., Hummel, E., DeVay, R.M., Lackner, L.L., Westermann, B., Schuldiner, M., Weissman, J.S., and Nunnari, J. (2011). A mitochondrial-focused genetic interaction map reveals a scaffold-like complex required for inner membrane organization in mitochondria. J. Cell Biol. *195*, 323–340. https://doi.org/10.1083/JCB.201107053.

Horvath, S.E., and Daum, G. (2013). Lipids of mitochondria. Prog. Lipid Res. *52*, 590–614. https://doi.org/10.1016/J.PLIPRES.2013.07.002.

Huang, Y., Chen, Y., Lin, X., Lin, Q., Han, M., and Guo, G. (2017). Clinical significance of SLP-2 in hepatocellular carcinoma tissues and its regulation in cancer cell proliferation, migration, and EMT. Onco. Targets. Ther. *10*, 4665–4673. https://doi.org/10.2147/OTT.S144638.

Jenkinson, E.M., Rehman, A.U., Walsh, T., Clayton-Smith, J., Lee, K., Morell, R.J., Drummond, M.C., Khan, S.N., Naeem, M.A., Rauf, B., et al. (2013). Perrault syndrome is caused by recessive mutations in CLPP, encoding a mitochondrial ATP-dependent chambered protease. Am. J. Hum. Genet. *92*, 605–613. https://doi.org/10.1016/J.AJHG.2013.02.013.

Jia, L., Dienhart, M., Schramp, M., McCauley, M., Hell, K., and Stuart, R.A. (2003). Yeast Oxa1 interacts with mitochondrial ribosomes: the importance of the C-terminal region of Oxa1. EMBO J. *22*, 6438–6447. https://doi.org/10.1093/EMBOJ/CDG624.

Jian, C., Xu, F., Hou, T., Sun, T., Li, J., Cheng, H., and Wang, X. (2017). Deficiency of PHB complex impairs respiratory supercomplex formation and activates mitochondrial flashes. J. Cell Sci. *130*, 2620–2630. https://doi.org/10.1242/JCS.198523.

Jin, S. (2010). Mitochondrial membrane potential regulates PINK1 import and proteolytic destabilization by PARL. J. Cell Biol. *191*, 933–942. .

Jones, A.J.Y., Blaza, J.N., Varghese, F., and Hirst, J. (2017). Respiratory Complex I in Bos taurus and Paracoccus denitrificans Pumps Four Protons across the Membrane for Every NADH Oxidized. J. Biol. Chem. *292*, 4987–4995. https://doi.org/10.1074/JBC.M116.771899.

Jourdain, A.A., Boehm, E., Maundrell, K., and Martinou, J.C. (2016). Mitochondrial RNA granules: Compartmentalizing mitochondrial gene expression. J. Cell Biol. *212*, 611–614. https://doi.org/10.1083/JCB.201507125.

Kang, Y., Stroud, D.A., Baker, M.J., De Souza, D.P., Frazier, A.E., Liem, M., Tull, D., Mathivanan, S., McConville, M.J., Thorburn, D.R., et al. (2017). Sengers Syndrome-Associated Mitochondrial Acylglycerol Kinase Is a Subunit of the Human TIM22 Protein Import Complex. Mol. Cell *67*, 457-470.e5. https://doi.org/10.1016/J.MOLCEL.2017.06.014.

Kang, Y., Fielden, L.F., and Stojanovski, D. (2018). Mitochondrial protein transport in health and disease. Semin. Cell Dev. Biol. *76*, 142–153. https://doi.org/10.1016/J.SEMCDB.2017.07.028.

Kasashima, K., Sumitani, M., Satoh, M., and Endo, H. (2008). Human prohibitin 1 maintains the organization and stability of the mitochondrial nucleoids. Exp. Cell Res. https://doi.org/10.1016/j.yexcr.2008.01.005.

Kaushal, P.S., Sharma, M.R., Booth, T.M., Haque, E.M., Tung, C.S., Sanbonmatsu, K.Y., Spremulli, L.L., and Agrawal, R.K. (2014). Cryo-EM structure of the small subunit of the mammalian mitochondrial ribosome. Proc. Natl. Acad. Sci. U. S. A. *111*, 7284–7289. https://doi.org/10.1073/PNAS.1401657111/-/DCSUPPLEMENTAL/PNAS.201401657SI.PDF.

Keckesova, Z., Donaher, J.L., De Cock, J., Freinkman, E., Lingrell, S., Bachovchin, D.A., Bierie, B., Tischler, V., Noske, A., Okondo, M.C., et al. (2017). LACTB is a tumour suppressor that modulates lipid metabolism and cell state. Nat. 2017 5437647 *543*, 681–686. https://doi.org/10.1038/nature21408.

Khosravi, S., and Harner, M.E. (2020). The MICOS complex, a structural element of mitochondria with versatile functions. Biol. Chem. *401*, 765–778. https://doi.org/10.1515/HSZ-2020-0103/ASSET/GRAPHIC/J_HSZ-2020-0103_FIG_005.JPG.

König, T., Tröder, S.E., Bakka, K., Korwitz, A., Richter-Dennerlein, R., Lampe, P.A., Patron, M., Mühlmeister, M., Guerrero-Castillo, S., Brandt, U., et al. (2016). The m-AAA Protease Associated with Neurodegeneration Limits MCU Activity in Mitochondria. Mol. Cell *64*, 148–162. https://doi.org/10.1016/J.MOLCEL.2016.08.020.

Koppen, M., Metodiev, M.D., Casari, G., Rugarli, E.I., and Langer, T. (2007). Variable and tissue-specific subunit composition of mitochondrial m-AAA protease complexes linked to hereditary spastic paraplegia. Mol. Cell. Biol. *27*, 758–767. https://doi.org/10.1128/MCB.01470-06.

Kotrys, A. V., and Szczesny, R.J. (2020). Mitochondrial Gene Expression and Beyond—Novel Aspects of Cellular Physiology. Cells *9*. https://doi.org/10.3390/CELLS9010017.

Krämer, L., Groh, C., and Herrmann, J.M. (2021). The proteasome: friend and foe of mitochondrial biogenesis. FEBS Lett. *595*, 1223–1238. https://doi.org/10.1002/1873-3468.14010.

Krebs, H.A., and Johnson, W.A. (1980). The role of citric acid in intermediate metabolism in animal tissues. FEBS Lett. *117*, K2–K10. https://doi.org/10.1016/0014-5793(80)80564-3.

Kühlbrandt, W. (2015). Structure and function of mitochondrial membrane protein

complexes. BMC Biol. https://doi.org/10.1186/s12915-015-0201-x.

Kummer, E., and Ban, N. (2021). Mechanisms and regulation of protein synthesis in mitochondria. Nat. Rev. Mol. Cell Biol. 2021 225 *22*, 307–325. https://doi.org/10.1038/s41580-021-00332-2.

Kummer, E., Leibundgut, M., Rackham, O., Lee, R.G., Boehringer, D., Filipovska, A., and Ban, N. (2018). Unique features of mammalian mitochondrial translation initiation revealed by cryo-EM. Nature *560*, 263–267. https://doi.org/10.1038/S41586-018-0373-Y.

Lagouge, M., Mourier, A., Lee, H.J., Spåhr, H., Wai, T., Kukat, C., Silva Ramos, E., Motori, E., Busch, J.D., Siira, S., et al. (2015). SLIRP Regulates the Rate of Mitochondrial Protein Synthesis and Protects LRPPRC from Degradation. PLoS Genet. *11*. https://doi.org/10.1371/JOURNAL.PGEN.1005423.

Lapatsina, L., Brand, J., Poole, K., Daumke, O., and Lewin, G.R. (2012). Stomatin-domain proteins. Eur. J. Cell Biol. https://doi.org/10.1016/j.ejcb.2011.01.018.

Lapuente-Brun, E., Moreno-Loshuertos, R., Acín-Pérez, R., Latorre-Pellicer, A., Colaś, C., Balsa, E., Perales-Clemente, E., Quirós, P.M., Calvo, E., Rodríguez-Hernández, M.A., et al. (2013). Supercomplex assembly determines electron flux in the mitochondrial electron transport chain. Science *340*, 1567–1570. https://doi.org/10.1126/SCIENCE.1230381.

Lee, K.W., and Bogenhagen, D.F. (2014). Assignment of 2'-O-methyltransferases to modification sites on the mammalian mitochondrial large subunit 16 S ribosomal RNA (rRNA). J. Biol. Chem. *289*, 24936–24942. https://doi.org/10.1074/JBC.C114.581868.

Lee, R.G., Gao, J., Siira, S.J., Shearwood, A.M., Ermer, J.A., Hofferek, V., Mathews, J.C., Zheng, M., Reid, G.E., Rackham, O., et al. (2020a). Cardiolipin is required for membrane docking of mitochondrial ribosomes and protein synthesis. J. Cell Sci. *133*. https://doi.org/10.1242/JCS.240374/266511/AM/CARDIOLIPIN-IS-REQUIRED-FOR-MEMBRANE-DOCKING-OF.

Lee, R.G., Gao, J., Siira, S.J., Shearwood, A.M., Ermer, J.A., Hofferek, V., Mathews, J.C., Zheng, M., Reid, G.E., Rackham, O., et al. (2020b). Cardiolipin is required for membrane docking of mitochondrial ribosomes and protein synthesis. J. Cell Sci. *133*. https://doi.org/10.1242/JCS.240374/266511/AM/CARDIOLIPIN-IS-REQUIRED-FOR-MEMBRANE-DOCKING-OF.

Letts, J.A., and Sazanov, L.A. (2017). Clarifying the supercomplex: the higher-order organization of the mitochondrial electron transport chain. Nat. Struct. Mol. Biol. 2017

2410 *24*, 800–808. https://doi.org/10.1038/nsmb.3460.

Li, H., Frankenfield, A.M., Houston, R., Sekine, S., and Hao, L. (2021). Thiol-Cleavable Biotin for Chemical and Enzymatic Biotinylation and Its Application to Mitochondrial TurboID Proteomics. J. Am. Soc. Mass Spectrom. *32*, 2358–2365. https://doi.org/10.1021/JASMS.1C00079/SUPPL_FILE/JS1C00079_SI_001.PDF.

Lill, R., Lill, R., and Freibert, S.A. (2020). Mechanisms of Mitochondrial Iron-Sulfur Protein Biogenesis. Annu. Rev. Biochem. *89*, 471–499. https://doi.org/10.1146/ANNUREV-BIOCHEM-013118-111540.

Lin, H., Miyauchi, K., Harada, T., Okita, R., Takeshita, E., Komaki, H., Fujioka, K., Yagasaki, H., Goto, Y.I., Yanaka, K., et al. (2018). CO 2-sensitive tRNA modification associated with human mitochondrial disease. Nat. Commun. *9*. https://doi.org/10.1038/S41467-018-04250-4.

Ling, M., Merante, F., Chen, H.S., Duff, C., Duncan, A.M.V., and Robinson, B.H. (1997). The human mitochondrial elongation factor tu (EF-Tu) gene: cDNA sequence, genomic localization, genomic structure, and identification of a pseudogene. Gene *197*, 325–336. https://doi.org/10.1016/S0378-1119(97)00279-5.

Love, M.I., Huber, W., and Anders, S. (2014). Moderated estimation of fold change and dispersion for RNA-seq data with DESeq2. Genome Biol. *15*, 1–21. https://doi.org/10.1186/S13059-014-0550-8/FIGURES/9.

Lussey-Lepoutre, C., Hollinshead, K.E.R., Ludwig, C., Menara, M., Morin, A., Castro-Vega, L.J., Parker, S.J., Janin, M., Martinelli, C., Ottolenghi, C., et al. (2015). Loss of succinate dehydrogenase activity results in dependency on pyruvate carboxylation for cellular anabolism. Nat. Commun. *6*. https://doi.org/10.1038/NCOMMS9784.

Ma, C., Wang, C., Luo, D., Yan, L., Yang, W., Li, N., and Gao, N. (2022). Structural insights into the membrane microdomain organization by SPFH family proteins. Cell Res. 2021 322 *32*, 176–189. https://doi.org/10.1038/s41422-021-00598-3.

MacVicar, T., Ohba, Y., Nolte, H., Mayer, F.C., Tatsuta, T., Sprenger, H.G., Lindner, B., Zhao, Y., Li, J., Bruns, C., et al. (2019). Lipid signalling drives proteolytic rewiring of mitochondria by YME1L. Nature https://doi.org/10.1038/s41586-019-1738-6.

Maranzana, E., Barbero, G., Falasca, A.I., Lenaz, G., and Genova, M.L. (2013). Mitochondrial respiratory supercomplex association limits production of reactive oxygen species from complex I. Antioxid. Redox Signal. *19*, 1469–1480. https://doi.org/10.1089/ARS.2012.4845.

Matsushima, Y., Goto, Y.I., and Kaguni, L.S. (2010). Mitochondrial Lon protease

regulates mitochondrial DNA copy number and transcription by selective degradation of mitochondrial transcription factor A (TFAM). Proc. Natl. Acad. Sci. U. S. A. *107*, 18410–18415. https://doi.org/10.1073/PNAS.1008924107.

Merkwirth, C., Dargazanli, S., Tatsuta, T., Geimer, S., Lower, B., Wunderlich, F.T., von Kleist-Retzow, J.-C., Waisman, A., Westermann, B., and Langer, T. (2008). Prohibitins control cell proliferation and apoptosis by regulating OPA1-dependent cristae morphogenesis in mitochondria. Genes Dev. *22*, 476–488. https://doi.org/10.1101/gad.460708.

Merkwirth, C., Martinelli, P., Korwitz, A., Morbin, M., Brönneke, H.S., Jordan, S.D., Rugarli, E.I., and Langer, T. (2012). Loss of Prohibitin Membrane Scaffolds Impairs Mitochondrial Architecture and Leads to Tau Hyperphosphorylation and Neurodegeneration. PLoS Genet. https://doi.org/10.1371/journal.pgen.1003021.

Metodiev, M.D., Lesko, N., Park, C.B., Cámara, Y., Shi, Y., Wibom, R., Hultenby, K., Gustafsson, C.M., and Larsson, N.G. (2009a). Methylation of 12S rRNA is necessary for in vivo stability of the small subunit of the mammalian mitochondrial ribosome. Cell Metab. *9*, 386–397. https://doi.org/10.1016/J.CMET.2009.03.001.

Metodiev, M.D., Lesko, N., Park, C.B., Cámara, Y., Shi, Y., Wibom, R., Hultenby, K., Gustafsson, C.M., and Larsson, N.G. (2009b). Methylation of 12S rRNA Is Necessary for In Vivo Stability of the Small Subunit of the Mammalian Mitochondrial Ribosome. Cell Metab. *9*, 386–397. https://doi.org/10.1016/J.CMET.2009.03.001.

Metodiev, M.D., Spåhr, H., Loguercio Polosa, P., Meharg, C., Becker, C., Altmueller, J., Habermann, B., Larsson, N.G., and Ruzzenente, B. (2014). NSUN4 is a dual function mitochondrial protein required for both methylation of 12S rRNA and coordination of mitoribosomal assembly. PLoS Genet. *10*. https://doi.org/10.1371/JOURNAL.PGEN.1004110.

Mick, D.U., Dennerlein, S., Wiese, H., Reinhold, R., Pacheu-Grau, D., Lorenzi, I., Sasarman, F., Weraarpachai, W., Shoubridge, E.A., Warscheid, B., et al. (2012). MITRAC links mitochondrial protein translocation to respiratory-chain assembly and translational regulation. Cell *151*, 1528–1541. https://doi.org/10.1016/J.CELL.2012.11.053.

Mick, E., Titov, D. V., Skinner, O.S., Sharma, R., Jourdain, A.A., and Mootha, V.K. (2020). Distinct mitochondrial defects trigger the integrated stress response depending on the metabolic state of the cell. Elife *9*. https://doi.org/10.7554/ELIFE.49178.

Mignotte, B., Barat, M., and Mounolou, J.C. (1985). Characterization of a mitochondrial

protein binding to single-stranded DNA. Nucleic Acids Res. *13*, 1703–1716. https://doi.org/10.1093/NAR/13.5.1703.

Mitchell, P. (1961). Coupling of phosphorylation to electron and hydrogen transfer by a chemi-osmotic type of mechanism. Nature *191*, 144–148. https://doi.org/10.1038/191144A0.

Mitchell, P. (1976). Possible molecular mechanisms of the protonmotive function of cytochrome systems. J. Theor. Biol. *62*, 327–367. https://doi.org/10.1016/0022-5193(76)90124-7.

Mitsopoulos, P., Chang, Y.-H., Wai, T., König, T., Dunn, S.D., Langer, T., and Madrenas, J. (2015a). Stomatin-like protein 2 is required for in vivo mitochondrial respiratory chain supercomplex formation and optimal cell function. Mol. Cell. Biol. https://doi.org/10.1128/MCB.00047-15.

Mitsopoulos, P., Chang, Y.-H., Wai, T., König, T., Dunn, S.D., Langer, T., and Madrenas, J. (2015b). Stomatin-Like Protein 2 Is Required for In Vivo Mitochondrial Respiratory Chain Supercomplex Formation and Optimal Cell Function . Mol. Cell. Biol. *35*, 1838–1847. https://doi.org/10.1128/MCB.00047-15/ASSET/A6F7CED5-B3C0-4FDA-BF8A-7A73003F2213/ASSETS/GRAPHIC/ZMB9991008310006.JPEG.

Mitsopoulos, P., Lapohos, O., Weraarpachai, W., Antonicka, H., Chang, Y.H., and Madrenas, J. (2017). Stomatin-like protein 2 deficiency results in impaired mitochondrial translation. PLoS One *12*, 1–13. https://doi.org/10.1371/journal.pone.0179967.

Morrow, I.C., and Parton, R.G. (2005). Flotillins and the PHB Domain Protein Family: Rafts, Worms and Anaesthetics. Traffic *6*, 725–740. https://doi.org/10.1111/j.1600-0854.2005.00318.x.

Mukherjee, I., Ghosh, M., and Meinecke, M. (2021). MICOS and the mitochondrial inner membrane morphology – when things get out of shape. FEBS Lett. *595*, 1159–1183. https://doi.org/10.1002/1873-3468.14089.

Mzhavia, N., Berman, Y.L., Qian, Y., Yan, L., and Devi, L.A. (1999). Cloning, expression, and characterization of human metalloprotease 1: a novel member of the pitrilysin family of metalloendoproteases. DNA Cell Biol. *18*, 369–380. https://doi.org/10.1089/104454999315268.

Nagaike, T., Suzuki, T., Tomari, Y., Takemoto-Hori, C., Negayama, F., Watanabe, K., and Ueda, T. (2001). Identification and characterization of mammalian mitochondrial tRNA nucleotidyltransferases. J. Biol. Chem. *276*, 40041–40049.

https://doi.org/10.1074/JBC.M106202200.

Navaratnarajah, T., Anand, R., Reichert, A.S., and Distelmaier, F. (2021). The relevance of mitochondrial morphology for human disease. Int. J. Biochem. Cell Biol. *134*. https://doi.org/10.1016/J.BIOCEL.2021.105951.

Nijtmans, L.G.J., De Jong, L., Sanz, M.A., Coates, P.J., Berden, J.A., Back, J.W., Muijsers, A.O., Van Der Spek, H., and Grivell, L.A. (2000). Prohibitins act as a membrane-bound chaperone for the stabilization of mitochondrial proteins. EMBO J. *19*, 2444. https://doi.org/10.1093/EMBOJ/19.11.2444.

Nikkanen, J., Forsström, S., Euro, L., Paetau, I., Kohnz, R.A., Wang, L., Chilov, D., Viinamäki, J., Roivainen, A., Marjamäki, P., et al. (2016). Mitochondrial DNA Replication Defects Disturb Cellular dNTP Pools and Remodel One-Carbon Metabolism. Cell Metab. *23*, 635–648. https://doi.org/10.1016/J.CMET.2016.01.019.

Nolden, M., Ehses, S., Koppen, M., Bernacchia, A., Rugarli, E.I., and Langer, T. (2005). The m-AAA protease defective in hereditary spastic paraplegia controls ribosome assembly in mitochondria. Cell *123*, 277–289. https://doi.org/10.1016/J.CELL.2005.08.003/ATTACHMENT/07A081BF-2567-42BE-9AB2-B99378B1A9D6/MMC1.PDF.

Nunnari, J., and Suomalainen, A. (2012). Mitochondria: In sickness and in health. Cell https://doi.org/10.1016/j.cell.2012.02.035.

Ohba, Y., MacVicar, T., and Langer, T. (2020). Regulation of mitochondrial plasticity by the i-AAA protease YME1L. Biol. Chem. *401*, 877–890. https://doi.org/10.1515/HSZ-2020-0120/ASSET/GRAPHIC/J_HSZ-2020-0120_FIG_005.JPG.

Ojala, D., Montoya, J., and Attardi, G. (1981). tRNA punctuation model of RNA processing in human mitochondria. Nature *290*, 470–474. https://doi.org/10.1038/290470A0.

Okamoto, H., Miyagawa, A., Shiota, T., Tamura, Y., and Endo, T. (2014). Intramolecular disulfide bond of Tim22 protein maintains integrity of the TIM22 complex in the mitochondrial inner membrane. J. Biol. Chem. *289*, 4827–4838. https://doi.org/10.1074/JBC.M113.543264.

Olichon, A., Baricault, L., Gas, N., Guillou, E., Valette, A., Belenguer, P., and Lenaers, G. (2003). Loss of OPA1 perturbates the mitochondrial inner membrane structure and integrity, leading to cytochrome c release and apoptosis. J. Biol. Chem. *278*, 7743–7746. https://doi.org/10.1074/JBC.C200677200.

Otto, G.P., and Nichols, B.J. (2011). The roles of flotillin microdomains – endocytosis and beyond. J. Cell Sci. *124*, 3933–3940. https://doi.org/10.1242/JCS.092015.

Pakos-Zebrucka, K., Koryga, I., Mnich, K., Ljujic, M., Samali, A., and Gorman, A.M. (2016). The integrated stress response. EMBO Rep. *17*, 1374–1395. https://doi.org/10.15252/EMBR.201642195.

Palade, G.E. (1953). An electron microscope study of the mitochondrial structure. J. Histochem. Cytochem. *1*, 188–211. https://doi.org/10.1177/1.4.188.

Palty, R., Silverman, W.F., Hershfinkel, M., Caporale, T., Sensi, S.L., Parnis, J., Nolte, C., Fishman, D., Shoshan-Barmatz, V., Herrmann, S., et al. (2010). NCLX is an essential component of mitochondrial Na+/Ca 2+ exchange. Proc. Natl. Acad. Sci. U. S. A. *107*, 436–441. https://doi.org/10.1073/PNAS.0908099107/SUPPL_FILE/PNAS.200908099SI.PDF.

Patron, M., Tarasenko, D., Nolte, H., Kroczek, L., Ghosh, M., Ohba, Y., Lasarzewski, Y., Ahmadi, Z.A., Cabrera-Orefice, A., Eyiama, A., et al. (2022). Regulation of mitochondrial proteostasis by the proton gradient. EMBO J. 110476. https://doi.org/10.15252/embj.2021110476.

Pearce, M.M.P., Wormer, D.B., Wilkens, S., and Wojcikiewicz, R.J.H. (2009). An endoplasmic reticulum (ER) membrane complex composed of SPFH1 and SPFH2 mediates the ER-associated degradation of inositol 1,4,5-trisphosphate receptors. J. Biol. Chem. *284*, 10433–10445. https://doi.org/10.1074/JBC.M809801200/ATTACHMENT/B3656BE2-4722-49CA-8AA9-66C21314D203/MMC1.PDF.

Phasukkijwatana, N., Kunhapan, B., Stankovich, J., Chuenkongkaew, W.L., Thomson, R., Thornton, T., Bahlo, M., Mushiroda, T., Nakamura, Y., Mahasirimongkol, S., et al. (2010). Genome-wide linkage scan and association study of PARL to the expression of LHON families in Thailand. Hum. Genet. *128*, 39–49. https://doi.org/10.1007/S00439-010-0821-8.

Pierson, T.M., Adams, D., Bonn, F., Martinelli, P., Cherukuri, P.F., Teer, J.K., Hansen, N.F., Cruz, P., Mullikin, J.C., Blakesley, R.W., et al. (2011). Whole-exome sequencing identifies homozygous AFG3L2 mutations in a spastic ataxia-neuropathy syndrome linked to mitochondrial m-AAA proteases. PLoS Genet. *7*. https://doi.org/10.1371/JOURNAL.PGEN.1002325.

Pinke, G., Zhou, L., and Sazanov, L.A. (2020). Cryo-EM structure of the entire mammalian F-type ATP synthase. Nat. Struct. Mol. Biol. *27*, 1077–1085.

https://doi.org/10.1038/S41594-020-0503-8.

Pinti, M., Gibellini, L., Nasi, M., De Biasi, S., Bortolotti, C.A., Iannone, A., and Cossarizza, A. (2016). Emerging role of Lon protease as a master regulator of mitochondrial functions. Biochim. Biophys. Acta - Bioenerg. *1857*, 1300–1306. https://doi.org/10.1016/J.BBABIO.2016.03.025.

Poveda-Huertes, D., Mulica, P., and Vögtle, F.N. (2017). The versatility of the mitochondrial presequence processing machinery: cleavage, quality control and turnover. Cell Tissue Res. *367*, 73–81. https://doi.org/10.1007/S00441-016-2492-9.

Powell, C.A., and Minczuk, M. (2020). TRMT2B is responsible for both tRNA and rRNA m5U-methylation in human mitochondria. RNA Biol. *17*, 451. https://doi.org/10.1080/15476286.2020.1712544.

Price, M.P., Thompson, R.J., Eshcol, J.O., Wemmie, J.A., and Benson, C.J. (2004a). Stomatin modulates gating of acid-sensing ion channels. J. Biol. Chem. https://doi.org/10.1074/jbc.M407708200.

Price, M.P., Thompson, R.J., Eshcol, J.O., Wemmie, J.A., and Benson, C.J. (2004b). Stomatin modulates gating of acid-sensing ion channels. J. Biol. Chem. *279*, 53886–53891. https://doi.org/10.1074/JBC.M407708200.

Rainbolt, T.K., Atanassova, N., Genereux, J.C., and Wiseman, R.L. (2013). Stress-Regulated Translational Attenuation Adapts Mitochondrial Protein Import through Tim17A Degradation. Cell Metab. *18*, 908–919. https://doi.org/10.1016/J.CMET.2013.11.006.

Rampelt, H., Zerbes, R.M., van der Laan, M., and Pfanner, N. (2017). Role of the mitochondrial contact site and cristae organizing system in membrane architecture and dynamics. Biochim. Biophys. Acta - Mol. Cell Res. https://doi.org/10.1016/j.bbamcr.2016.05.020.

Rasheed, M., & G.T.-A. of P., and 2018, undefined Succinate dehydrogenase complex: an updated review. Meridian.Allenpress.Com.

Rath, S., Sharma, R., Gupta, R., Ast, T., Chan, C., Durham, T.J., Goodman, R.P., Grabarek, Z., Haas, M.E., Hung, W.H.W., et al. (2021). MitoCarta3.0: an updated mitochondrial proteome now with sub-organelle localization and pathway annotations. Nucleic Acids Res. *49*, D1541–D1547. https://doi.org/10.1093/NAR/GKAA1011.

Rey, T., Zaganelli, S., Cuillery, E., Vartholomaiou, E., Croisier, M., Martinou, J.C., and Manley, S. (2020). Mitochondrial RNA granules are fluid condensates positioned by membrane dynamics. Nat. Cell Biol. 2020 2210 *22*, 1180–1186.

https://doi.org/10.1038/s41556-020-00584-8.

Richter-Dennerlein, R., Korwitz, A., Haag, M., Tatsuta, T., Dargazanli, S., Baker, M., Decker, T., Lamkemeyer, T., Rugarli, E.I., and Langer, T. (2014). DNAJC19, a mitochondrial cochaperone associated with cardiomyopathy, forms a complex with prohibitins to regulate cardiolipin remodeling. Cell Metab. *20*, 158–171. https://doi.org/10.1016/j.cmet.2014.04.016.

Richter-Dennerlein, R., Dennerlein, S., and Rehling, P. (2015). Integrating mitochondrial translation into the cellular context. Nat. Rev. Mol. Cell Biol. 2015 1610 *16*, 586–592. https://doi.org/10.1038/nrm4051.

Richter-Dennerlein, R., Oeljeklaus, S., Lorenzi, I., Ronsör, C., Bareth, B., Schendzielorz, A.B., Wang, C., Warscheid, B., Rehling, P., and Dennerlein, S. (2016a). Mitochondrial Protein Synthesis Adapts to Influx of Nuclear-Encoded Protein. Cell *167*, 471-483.e10. https://doi.org/10.1016/J.CELL.2016.09.003.

Richter-Dennerlein, R., Oeljeklaus, S., Lorenzi, I., Ronsör, C., Bareth, B., Schendzielorz, A.B., Wang, C., Warscheid, B., Rehling, P., and Dennerlein, S. (2016b). Mitochondrial Protein Synthesis Adapts to Influx of Nuclear-Encoded Protein. Cell *167*, 471-483.e10. https://doi.org/10.1016/J.CELL.2016.09.003.

Richter, F., Dennerlein, S., Nikolov, M., Jans, D.C., Naumenko, N., Aich, A., MacVicar, T., Linden, A., Jakobs, S., Urlaub, H., et al. (2019). ROMO1 is a constituent of the human presequence translocase required for YME1L protease import. J. Cell Biol. *218*, 598–614. https://doi.org/10.1083/JCB.201806093.

Rizzuto, R., Bernardi, P., and Pozzan, T. (2000). Mitochondria as all-round players of the calcium game. J. Physiol. *529 Pt 1*, 37–47. https://doi.org/10.1111/J.1469-7793.2000.00037.X.

Rumyantseva, A., Motori, E., and Trifunovic, A. (2020). DARS2 is indispensable for Purkinje cell survival and protects against cerebellar ataxia. Hum. Mol. Genet. *29*, 2845–2854. https://doi.org/10.1093/HMG/DDAA176.

Ruzzenente, B., Metodiev, M.D., Wredenberg, A., Bratic, A., Park, C.B., Cámara, Y., Milenkovic, D., Zickermann, V., Wibom, R., Hultenby, K., et al. (2012). LRPPRC is necessary for polyadenylation and coordination of translation of mitochondrial mRNAs. EMBO J. *31*, 443. https://doi.org/10.1038/EMBOJ.2011.392.

Ryan, D.G., Yang, M., Prag, H.A., Blanco, G.R., Nikitopoulou, E., Segarra-Mondejar, M., Powell, C.A., Young, T., Burger, N., Miljkovic, J.L., et al. (2021). Disruption of the TCA cycle reveals an ATF4-dependent integration of redox and amino acid

metabolism. Elife *10*. https://doi.org/10.7554/ELIFE.72593.

Rydning, S.L., Dudesek, A., Rimmele, F., Funke, C., Krüger, S., Biskup, S., Vigeland, M.D., Hjorthaug, H.S., Sejersted, Y., Tallaksen, C., et al. (2018). A novel heterozygous variant in ERLIN2 causes autosomal dominant pure hereditary spastic paraplegia. Eur. J. Neurol. *25*, 943-e71. https://doi.org/10.1111/ENE.13625.

Safra, M., Sas-Chen, A., Nir, R., Winkler, R., Nachshon, A., Bar-Yaacov, D., Erlacher, M., Rossmanith, W., Stern-Ginossar, N., and Schwartz, S. (2017). The m1A landscape on cytosolic and mitochondrial mRNA at single-base resolution. Nature *551*, 251–255. https://doi.org/10.1038/NATURE24456.

Saita, S., Nolte, H., Fiedler, K.U., Kashkar, H., Saskia, A.V., Zahedi, R.P., Krüger, M., and Langer, T. (2017). PARL mediates Smac proteolytic maturation in mitochondria to promote apoptosis. Nat. Cell Biol. 2017 194 *19*, 318–328. https://doi.org/10.1038/ncb3488.

Saita, S., Tatsuta, T., Lampe, P.A., König, T., Ohba, Y., and Langer, T. (2018). PARL partitions the lipid transfer protein STARD7 between the cytosol and mitochondria. EMBO J. *37*, e97909. https://doi.org/10.15252/EMBJ.201797909.

Saitoh, T., Igura, M., Obita, T., Ose, T., Kojima, R., Maenaka, K., Endo, T., and Kohda, D. (2007). Tom20 recognizes mitochondrial presequences through dynamic equilibrium among multiple bound states. EMBO J. *26*, 4777–4787. https://doi.org/10.1038/SJ.EMBOJ.7601888.

Santel, A., and Fuller, M.T. (2001). Control of mitochondrial morphology by a human mitofusin. J. Cell Sci. *114*, 867–874. https://doi.org/10.1242/JCS.114.5.867.

Sanz, M.A., Tsang, W.Y., Willems, E.M., Grivell, L.A., Lemire, B.D., Van der Spek, H., and Nijtmans, L.G.J. (2003). The Mitochondrial Prohibitin Complex Is Essential for Embryonic Viability and Germline Function in Caenorhabditis elegans *. J. Biol. Chem. *278*, 32091–32099. https://doi.org/10.1074/JBC.M304877200.

Sasaki, K., Uchiumi, T., Toshima, T., Yagi, M., Do, Y., Hirai, H., Igami, K., Gotoh, K., and Kang, D. (2020). Mitochondrial translation inhibition triggers ATF4 activation, leading to integrated stress response but not to mitochondrial unfolded protein response. Biosci. Rep. *40*. https://doi.org/10.1042/BSR20201289.

Sasarman, F., Brunel-Guitton, C., Antonicka, H., Wai, T., Shoubridge, E.A., Allen, B., Burelle, Y., Charron, G., Coderre, L., DesRosiers, C., et al. (2010). LRPPRC and SLIRP interact in a ribonucleoprotein complex that regulates posttranscriptional gene expression in mitochondria. Mol. Biol. Cell *21*, 1315–1323.

https://doi.org/10.1091/MBC.E10-01-0047.

Schägger, H., and Pfeiffer, K. (2000). Supercomplexes in the respiratory chains of yeast and mammalian mitochondria. EMBO J. *19*, 1777–1783. https://doi.org/10.1093/EMBOJ/19.8.1777.

Schlame, M., and Ren, M. (2006). Barth syndrome, a human disorder of cardiolipin metabolism. FEBS Lett. *580*, 5450–5455. https://doi.org/10.1016/J.FEBSLET.2006.07.022.

Schlame, M., and Ren, M. (2009). The role of cardiolipin in the structural organization of mitochondrial membranes. Biochim. Biophys. Acta - Biomembr. *1788*, 2080–2083. https://doi.org/10.1016/J.BBAMEM.2009.04.019.

Schubert, U., Antón, L.C., Gibbs, J., Norbury, C.C., Yewdell, J.W., and Bennink, J.R. (2000). Rapid degradation of a large fraction of newly synthesized proteins by proteasomes. Nature *404*, 770–774. https://doi.org/10.1038/35008096.

Schwaiger, M., Rampler, E., Hermann, G., Miklos, W., Berger, W., and Koellensperger, G. (2017). Anion-Exchange Chromatography Coupled to High-Resolution Mass Spectrometry: A Powerful Tool for Merging Targeted and Non-targeted Metabolomics. Anal. Chem. *89*, 7667–7674. https://doi.org/10.1021/ACS.ANALCHEM.7B01624/ASSET/IMAGES/LARGE/AC-2017-01624X_0003.JPEG.

Sekine, S., Kanamaru, Y., Koike, M., Nishihara, A., Okada, M., Kinoshita, H., Kamiyama, M., Maruyama, J., Uchiyama, Y., Ishihara, N., et al. (2012). Rhomboid protease PARL mediates the mitochondrial membrane potential loss-induced cleavage of PGAM5. J. Biol. Chem. *287*, 34635–34645. https://doi.org/10.1074/JBC.M112.357509/ATTACHMENT/EE7740A3-5A3A-4E22-8FDA-BC5AEB339263/MMC1.PDF.

Sharma, M.R., Koc, E.C., Datta, P.P., Booth, T.M., Spremulli, L.L., and Agrawal, R.K. (2003). Structure of the mammalian mitochondrial ribosome reveals an expanded functional role for its component proteins. Cell *115*, 97–108. https://doi.org/10.1016/S0092-8674(03)00762-1.

Shoubridge, E.A. (2000). Mitochondrial DNA segregation in the developing embryo. Hum. Reprod. *15 Suppl 2*, 229–234. https://doi.org/10.1093/HUMREP/15.SUPPL_2.229.

De Silva, D., Tu, Y.T., Amunts, A., Fontanesi, F., and Barrientos, A. (2015). Mitochondrial ribosome assembly in health and disease. Cell Cycle *14*, 2226.

https://doi.org/10.1080/15384101.2015.1053672.

Sinha, D., Joshi, N., Chittoor, B., Samji, P., and D'Silva, P. (2010). Role of Magmas in protein transport and human mitochondria biogenesis. Hum. Mol. Genet. *19*, 1248–1262. https://doi.org/10.1093/HMG/DDQ002.

Sinha, D., Srivastava, S., Krishna, L., and D'Silva, P. (2014). Unraveling the Intricate Organization of Mammalian Mitochondrial Presequence Translocases: Existence of Multiple Translocases for Maintenance of Mitochondrial Function. Mol. Cell. Biol. *34*, 1757–1775. https://doi.org/10.1128/MCB.01527-13/ASSET/3DB5F926-D1DA-49CD-A562-992957B8E71A/ASSETS/GRAPHIC/ZMB9991004180013.JPEG.

Sirrenberg, C., Bauer, M.F., Guiard, B., Neupert, W., and Brunner, M. (1996). Import of carrier proteins into the mitochondrial inner membrane mediated by Tim22. Nature *384*, 582–585. https://doi.org/10.1038/384582A0.

Smirnova, E., Griparic, L., Shurland, D.L., and Van der Bliek, A.M. (2001). Dynamin-related protein Drp1 is required for mitochondrial division in mammalian cells. Mol. Biol. Cell *12*, 2245–2256. https://doi.org/10.1091/MBC.12.8.2245.

Sohal, R.S. (1970). Mitochondrial changes in the heart of Drosophila repleta, Wollaston with age. Exp. Gerontol. *5*, 213–214. https://doi.org/10.1016/0531-5565(70)90040-9.

Sousa, J.S., Mills, D.J., Vonck, J., and Kühlbrandt, W. (2016). Functional asymmetry and electron flow in the bovine respirasome. Elife *5*. https://doi.org/10.7554/ELIFE.21290.

Spelbrink, J.N., Li, F.Y., Tiranti, V., Nikali, K., Yuan, Q.P., Tariq, M., Wanrooij, S., Garrido, N., Comi, G., Morandi, L., et al. (2001). Human mitochondrial DNA deletions associated with mutations in the gene encoding Twinkle, a phage T7 gene 4-like protein localized in mitochondria. Nat. Genet. *28*, 223–231. https://doi.org/10.1038/90058.

Spencer, A.C., and Spremulli, L.L. (2004). Interaction of mitochondrial initiation factor 2 with mitochondrial fMet-tRNA. Nucleic Acids Res. *32*, 5464–5470. https://doi.org/10.1093/NAR/GKH886.

Sprenger, H.-G., Wani, G., Hesseling, A., König, T., Patron, M., MacVicar, T., Ahola, S., Wai, T., Barth, E., Rugarli, E.I., et al. (2019). Loss of the mitochondrial i-AAA protease YME1L leads to ocular dysfunction and spinal axonopathy. EMBO Mol. Med. *11*, e9288. https://doi.org/10.15252/EMMM.201809288.

Sprenger, H.G., MacVicar, T., Bahat, A., Fiedler, K.U., Hermans, S., Ehrentraut, D., Ried, K., Milenkovic, D., Bonekamp, N., Larsson, N.G., et al. (2021). Cellular

pyrimidine imbalance triggers mitochondrial DNA–dependent innate immunity. Nat. Metab. 2021 35 *3*, 636–650. https://doi.org/10.1038/s42255-021-00385-9.

Steglich, G., Neupert, W., and Langer, T. (1999). Prohibitins regulate membrane protein degradation by the m-AAA protease in mitochondria. Mol. Cell. Biol. https://doi.org/10.1128/MCB.19.5.3435.

Stephan, T., Brüser, C., Deckers, M., Steyer, A.M., Balzarotti, F., Barbot, M., Behr, T.S., Heim, G., Hübner, W., Ilgen, P., et al. (2020a). MICOS assembly controls mitochondrial inner membrane remodeling and crista junction redistribution to mediate cristae formation. EMBO J. *39*, e104105. https://doi.org/10.15252/EMBJ.2019104105.

Stephan, T., Brüser, C., Deckers, M., Steyer, A.M., Balzarotti, F., Barbot, M., Behr, T.S., Heim, G., Hübner, W., Ilgen, P., et al. (2020b). MICOS assembly controls mitochondrial inner membrane remodeling and crista junction redistribution to mediate cristae formation. EMBO J. *39*, e104105. https://doi.org/10.15252/EMBJ.2019104105.

Sterky, F.H., Ruzzenente, B., Gustafsson, C.M., Samuelsson, T., and Larsson, N.-G. (2010). LRPPRC is a mitochondrial matrix protein that is conserved in metazoans. Biochem. Biophys. Res. Commun. *398*, 759–764. https://doi.org/10.1016/J.BBRC.2010.07.019.

Stiburek, L., Cesnekova, J., Kostkova, O., Fornuskova, D., Vinsova, K., Wenchich, L., Houstek, J., and Zeman, J. (2012). YME1L controls the accumulation of respiratory chain subunits and is required for apoptotic resistance, cristae morphogenesis, and cell proliferation. Mol. Biol. Cell *23*, 1010–1023. https://doi.org/10.1091/MBC.E11-08-0674/ASSET/IMAGES/LARGE/1010FIG7.JPEG.

Supale, S., Thorel, F., Merkwirth, C., Gjinovci, A., Herrera, P.L., Scorrano, L., Meda, P., Langer, T., and Maechler, P. (2013). Loss of prohibitin induces mitochondrial damages altering β-cell function and survival and is responsible for gradual diabetes development. Diabetes *62*, 3488–3499. https://doi.org/10.2337/DB13-0152.

Suzuki, T., Nagao, A., and Suzuki, T. (2011). Human Mitochondrial tRNAs: Biogenesis, Function, Structural Aspects, and Diseases. Http://Dx.Doi.Org/10.1146/Annurev-Genet-110410-132531 *45*, 299–329. https://doi.org/10.1146/ANNUREV-GENET-110410-132531.

Suzuki, Y., Imai, Y., Nakayama, H., Takahashi, K., Takio, K., and Takahashi, R. (2001). A serine protease, HtrA2, is released from the mitochondria and interacts with XIAP, inducing cell death. Mol. Cell *8*, 613–621. https://doi.org/10.1016/S1097-2765(01)00341-0.

Swenson, S.A., Moore, C.M., Marcero, J.R., Medlock, A.E., Reddi, A.R., and Khalimonchuk, O. (2020). From Synthesis to Utilization: The Ins and Outs of Mitochondrial Heme. Cells *9*. https://doi.org/10.3390/CELLS9030579.

Szczepanowska, K., Maiti, P., Kukat, A., Hofsetz, E., Nolte, H., Senft, K., Becker, C., Ruzzenente, B., Hornig-Do, H.-T., Wibom, R., et al. (2016). CLPP coordinates mitoribosomal assembly through the regulation of ERAL1 levels. EMBO J. *35*, 2566–2583. https://doi.org/10.15252/EMBJ.201694253.

Szyrach, G., Ott, M., Bonnefoy, N., Neupert, W., and Herrmann, J.M. (2003). Ribosome binding to the Oxa1 complex facilitates co-translational protein insertion in mitochondria. EMBO J. *22*, 6448–6457. https://doi.org/10.1093/EMBOJ/CDG623.

Talim, B., Pyle, A., Griffin, H., Topaloglu, H., Tokatli, A., Keogh, M.J., Santibanez-Koref, M., Chinnery, P.F., and Horvath, R. (2013). Multisystem fatal infantile disease caused by a novel homozygous EARS2 mutation. Brain *136*, e228–e228. https://doi.org/10.1093/BRAIN/AWS197.

Tatsuta, T., Model, K., and Langer, T. (2005). Formation of membrane-bound ring complexes by prohibitins in mitochondria. Mol. Biol. Cell *16*, 248–259. https://doi.org/10.1091/mbc.e04-09-0807.

Taylor, R.W., and Turnbull, D.M. (2005). Mitochondrial DNA mutations in human disease. Nat. Rev. Genet. *6*, 389–402. https://doi.org/10.1038/NRG1606.

Teresa Lobo-Jarne 1 , Eva Nývltová 2 , Rafael Pérez-Pérez 1 , Alba Timón-Gómez 2 , Thibaut Molinié 3 , Austin Choi 2 , Arnaud Mourier 3 , Flavia Fontanesi 4 , Cristina Ugalde 5, A.B. 6 (2018). Human COX7A2L Regulates Complex III Biogenesis and Promotes Supercomplex Organization Remodeling without Affecting Mitochondrial Bioenergetics. Cell Rep. https://doi.org/10.1016/j.celrep.2018.10.058.

Theiss, A.L., and Sitaraman, S. V. (2011). The role and therapeutic potential of prohibitin in disease. Biochim. Biophys. Acta - Mol. Cell Res. https://doi.org/10.1016/j.bbamcr.2011.01.033.

Timón-Gómez, A., Nývltová, E., Abriata, L.A., Vila, A.J., Hosler, J., and Barrientos, A. (2018). Mitochondrial cytochrome c oxidase biogenesis: Recent developments. Semin. Cell Dev. Biol. *76*, 163–178. https://doi.org/10.1016/J.SEMCDB.2017.08.055.

Tomecki, R., Dmochowska, A., Gewartowski, K., Dziembowski, A., and Stepien, P.P. (2004). Identification of a novel human nuclear-encoded mitochondrial poly(A) polymerase. Nucleic Acids Res. *32*, 6001–6014. https://doi.org/10.1093/NAR/GKH923.

Tondera, D., Grandemange, S., Jourdain, A., Karbowski, M., Mattenberger, Y., Herzig, S., Da Cruz, S., Clerc, P., Raschke, I., Merkwirth, C., et al. (2009). SlP-2 is required for stress-induced mitochondrial hyperfusion. EMBO J. https://doi.org/10.1038/emboj.2009.89.

Toompuu, M., Tuomela, T., Laine, P., Paulin, L., Dufour, E., and Jacobs, H.T. (2018). Polyadenylation and degradation of structurally abnormal mitochondrial tRNAs in human cells. Nucleic Acids Res. *46*, 5209–5226. https://doi.org/10.1093/NAR/GKY159.

Torrence, M.E., Macarthur, M.R., Hosios, A.M., Valvezan, A.J., Asara, J.M., Mitchell, J.R., and Manning, B.D. (2021). The mtorc1-mediated activation of atf4 promotes protein and glutathione synthesis downstream of growth signals. Elife *10*. https://doi.org/10.7554/ELIFE.63326.

Tsai, C.W., Wu, Y., Pao, P.C., Phillips, C.B., Williams, C., Miller, C., Ranaghan, M., and Tsai, M.F. (2017). Proteolytic control of the mitochondrial calcium uniporter complex. Proc. Natl. Acad. Sci. U. S. A. *114*, 4388–4393. https://doi.org/10.1073/PNAS.1702938114/SUPPL_FILE/PNAS.201702938SI.PDF.

Tsai, P.I., Lin, C.H., Hsieh, C.H., Papakyrikos, A.M., Kim, M.J., Napolioni, V., Schoor, C., Couthouis, J., Wu, R.M., Wszolek, Z.K., et al. (2018). PINK1 Phosphorylates MIC60/Mitofilin to Control Structural Plasticity of Mitochondrial Crista Junctions. Mol. Cell *69*, 744-756.e6. https://doi.org/10.1016/J.MOLCEL.2018.01.026.

Uchiumi, T., Ohgaki, K., Yagi, M., Aoki, Y., Sakai, A., Matsumoto, S., and Kang, D. (2010). ERAL1 is associated with mitochondrial ribosome and elimination of ERAL1 leads to mitochondrial dysfunction and growth retardation. Nucleic Acids Res. *38*, 5554. https://doi.org/10.1093/NAR/GKQ305.

Vercellino, I., and Sazanov, L.A. (2021). The assembly, regulation and function of the mitochondrial respiratory chain. Nat. Rev. Mol. Cell Biol. 2021 232 *23*, 141–161. https://doi.org/10.1038/s41580-021-00415-0.

Vogel, F., Bornhövd, C., Neupert, W., and Reichert, A.S. (2006). Dynamic subcompartmentalization of the mitochondrial inner membrane. J. Cell Biol. *175*, 237–247. https://doi.org/10.1083/JCB.200605138.

Van Vranken, J.G., Bricker, D.K., Dephoure, N., Gygi, S.P., Cox, J.E., Thummel, C.S., and Rutter, J. (2014). SDHAF4 promotes mitochondrial succinate dehydrogenase activity and prevents neurodegeneration. Cell Metab. *20*, 241. https://doi.org/10.1016/J.CMET.2014.05.012.

Wai, T., and Langer, T. (2016). Mitochondrial Dynamics and Metabolic Regulation. Trends Endocrinol. Metab. *27*, 105–117. https://doi.org/10.1016/J.TEM.2015.12.001.

Wai, T., Saita, S., Nolte, H., Müller, S., König, T., Richter-Dennerlein, R., Sprenger, H., Madrenas, J., Mühlmeister, M., Brandt, U., et al. (2016). The membrane scaffold SLP2 anchors a proteolytic hub in mitochondria containing PARL and the *i* -AAA protease YME1L. EMBO Rep. https://doi.org/10.15252/embr.201642698.

Walker, D.W., and Benzer, S. (2004). Mitochondrial "swirls" induced by oxygen stress and in the Drosophila mutant hyperswirl. Proc. Natl. Acad. Sci. U. S. A. *101*, 10290–10295. https://doi.org/10.1073/PNAS.0403767101.

Wang, C., Richter-Dennerlein, R., Pacheu-Grau, D., Liu, F., Zhu, Y., Dennerlein, S., and Rehling, P. (2020). MITRAC15/COA1 promotes mitochondrial translation in a ND2 ribosome-nascent chain complex. EMBO Rep. *21*. https://doi.org/10.15252/EMBR.201948833.

Wang, Y., Cao, W., Yu, Z., and Liu, Z. (2009). Downregulation of a mitochondria associated protein SLP-2 inhibits tumor cell motility, proliferation and enhances cell sensitivity to chemotherapeutic reagents. Cancer Biol. Ther. https://doi.org/10.4161/cbt.8.17.9283.

Waterham, H.R., Koster, J., van Roermund, C.W.T., Mooyer, P.A.W., Wanders, R.J.A., and Leonard, J. V. (2007). A lethal defect of mitochondrial and peroxisomal fission. N. Engl. J. Med. *356*, 1736–1741. https://doi.org/10.1056/NEJMOA064436.

Wei, Y., Chiang, W.C., Sumpter, R., Mishra, P., and Levine, B. (2017). Prohibitin 2 Is an Inner Mitochondrial Membrane Mitophagy Receptor. Cell https://doi.org/10.1016/j.cell.2016.11.042.

Weraarpachai, W., Sasarman, F., Nishimura, T., Antonicka, H., Auré, K., Rötig, A., Lombs, A., and Shoubridge, E.A. (2012). Mutations in C12orf62, a factor that couples COX I synthesis with cytochrome c oxidase assembly, cause fatal neonatal lactic acidosis. Am. J. Hum. Genet. *90*, 142–151. https://doi.org/10.1016/J.AJHG.2011.11.027.

Werner, S., and Neupert, W. (1972). Functional and Biogenetical Heterogeneity of the Inner Membrane of Rat-Liver Mitochondria. Eur. J. Biochem. *25*, 379–396. https://doi.org/10.1111/J.1432-1033.1972.TB01707.X.

Wheatley, D.N., Giddings, M.R., and Inglis, M.S. (1980). Kinetics of degradation of "short-" and "long-lived" proteins in cultured mammalian cells. Cell Biol. Int. Rep. *4*, 1081–1090. https://doi.org/10.1016/0309-1651(80)90045-4.

Wiedemann, N., and Pfanner, N. (2017). Mitochondrial Machineries for Protein Import and Assembly. Annu. Rev. Biochem https://doi.org/10.1146/annurev.

Van Wilpe, S., Ryan, M.T., Hill, K., Maarse, A.C., Meisinger, C., Brix, J., Dekker, P.J.T., Moczko, M., Wagner, R., Meijer, M., et al. (1999). Tom22 is a multifunctional organizer of the mitochondrial preprotein translocase. Nature *401*, 485–489. https://doi.org/10.1038/46802.

Wittig, I., Braun, H.P., and Schägger, H. (2006). Blue native PAGE. Nat. Protoc. *1*, 418–428. https://doi.org/10.1038/NPROT.2006.62.

Wong, J.M.T., Malec, P.A., Mabrouk, O.S., Ro, J., Dus, M., and Kennedy, R.T. (2016). Benzoyl chloride derivatization with liquid chromatography-mass spectrometry for targeted metabolomics of neurochemicals in biological samples. J. Chromatogr. A *1446*, 78–90. https://doi.org/10.1016/J.CHROMA.2016.04.006.

Wüst, R., Maurer, B., Hauser, K., Woitalla, D., Sharma, M., and Krüger, R. (2015). Mutation analyses and association studies to assess the role of the presenilin-associated rhomboid-like gene in Parkinson's disease. Neurobiol. Aging *39*, 217.e13-5. https://doi.org/10.1016/J.NEUROBIOLAGING.2015.11.025.

Xia, D., Esser, L., Tang, W.K., Zhou, F., Zhou, Y., Yu, L., and Yu, C.A. (2013). Structural analysis of cytochrome bc1 complexes: implications to the mechanism of function. Biochim. Biophys. Acta *1827*, 1278–1294. https://doi.org/10.1016/J.BBABIO.2012.11.008.

Xiao, B., Xie, Z., Guo, L., Wu, J., and Zhang, H. (2015). Stomatin-like protein 2 expression is associated with clinical survival in patients with cervical cancer. Int. J. Clin. Exp. Pathol.

Yakubovskaya, E., Mejia, E., Byrnes, J., Hambardjieva, E., and Garcia-Diaz, M. (2010). Helix unwinding and base flipping enable human MTERF1 to terminate mitochondrial transcription. Cell *141*, 982–993. https://doi.org/10.1016/J.CELL.2010.05.018.

Yamamoto, H., Esaki, M., Kanamori, T., Tamura, Y., Nishikawa, S. ichi, and Endo, T. (2002). Tim50 is a subunit of the TIM23 complex that links protein translocation across the outer and inner mitochondrial membranes. Cell *111*, 519–528. https://doi.org/10.1016/S0092-8674(02)01053-X.

Yang, C.T., Li, J.M., Li, L.F., Ko, Y.S., and Chen, J.T. (2018). Stomatin-like protein 2 regulates survivin expression in non-small cell lung cancer cells through β-catenin signaling pathway. Cell Death Dis. https://doi.org/10.1038/s41419-018-0461-9.

Yeo, J.H.C., Skinner, J.P.J., Bird, M.J., Formosa, L.E., Zhang, J.G., Kluck, R.M., Belz, G.T., and Chong, M.M.W. (2015). A Role for the Mitochondrial Protein Mrpl44 in Maintaining OXPHOS Capacity. PLoS One *10*. https://doi.org/10.1371/JOURNAL.PONE.0134326.

Yoshikawa, S., and Shimada, A. (2015). Reaction mechanism of cytochrome c oxidase. Chem. Rev. *115*, 1936–1989. https://doi.org/10.1021/CR500266A.

Youle, R.J., and Van Der Bliek, A.M. (2012). Mitochondrial fission, fusion, and stress. Science *337*, 1062–1065. https://doi.org/10.1126/SCIENCE.1219855.

Zeharia, A., Friedman, J.R., Tobar, A., Saada, A., Konen, O., Fellig, Y., Shaag, A., Nunnari, J., and Elpeleg, O. (2016). Mitochondrial hepato-encephalopathy due to deficiency of QIL1/MIC13 (C19orf70), a MICOS complex subunit. Eur. J. Hum. Genet. *24*, 1778–1782. https://doi.org/10.1038/EJHG.2016.83.

Zhu, J., Vinothkumar, K.R., and Hirst, J. (2016). Structure of mammalian respiratory complex I. Nature *536*, 354–358. https://doi.org/10.1038/NATURE19095.

Zorkau, M., Albus, C.A., Berlinguer-Palmini, R., Chrzanowska-Lightowlers, Z.M.A., and Lightowlers, R.N. (2021). High-resolution imaging reveals compartmentalization of mitochondrial protein synthesis in cultured human cells. Proc. Natl. Acad. Sci. U. S. A. *118*, e2008778118. https://doi.org/10.1073/PNAS.2008778118/SUPPL_FILE/PNAS.2008778118.SAPP.PDF.

Zurita Rendón, O., and Shoubridge, E.A. (2018). LONP1 Is Required for Maturation of a Subset of Mitochondrial Proteins, and Its Loss Elicits an Integrated Stress Response. Mol. Cell. Biol. *38*. https://doi.org/10.1128/MCB.00412-17/SUPPL_FILE/ZMB999101844S1.PDF.